DEVELOPMENT OF CONTRAST ENHANCEMENT ALGORITHMS FOR COASTAL APPLICATIONS USING SATELLITE IMAGES

Thesis

Submitted in partial fulfillment of the requirements for the award of the degree of

DOCTOR OF PHILOSOPHY

by

RAJU. A

DEPARTMENT OF APPLIED MECHANICS AND HYDRAULICS

NATIONAL INSTITUTE OF TECHNOLOGY KARNATAKA

SURATHKAL, MANGALORE – 575 025

November, 2014

D E C L A R A T I O N

By the Ph.D. Research Scholar

I hereby *declare* that the Research Synopsis entitled **Development of Contrast Enhancement Algorithms for Coastal Applications using Satellite Images**, which is being submitted to the **National Institute of Technology Karnataka**, **Surathkal** in partial fulfilment of the requirements for the award of the Degree of **Doctor of Philosophy** in **Civil Engineering**, is a *bonafide report of the research work carried out by me*. The material contained in this Research Synopsis has not been submitted to any University or Institution for the award of any degree.

RAJU. A

(Registration Number: 110632AM11F05)

Department of Applied Mechanics and Hydraulics

Place: NITK-Surathkal

Date: 07-11-2014

C E R T I F I C A T E

This is to *certify* that the Research Synopsis entitled "**Development of Contrast Enhancement Algorithms for Coastal Applications using Satellite Images**" submitted by **Mr. Raju. A** (Register Number 110632AM11F05) as the record of the research work carried out by him, is *accepted* as the *Research Synopsis submission* in partial fulfillment of the requirements for the award of degree of Doctor of Philosophy.

Dr. G. S. Dwarakish

Professor & Research Guide
Department of Applied Mechanics and Hydraulics

Dr. D. Venkat Reddy

Professor & Research Guide
Department of Civil Engineering

Dr. Subba Rao

Professor & Chairman DRPC
Department of Applied Mechanics and Hydraulics

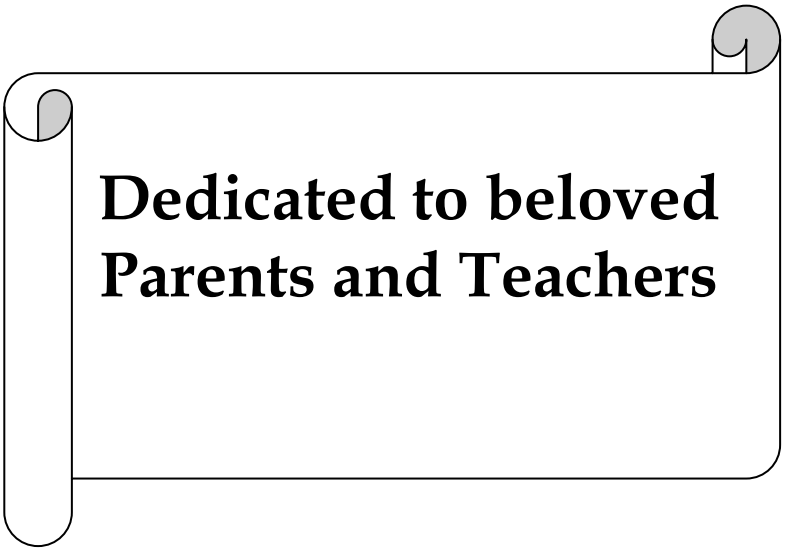
Dedicated to beloved
Parents and Teachers

ACKNOWLEDGEMENT

I am deeply indebted and thankful to my supervisors **Dr. G. S. Dwarakish**, Professor, Department of Applied Mechanics and Hydraulics and **Dr. D. Venkat Reddy**, Professor, Department of Civil Engineering, for their guidance, support, inspiring suggestions and encouragement throughout the research work, which made all the difference. It is my privilege to work under them and it has provided an opportunity to gain knowledge in the field of Remote Sensing, Digital Image Processing and Coastal Engineering, and also created a platform to learn quality teaching skills from their experience.

I am grateful to Prof. Swapan Bhattacharya, Director, NITK, Surathkal and Prof. Sandeep Sancheti, Former Director, NITK, Surathkal for permitting to utilize the infrastructure facilities throughout the research work.

I profusely thank my Research Progress Assessment Committee Members, Dr. Subba Rao, Professor and Head, Department of Applied Mechanics and Hydraulics and Dr. Aparna. P, Assistant Professor, Department of Electronics and Communications Engineering for their valuable timely suggestions and appraisal.

I sincerely thank Dr. M. K. Nagaraj, Professor and Former Head, Department of Applied Mechanics and Hydraulics and Dr. Katta Venkataramana, Professor and Head, Department of Civil Engineering, for their constant encouragement and cooperation during the research work.

I thank all the faculty members, technical and office staff of Department of Applied Mechanics and Hydraulics for their continuous moral support.

I acknowledge to Miss. Ganasri B P, Research Scholar, for her unique support and, Miss. Nujuma Nazimudhin, Mr. Sri Ram Kumar and Miss. Deepthi I Gopinath Post Graduate students for their support and fruitful discussions during the work.

My special and heartfelt thanks to my father, Mr. Ramalaxmaiah, mother Smt. Bhagyalaxmi, brother, Mr. Sanjeev and sister Miss. Samatha for their endless love, encouragement, strength and confidence.

My wholehearted thanks to all those who have helped me directly or indirectly to achieve my dream and goal.

RAJU. A

Date: 07-11-2014

ABSTRACT

Remotely sensed satellite images are used in many earth science applications such as geosciences studies, astronomy, and geographical information systems. One of the most important quality factors in satellite images comes from its contrast. Contrast enhancement is frequently referred to as one of the most important issues in image processing. Contrast is created by the difference in luminance reflectance from two adjacent surfaces. Image enhancement is one of the most interesting and important phase in the domain of digital image processing. The main purpose of image enhancement is to bring out details that are hidden in image, or to increase the contrast in a low contrast image. The quality of the remote sensing image depends on the reflected electromagnetic radiation from earth surfaces features. Lack of consistent and similar amounts of energy reflected by different features, results a low contrast satellite image. Enhancement of contrast is desirable for satellite images to identify and extract features, where features are essential in studying earth applications.

The present study is carried out with a view to develop contrast enhancement algorithms for coastal applications using satellite images. Histogram Equalization (HE) is an effective and well-known indirect contrast enhancement method, where histogram of the image is modified. Because of stretching the global distribution of the intensity, the information laid on the histogram of the image will be lost by over enhancement and introducing unwanted artefacts. To overcome these drawbacks several HE-based methods are introduced. With the comparative study of existing HE-based methods, the present study has developed contrast enhancement algorithms for coastal applications such as, automatic shoreline detection, suspended sediment transport and land use and land cover assessment for Mangalore Coast, West Coast of India, starting from Thalapady in the South and Mulky in the North.

The study has developed an automatic shoreline detection algorithm using clipped histogram equalization and thresholding techniques. Clipped histogram equalization method highlighted the coastal objects and thresholding operation precisely separated the land and water regions. The smoothed shoreline is extracted using Robert's edge detector. The study area is divided into Mulky-Pavanje rivermouth and Netravati-Gurpur rivermouth areas. The shorelines of both the regions are extracted from Indian Remote Sensing Satellite (IRS P6) LISS-III (2005, 2007 and 2010) and IRS R2 LISS-III (2013) satellite images using developed automatic shoreline detection method. The delineated shorelines have been analyzed using Digital Shoreline Analysis System (DSAS), a GIS Software tool for estimation of shoreline change rates through two statistical techniques such as, End Point Rate (EPR) and Linear Regression Rate (LRR).

To enhance IRS-P4 OCM Oceasat-2 satellite image for sediment movement direction, study developed Clipped Histogram Equalization and Principal Component Analysis (PCA) based algorithm. The movement of dispersed suspended sediment pattern of Mangalore Coast, West Coast of India is detected and mapped using qualitative analysis. The study is mainly focused on suspended sediment distributions at Netravati-Gurpur Rivermouth along Mangalore Coast.

To improve the assessment of land use and land cover, study developed contrast enhancement algorithm using clipped histogram equalization and Principal Component Analysis (PCA). IRS-R2 LISS III 2013 satellite image is used for assess the developed algorithm. For assessment, the study area is divided into Mulky-Pavanje rivermouth area, New Mangalore Port Trust (NMPT) area and Netravati-Gurpur rivermouth area. The IRS-R2 LISS III 2013 satellite image is classified using maximum likelihood supervised classification method by considering GPS values and Google Earth map as reference in selection of training samples during the classification. The developed contrast enhancement algorithm has increased the

accuracy assessment of LULC classification to 85.42%, 89.66% and 86.93% for Mulky-Pavanje rivermouth area, New Mangalore Port Trust (NMPT) area and Netravati-Gurpur rivermouth area respectively.

TABLE OF CONTENTS

LIST OF FIGURES

LIST OF TABLES

NOMENCLATURE

2DHE	:	Two-Dimensional Histogram Equalization
AMBE	:	Absolute Mean Brightness Error
BBHE	:	Brightness Preserving Bi-Histogram Equalization
BHENM	:	Bi-Histogram Equalization with Neighbourhood Metric
BHEPL	:	Bi-Histogram Equalization Plateau Limit
Bi-HE	:	Bi-Histogram Equalization
BPDFHE	:	Brightness Preserving Dynamic Fuzzy Histogram Equalization
BPDHE	:	Brightness Preserving Dynamic Histogram Equalization
BPHEME	:	Brightness Preserving Histogram Equalization with Maximum Entropy
BPWCHE	:	Brightness Preserving Weight Clustering Histogram Equalization
BUBO	:	Bin Underflow and Bin Overflow
CDF	:	Cumulative Distribution Function
CHE	:	Clipped Histogram Equalization
DBMS	:	Data Base Management System
DHE	:	Dynamic Histogram Equalization
DN	:	Digital Number
DPHE	:	Double Plateaus Histogram Equalization
DSAS	:	Digital Shoreline Analysis System
DSIHE	:	Dualistic Sub-Image Histogram Equalization
DWT	:	Discrete Wavelet Transform
EPR	:	End point Rate
ERDAS	:	Earth Resources Data Analysis System
ERS	:	European Remote Sensing Satellite
ESIHE	:	Exposure based Sub-Image Histogram Equalization
ESRI	:	Environmental Systems Research Institute
FCC	:	False Colour Composition
FGLG	:	Fast Gray-Level Grouping
FHQ	:	Flexible Histogram Quantization
GC-CHE	:	Gain-Controllable Clipped Histogram Equalization
GHE	:	Global Histogram Equalization
GIS	:	Geographical Information System
GL	:	Grey Level
GPS	:	Global Positioning System
HE	:	Histogram Equalization
IGDC	:	International Geographic Data Committee
IQM	:	Image Quality Measure
IRS	:	Indian Remote Sensing Satellite
LISS	:	Linear Imaging Self-scanning Sensor
LRR	:	Linear Regression Rate
LULC	:	Land Use and Land Cover

MLC	:	Maximum Likelihood Classifier
MMBEBHE	:	Minimum Mean Brightness Error Bi-Histogram Equalization
MMLSEMHE	:	Minimum Middle Level Squared Error Multi Histogram Equalization
MPHEBP	:	Multi-Peak Histogram Equalization with Brightness Preserving
MSMR	:	Multi-frequency Scanning Microwave Radiometer
Multi-HE	:	Multi-Histogram Equalization
MWCVMHE	:	Minimum Within-Class Variance Multi-Histogram Equalization
NIR	:	Near Infrared
NMPT	:	New Mangalore Port Trust
NRSC	:	National Remote Sensing Centre
OCM	:	Ocean Colour Monitor
OCMDAS	:	OCM Data Analysis Software
PAN	:	Panchromatic
PCA	:	Principal Component Analysis
PDF	:	Probability Density Function
PSNR	:	Peak-Signal to Noise Ratio
QDHE	:	Quadrants Dynamic Histogram Equalization
RLBHE	:	Range Limited Bi-Histogram Equalization
RMSHE	:	Recursive Mean-Separate Histogram Equalization
ROI	:	Region of Interest
RS	:	Remote Sensing
RSIHE	:	Recursive Sub-Image Histogram Equalization
RSWHE	:	Recursively Separated and Weighted Histogram Equalization
SAC	:	Space Application Centre
SAPHE	:	Self-Adaptive Plateau Histogram Equalization
SAR	:	Synthetic Aperture Radar
SCHE	:	Spatially Controlled Histogram Equalization
SD	:	Standard Deviation
SQL	:	Structured Query Language
SSC	:	Suspended Sediment Concentration
SVD	:	Singular Value Decomposition
TOA	:	Top of the Atmosphere
WAMSHE	:	Weighted Average Multi Segment Histogram Equalization

CHAPTER 1
INTRODUCTION

1.1. General

Remotely sensed satellite images are used in many earth science applications such as geoscience studies, water resources and coastal processes. In order to conserve sustainable development of coastal zones, it is essential to develop accurate and complete databases by continuous monitoring of coastal zones. Monitoring and development of database for large and inaccessible coastal areas is complex through conventional methods, because of huge man power, cost ineffective and time consuming by these methods. The advanced scientific tools of Remote Sensing, Geographical Information System (GIS) and Global Positioning System (GPS) are overcoming the drawbacks of conventional methods used in coastal studies and provide accurate database. By integrating, the generated database can be efficiently analysed using these tools to develop proper coastal zone management plans. Periodical monitoring of coastal changes with less cost and at faster rate is the major advantage of remote sensing. The moderate and high spatial resolution and multi-spectral remotely sensed data generated from various satellite platforms provide detailed information about coastal zones. Due to inherent advantages such as easy availability, synoptic and repetitive global coverage, multi-spectral and moderate to high-spatial resolution, the remote sensing data is more suitable for coastal zone monitoring and management studies in an efficient manner.

In most of the remotely sensed satellite images, the important quality factor comes from its contrast. The quality of the remotely sensed image depends on the reflected electromagnetic radiation from the earth surface features. Due to lack of uniformity in features and similar amounts of energy reflected by different features, results a low contrast satellite image. If one material reflects high amount of energy in a certain wavelength and another material reflects much less energy in the same

wavelength also creates a low contrast image. Contrast enhancement is one of the most important issues in the image processing, which improve the quality of a low contrast satellite image, by bringing out all the hidden objects information without over-enhancing the other objects in the image. If the contrast of an image is highly concentrated on a specific range, then the information may be lost in those areas which are excessively and uniformly concentrated. The problem is to enhance the contrast of an image in order to represent all the information in the input image. Enhancement of contrast is desirable for satellite images to identify and extract features, which are essential for studying geoscience/earth science applications.

1.2. Remote Sensing

Remote Sensing (RS) is the science and art of obtaining information about an object, area or phenomenon through the analysis of data acquired by a device that is not in contact with the object, area or phenomenon under investigation (Lillesand and Kiefer 1994). In Earth's perspective, remote sensing is the process of obtaining the information about the Earth's surface features using on-board sensors or camera systems from the satellite platform without being in direct contact with it. The data collected by these sensors are in the form of electromagnetic energy (EM) which are emitted or reflected by the object at different wavelengths depending on its physical properties. In addition to this, objects emit radiation depending up on their temperature and emissivity. Every pixel of the digital remote sensing data represents an average value of the EM energy and is recorded as a Digital Number (DN). The recorded energy at different wavelengths follows a pattern which is the unique characteristic of that object and is known as the spectral signature of the object or class. Proper interpretation of the spectral signature leads to the identification of the object and segregation of different classes. Certain regions or bands of the electromagnetic spectrum are optimum for obtaining biophysical information. The

bands are normally selected to maximize the contrast between the object of interest and its background.

Remote sensing is a process enabled for mapping, monitoring and management of various resources namely, agriculture, forestry, geology, water, ocean etc. Indian Remote Sensing Satellites (IRS) such as IRS-1A (1988), IRS 1B (1991), IRS-P2 (1994), IRS-1C (1995), IRS-P3 (1996), IRS-1D (1997), IRS-P4 Oceansat-1 (1999), IRS-P6 Resourcesat-1 (2003), IRS-P5 Cartosat-1 (2005), IRS-P7 Cartosat-2 (2007), Oceansat-2 etc. facilitate a variety of applications including natural resource monitoring, environmental assessments and disaster management related activities. After the successful launch of Bhaskara I and Bhaskara II in 1979 and 1981 respectively, India lunched the first remote sensing satellite IRS-1A in 1988 for various land-based applications. IRS-P5 Cartosat-1 is mainly planned for cartographic applications with two PAN cameras that take black and white stereoscopic pictures of the earth in the visible region of the electromagnetic spectrum with spatial resolution of 2.5 meters.

IRS-P6 Resourcesat-1 is launched in 2003 with LISS-IV camera (5.8 m resolution), LISS-III (23.5 m resolution) and AWiFS (60 m resolution). It is a follow-on satellite for Earth observation that will provide continuity to IRS-1C and 1D and enhances the service capabilities in the areas of agriculture, disaster management, and land and water resources with better resolution imagery. IRS-P4 was the first Indian satellite for Ocean applications launched in 1999 with on-board an Ocean Colour Monitor (OCM) and a Multi-frequency Scanning Microwave Radiometer (MSMR) cameras. OCM is a solid state camera operating in eight narrow spectral bands with 360 m spatial resolution and collect data of chlorophyll concentration, detect and monitor phytoplankton blooms and obtain data of atmospheric aerosols and suspended sediments in the water. MSMR, which operates in four microwave frequencies both in vertical and horizontal polarisation is used to collect data of sea surface temperature,

wind speed, cloud water content and water vapour content in the atmosphere above the ocean.

The Indian satellites with their improved spatial resolution, extended spectral range and increased repetivity leads new studies of coastal zone. Preliminary analysis of IRS-IC, ID data indicates that coral reef zonation, identification of coastal vegetation and mangroves, mudflats, beach, dune vegetation, saline areas, etc. as well as suspended sediment patterns along the coast. IRS-IC Linear Imaging Self Scanner (LISS) III and Panchromatic (PAN) merged data are more suitable for coral reef zonation studies through identification of reef crest, algal ridge, reef edge, moat, coral knolls, reef platform, reef flat. The PAN data combined with the LISS III and LISS IV data provides detailed information about area of reclamation, construction of coastal structures and ecologically sensitive areas, which are vital for the coastal zone regularity authorities, while developing comprehensive Integrated Coastal Zone Management Plan (ICZMP).

1.3. Digital Image Processing

Digital image processing system consists of the computer hardware and the image processing software needed to analyze digital image data (Jensen 1996). Satellite digital image processing is categorized into image rectification and restoration, enhancement and classification. The image rectification and restoration are initial processes of raw image data to correct geometric distortion, to calibrate the data radiometrically and to eliminate noise exist in the satellite data (Lillesand and Kiefer 1994). The image rectification and restoration processes are often termed as pre-processing procedure, because they normally precede with further manipulation and analysis of the image data to extract specific information. The enhancement procedures are applied to image data in order to effectively display the data for subsequent visual interpretation. It involves techniques for increasing the visual

distinction between features in a scene. The image classification is to automatically categorize all pixels in an image into land cover classes or themes. Generally, multispectral data are used to perform the classification, and the spectral pattern present within the data for each pixel is used as numerical basis for categorization. That is, different feature types manifest different combination of DNs based on their inherent spectral reflectance and emittance properties.

1.4. Digital Image Enhancement

Image enhancement is one of the most interesting and important phases in the domain of digital image processing. It is used to transform an image, based on the psychological characteristics of the human visual system (Neycenssac 1993). Image enhancement algorithms are applied to remotely sensed data to improve the appearance of an image for human visual analysis or occasionally for subsequent machine analysis. In most of the satellite images the quality factor comes from its contrast. Image enhancement techniques improve the quality of an image as perceived by a human. A wide variety of image enhancement techniques are used for improving the image quality such as, contrast stretch, density slicing, edge enhancement, and spatial filtering. After the image is geometrically and radiometrically corrected, image enhancement is applied separately to each band of a multi-spectral image.

1.4.1. Contrast Enhancement

Contrast is created by the difference in luminance reflectance from two adjacent surfaces. Contrast enhancement is an important area in image processing for both human and computer vision. Contrast generally refers to the difference in luminance or grey level values in an image and is one of the important characteristics of image enhancement. It can be defined as the ratio of the maximum intensity to the minimum intensity over an image. Contrast ratio has a strong bearing on the resolving power and detectability of an image. The quality of interpretation of satellite image improves

with the higher value of contrast ratio. Usually, contrast refers to the difference in luminance between an object and its surrounding region.

In psychovisual studies, the contrast *C* is defined as (Morrow 1992);

$$C = \frac{(f-b)}{b} \qquad (1.1)$$

Where, *f* is the object luminance and *b* is the surrounding luminance. In optical studies, the contrast *C* is defined as (Morrow, 1992);

$$C = \frac{(f-b)}{(f+b)} \qquad (1.2)$$

Where, *f* is the maximum luminance of the image and *b* is the minimum luminance of the image.

Generally, remote sensors record reflected and emitted radiant flux leaving from Earth's surface materials. Unfortunately, different materials often reflect similar amounts of radiant flux throughout the visible, near-infrared, and mid-infrared portion of the electromagnetic spectrum, resulting in a relatively low contrast image. In addition to this, the low sensitivity of the detectors also creates low-contrast remotely sensed image because of its insufficient radiometric sensitivity of a detector to record the full range of intensities of reflected or emitted energy emanating from the earth surface. There are two digital contrast enhancement techniques, namely, linear and nonlinear contrast enhancement methods.

1.4.1.1. Linear Contrast Enhancement

The main object of contrast stretching is to expand the narrow range of brightness values typically present in an input image over a wider range of gray values. In this

method, the grey values in the input image and the modified output image follow a linear relation. A density number in the low range of the original histogram is assigned to extremely black color (0 DN value) and a value at the high end is assigned to extremely white colour (255 DN value). The remaining pixel values are distributed linearly between these extremes. The features or information that is unclear on the original image will be now clearly visible in the contrast stretched image. To provide optimal contrast and colour variation in colour composites, the small range of grey values in each band is stretched to the full brightness range of the output or display unit. To perform a linear contrast enhancement, first determine the minimum and maximum brightness values in the band, min_k and max_k respectively and then, the output brightness value BV_{out}, is computed according to the equation (1.3);

$$BV_{out} = \left(\frac{BV_{in} - min_k}{max_k - min_k}\right) quant_k \qquad (1.3)$$

Where, BV_{in} is the brightness values of original image, $quant_k$ is the range of the brightness values (0 to 255 for 8-bit data).

1.4.1.2. Nonlinear Contrast Enhancement

In this method, the input and output data values follow a nonlinear transformation. The general form of the nonlinear contrast enhancement is defined by $y=f(x)$, where x, is the input data value and y, is the output data value. The nonlinear contrast enhancement techniques have been found to be useful for enhancing the colour contrast between the nearly classes and subclasses of a main class. Histogram Equalization (HE) is the most useful nonlinear contrast enhancement method. Another type of nonlinear contrast enhancement is scaling the input image data logarithmically. This method enhances the brightness values of darker region of the histogram by scaling the input data using an inverse log function.

1.4.1.2.1. Histogram Equalization

Histogram is a graphical representation of the information content of a remotely sensed image. Histogram Equalization (HE) (Hummel 1977) and histogram specification are two well-known indirect contrast enhancement methods, where histogram of the image is modified. HE is a distinguished and widely used contrast enhancement technique (Kim 1997; Gonzalez and Woods 1992; Jain 1989; Zimmerman et al. 1988; Kim et al. 1998). Applications of HE are found in many areas such as medical image processing (Kong and Ibrahim 2008), radar image processing (Kim 1997), sonar image processing (Chen and Ramli 2004), texture synthesis, and speech recognition and so on (Pei et al. 2004; Dhnawan et al. 1986; Rangayyan and Nguyen 1986) due to its efficiency. HE, redistribute the histogram of the original image to produce an uniform population density and it is obtained by grouping certain neighboring grey values. Consequently the number of grey levels in the enhanced image is less than the number of grey levels in the original image. The algorithm of histogram equalization is as follows;

Let, X is a input image and then, probability density function $p\ (X_k)$ is defined as;

$$p(X_k) = \frac{n^k}{n} \qquad (1.4)$$

Where X_k is the k^{th} brightness level, n^k is the number of brightness level, n is the total number of pixels in the image, $p(X_k)$ is the probability of occurrence of brightness-level X_k and k= 0,1,2,3…(L-1). In fact, a plot of $\underline{n^k}$ vs. X_k is known as histogram of X. Based on the probability density function, the cumulative density function is defined as;

$$c(x) = \sum_{j=0}^{k} p(X_j) \qquad (1.5)$$

Where $X_k=x$, for k= 0, 1, 2…, L-1. Note that $c(X_{L-1})=1$ by definition. HE is a scheme that maps the input image into the entire dynamic range, (X_0, X_{L-1}), by using cumulative density function as a transform function. Based on cumulative function, the transform function is defines as;

$$f(x)=X_0+(X_{L-1}- X_0).c(x) \qquad (1.6)$$

Then the output image of histogram equalization, Y={Y (i,j)}, is expressed as;

$$Y = f(X) = \{f(X(i,j))|\forall X(i,j) \in X_L\} \qquad (1.7)$$

HE applies to the individual bands of the multi-spectral dataset and provides better contrast enhancement to the most populated range of brightness values in the image. It is entirely different from other contrast enhancement techniques because the data has been redistributed to the cumulative frequency histogram. However, HE is rarely employed in consumer electronic products, since it tends to introduce some annoying artefacts and unnatural enhancement, including intensity saturation effect (Kong and Ibrahim 2008).

1.4.2. Filtering Techniques

Filtering is the process that selectively enhances or suppresses particular wavelengths or pixel DN values (brightness values) within an image. Spatial frequency describes the brightness values over a spatial region and defined as the number of changes in brightness value per unit distance for any particular area of an image. If an area in an image has very few changes in brightness value, then it is referred to as low frequency area and similarly, if the brightness values change dramatically over a short distance it is stated as high frequency area. Spatial approach is necessary to adopt to extract qualitative information from remotely sensed imagery using two different methods such as convolution filtering in the spatial domain and Fourier analysis in the frequency domain. Convolution filtering

is relatively easy to understand and used to enhance low-frequency and high-frequency regions, in addition to edges in the imagery. Fourier analysis mathematically divides an image into its spatial frequency components, resulting in a Fourier transform of the image. Low-pass or low-frequency filters are used to block the high frequency details in an image, and high-pass filters are applied to remove the slowly varying components and enhance the high-frequency local variations in an image.

Median filter is the non-linear, low-pass filter useful for removing noise in an image, by which individual pixels are missing. Median filter contains a spatial filtering operation, selects the median value of the nine pixels of 3x3 convolution mask and it is placed in the central value of the mask or kernel. The convolution masks of median filter are 3x3, 5x5, 7x7 and 5x5 and 7x7 Octagonal. Median filter reduce the variance of the intensities in the image.

1.4.3. Principal Component Analysis

Principal Component Analysis (PCA) or Kar-hunen-Loeve analysis is used to compress the information content of a number of bands of imagery into just two or three transformed principal component images (Press et al. 1992, Wang 1993). The transformation of the raw remote sensor data using PCA, results a new principal component images that may be more interpretable than the original data (Singh and Harrison 1985). Principal component analysis is a pre-processing transformation that creates new images from the uncorrelated values of different images. The aim of PCA is to translate or rotate the original axes, so that, the brightness values on original axes are redistributed on to a new set of axes or dimensions. Principal component transformations are used for spectral pattern recognition as well as image enhancement. PCA operates on all bands together and describe the data more efficiently than the original band reflectance values. The first principal component accounts for a maximum portion of the variance in the data set, often as high as 98%. Subsequent principal components account for successively smaller portions of the

remaining variance. Principal component images may be analysed as separate black and white images, or any three component images may be colour coded to form a colour composite. Principal component enhancement techniques are particularly appropriate in areas where little a priori information concerning the region is available.

1.5. Geographical Information System

A Geographical Information System (GIS) is defined as "a powerful set of tools for collecting, storing, retrieving at will, transforming and displaying spatial data from the real world for a particular set of purposes" (Burrough 1998). GIS is capable of handling both spatial data and attribute data of earth surface features. GIS permits to automate mapping and also got the capability of recording and analyzing descriptive characteristics about earth surface features (Lillesand et al. 2004). A Data Base Management System (DBMS) is built in GIS to store and manipulate attribute data of features and it is designed with user friendly commands in Structured Query Language (SQL). GIS has the ability to spatially interrelate multiple types of information stemming from a range of sources. GIS convert data from one coordinate system to another, to understand the characteristics of the various types of coordinate systems, either by using raster or vector data format.

1.6. Coastal Processes

Coastal zone is the triple interface of the land, ocean and atmosphere. Cracknell (1999) defined coastal zone as the region between the 200 m bathymetric contour at sea to the 200 m elevation contour on the land. Coastal zones are one of the most complicated ecosystems with a large number of living and non-living resources (Constanza et al. 1997). Coastal zones are exposed to a series of dynamic natural processes like coastal erosion, sediment transport, environmental pollution, and

coastal development that usually causes changes in long and short time spans. These coastal changes influences the loss of life and property, security of harbors, change of the coastal socio-economic condition, and decrease in coastal land resources. So, coastal zone monitoring is a significant task in national development and environmental protection, in which, extraction of shoreline is the fundamental study of necessity (Rasuly et al. 2010). The effects of waves, tides, currents and winds are primary natural factors that influence the change in configuration of the coast. Anthropogenic effects that trigger the beach erosion are, construction of coastal structures in the zone of high littoral drift, mining of beach sand and offshore dredging.

1.6.1. Shoreline

Shoreline is considered as one of the most dynamic processes in coastal area (Bagli and Soile 2003; Mills et al. 2005) and it is the physical interface of the land and water (Dolan et al. 1980). It is formed by a number of geological factors such as interaction, sediment deposition of rivers and oceans, various weather and sea conditions, as well as the frequent human social and economic activities (Boak and Turner 2005). Shoreline is defined as the line of contact between the high water line and the shore (CERC 1984). It is one of the 27 features recognized by International Geographic Data Committee (IGDC) (Li et al. 2001). It undergoes short-term and long-term changes, caused by hydrodynamic changes (e.g. river cycles, sea level rise), geomorphological changes (e.g. barrier island formation, spit development) and other factors (e.g. sudden and rapid seismic and storm events) (Scott 2005).

1.6.2. Shoreline Changes

The study of shoreline change rate is essential for a wide range of coastal applications, such as development of setback planning, hazard zoning, erosion-

accretion studies, regional sediment budgets and conceptual or predictive modeling of coastal morphodynamics (Sherman and Bauer 1993; Al Bakri 1996; Zuzek et al. 2003; Maiti and Battacharya 2009). The location of the shoreline provides the data in respect to shoreline reorientation adjacent to structures (Komar 1998) and beach width and volume (Smith and Jackson 1992), and it is used to quantify historical rate of change of shoreline (Dolan et al. 1991; Moore 2000).

Coastal erosion is due to natural processes (Waves, Tides, Littoral current, Littoral drift and Storms) and also due to human interference through construction of coastal protection structures (Breakwaters, Seawalls, Groins, Jetties and approach channels of ports and harbours) (Dwarakish and Natesan 2002; Antonio et al. 2010). In addition to these, nearshore breaking waves and currents transport coastal sediments from one part of shoreline to another part called littoral transport, causing coastal erosion/accretion and leads to shoreline change (Jorge and Albert 1996; Anil et al. 2007; Rao et al. 2009). Normally, beaches grow during fair weather and retreat (they are eroded) during storms.

1.6.3. Karnataka Coast

The coastline along the Peninsular Indian mainland stretches about 5423 km and the islands of Andaman, Nicobar, Lakshadweep and Maldives, which extend to about 2094 km. The seasons, Southwest monsoon (June to September), Northeast monsoon (October to January) and dry weather period (February to May) dominate the oceanography of the Indian coastal region. While both the monsoons have equal impact along the southern part of the East Coast and only Southwest monsoon has a significant effect on the West Coast. Tides along the Indian coast are semi diurnal with tidal range (0.5 m to 6 m) varying from place to place (Dwarakish, 2001).

Karnataka coast stretches about 290 km and covers Dakshina Kannada, Udupi and Uttara Kannada districts. It is covered by 75% of open sand beaches, 11% rocky coast

and 14% muddy flats (Sanil et al. 2006). Erosion along the beaches near the rivermouth is being most common problem noticed along the Karnataka coast (Dattatri et al. 1997). Infact, there are number of rivermouths along Karnataka coast that are being developed into fishery and general harbours where sedimentation in the navigational channel is a major problem (Dattatri and Kamath 1997; Hegde et al. 2004).

Karnataka Coast is being a center for developmental activities due to its rich ocean resources and favorable conditions for the development of port based major industries like refineries, fertilizer industries, leather industries, thermal power plants, coastal irrigation, development of marine structures, etc. As a result of these anthropogenic activities, natural processes are being disturbed, leading to a significant modification in the coastal configuration, particularly around the rivermouths (Dwarakish et al. 1997; Hegde et al. 2009; Avinash et al. 2010). In addition to this, sediments brought by the rivers causing shoreline erosion/accretion and rapid change in rivermouth configurations. The morphological features (tidal bar, spit formation, lagoons etc.) are the main responsible factors, which lead sedimentation in the rivermouth (Bhat and Subrahmanya 2000; Raghavan et al. 2001; Santosh and Reddy 2002). It is estimated that, out of 290 km length of Karnataka coastline, about 80 km (27.6%) is vulnerable to severe erosion during the SW monsoon (Jayappa et al. 2003).

1.6.4. Mangalore Coast

Mangalore Coast is a part of coastal areas of Dakshina Kannada District, Karnataka State, India. It stretches from Talapadi in the South to Mulky in the North along West Coast of India with coastline of 40 km and it is bordered by the Arabian Sea on the West and the Western Ghats on the East. The rivers Netravati, Gurpur, Mulky and Pavanje are originated in the Western Ghats and flow westward and take an almost right angle turn near the coast and then flow either northward or southward direction close to or parallel to the coast before empty into the Arabian Sea. The Mangalore

Coast is subjected to severe wave attack only during the monsoon months of June to September. Tides at Mangalore Coast are the mixed type with the semi diurnal components. Semi diurnal tides would mean 2 high waters and 2 low waters in a day. The currents along the coast during the months February to September is generally towards the South with velocities ranging from 0.22 to 0.80 knots and during the months November to January is towards North with velocities of 0.22 to 0.60 knots.

Mangalore Coast is having two rivermouths viz., Netravati-Gurpur rivermouth and Mulky-Pavanje rivermouth in addition to manmade structure, New Mangalore Port Trust (NMPT) at Panambur. Netravati-Gurpur rivermouth is with breakwaters and Mulky-Pavaje rivermouth is without breakwaters. To prevent the shifting nature of Netravati-Gurpur rivermouth and also to guide the sediment movement at rivermouth two breakwaters on either side of rivermouth were constructed during 1994. Due to rich ocean resources, favourable conditions for harbours and ports, and transportation, Mangalore Coast is getting more and more importance and there is an increase in trend of industrialization and urbanization. NMPT is one of the eleventh major ports of India and most of the large, medium and small scale industries are located near the port. NMPT is having two breakwaters of length 770 m on either side of approach channel (Dwarakish 2001).

1.6.5. Digital Shoreline Analysis System

The Digital Shoreline Analysis System (DSAS) is a freely available software application that works within the Environmental Systems Research Institute (ESRI) Geographic Information System (ArcGIS) software. DSAS computes rate-of-change statistics for a time series of shoreline vector data (Crowell and Leatherman 1999). User has to construct the baseline with defined distance both on-shore or off-shore side and it serves as the starting point for all transects cast by the DSAS application. A group of transects can be drawn in perpendicular to the baseline at a user-defined

spacing and the orientation of transect through the shorelines is highly dependent on the position of the baseline. The intersection of transect with each shoreline at the measurement points gives the shoreline-change rates. Shoreline change rates can be measured based on differences between shoreline positions through time with available statistical methods. The shoreline change rates are expressed as meters of change along transects per year.

The statistical methods available in DSAS includes Net Shoreline Movement (NSM), Shoreline Change Envelope (SCE), End Point Rate (EPR), Linear Regression Rate (LRR), Weighted Linear Regression Rate (WLR) and Least Median of Squares (LMS). EPR can be calculated by dividing the distance of shoreline movement by the time elapsed between the earliest and latest measurements at each transect. A linear regression rate statistics can be determined by fitting a least-squares regression line to all shoreline points for a particular transect and it is used to express the long-term rates of shoreline change. The net shoreline movement (NSM) reports a distance, not a rate and it is associated with the dates of only two shorelines. It reports the distance between the oldest and latest shorelines for each transect. DSAS merges the individual module calculations, after finishing the shoreline change rate computations; the output is presented as a table in ArcMap.

1.7. Coastal Sediment Transport

Monitoring and understanding of sediment transport is essential due to the adverse effects like siltation of harbours, accumulation of sand bars to create navigational hazards, seasonal blockage of estuaries or degradation of coastal environment. The longshore current plays an important role in transporting the sediments in the surf zone. Sediments are moved alongshore by waves and currents. This longshore transport is a constant process, and large volume of sediments may be transported from one point to another point. Beach material is also derived from erosion of the

coastal formation due to waves and currents, and in some cases, transported onshore by the movement of sediment from deeper water. Clay and silt do not usually settle on beaches because the waves create such turbulence in the water along the shore that, these fine particles are kept in suspension. The net sediment transport is the product of two processes namely (i) the periodic wave induced fluid motion that initiates sediment motion, and (ii) the superimposed currents which transport the sediment set in motion.

1.7.1. Determination of Sediment Distribution using Satellite Data

Remote sensing satellite images provides periodic, integrated, and synoptic views for determination of net direction and distribution of alongshore sediment transport economically, efficiently and quickly (Kunte and Wagle 1993). The penetration depth of electromagnetic (EM) energy is influenced by the material content and/or size of the suspended sediments (Whitelock et al. 1978). Turbid water is more reflective than clear water both in the visible and near infrared regions of the EM spectrum.

1.8. Land Use and Land Cover Mapping

Land cover mapping from multi-spectral remote sensing satellite data is based on spectral differences in land cover (Cihlar et al. 2001). Land cover information is significant in many scientific research fields such as urban land management, urban planning, and landscape pattern analysis, ecology, agriculture, forest, coastal processes and hydrology. Accurate and detailed land cover information derived from remotely sensed satellite imagery by the spatial resolution of the data and number of land cover feature classes identified by their reflectance properties (Comber et al. 2004). If the spatial frequency of land cover is moderate relative to the spatial resolution, then much spatial information will be lost within mixed pixels. Similarly, if the spatial resolution is fine, then high spatial frequency of land cover variation will result in a large number of mixed pixels with minimum loss in spatial information.

Classification techniques are regularly used to extract land cover information from remotely sensed satellite imagery. However, image classification is always a difficult task and the characteristics of the resulting land-cover maps derived from different satellite images are not always the same (Bonnett and Campbell 2002). Multi-temporal remotely sensed data are often used in understanding seasonal variations of land-cover and also in improving the land cover classification accuracy (Schriever and Congalton 1995). Multi-spectral classification is one of the most frequently used methods of information extraction. Multi-spectral classification is performed using variety of algorithms, including hard classification methods using supervised and unsupervised classification, soft classification techniques using linear spectral mixture modelling, fuzzy c-means classifiers, artificial neural networks and support vector machines and hybrid approaches using ancillary (collateral) information.

1.8.1. Classification Techniques

Classification techniques are used to automatically classify all pixels in an image into land cover classes. The actual multispectral classification performs using variety of classification approaches and the main classification algorithms are supervised classification and unsupervised classification.

1.8.1.1. Supervised Classification

In supervised classification, the training sites are selected to classify the image because the spectral characteristics of these training sites are used to train the classification algorithm for ultimate land-cover mapping of the rest of the image. For each training site multivariate statistical parameters (mean, standard deviation, covariance matrix, correlation matrix, etc.) are calculated and every pixel both inside and outside the training site is then evaluated and assigned to the class of which it has the highest likelihood of being a member. In supervised classification, a pixel is assigned to only one class, even though the sensor records radiant flux from a mixture of biophysical materials within the Instantaneous Filed of View (IFOV). Additional

training data are also collected and then applied the classification algorithm to yield a classification map. Three widely used supervised classification algorithms are, Parallelepiped Classifier, Minimum-Distance-to-Means Classifier and Maximum Likelihood Classifier (MLC).

1.8.1.1.1. Parallelepiped Classifier

The parallelepiped classifier considers the range of values in each class training set. This range may be defined by the highest and lowest digital number values in each band and appears as a rectangular area. According to the class range, an unknown pixel is classified in which it lies or the pixel is unknown if it lies outside all regions. The multidimensional analogs of these rectangular areas are called parallelepipeds. This method is a computationally efficient method of classifying remotely sensed data. But due to some parallelepipeds overlap, it is possible that an unknown class pixel might satisfy the criteria of being more than one class. In such cases it is usually assigned to the class for which it meets most of the criteria's.

1.8.1.1.2. Minimum-Distance-to-Means Classifier

Minimum-Distance-to-Means Classifier is commonly used simple computational method. Like parallelepiped method, mean or average spectral value of each class in each band is determined from the training data. To perform a minimum distance classification, the distance from each unknown pixel to each mean vector is calculated using Euclidean distance based on the Pythagorean Theorem. The minimum-distance-to-means strategy is mathematically simple and computationally efficient, but it has certain limitations.

1.8.1.1.3. Maximum Likelihood Classifier

Maximum likelihood Classification (MLC) is based on statistical decision principle to assist in the classification of overlapping signatures and pixels are assigned to the class of highest probability. In this method, data is assumed to be distributed according to a previously defined probability model, for which the parameters are determined from a given training set. Each data point is then classified independently by labeling it as belonging to the class, which is most possible given data, that data has the highest a posteriori probability. These posteriori probabilities are calculated using the Bayesian classification method. To calculate the probability, a multivariate Gaussian distribution with mean vector and covariance matrix is assumed for each class. The maximum likelihood classifier is considered to give more accurate results than parallelepiped classification. The maximum likelihood and Bayes's classifications require many more computations per pixel than either the parallelepiped or minimum-distance classification algorithms.

1.8.1.2. Unsupervised Classification

In an unsupervised classification, the numbers of land–cover types are identified as classes, because of lack of ground reference information or surface features within the scene are not well defined. Unlike supervised classification, unsupervised classification does not require analyst-specified training data. This method used to group the pixels with similar spectral characteristics into unique clusters. The analyst then combines and labels the spectral clusters into feature classes.

1.8.1.3. Accuracy Assessment

Accuracy of the classification basically indicates that what extent a category is correctly mapped on the remotely sensed images with reference to its geographic location on the ground. The classified map is considered as 100 percent accurate, when all the pixels classified in the remotely sensed data display correct geographic position of the various land use and land cover categories on the ground. Accuracy of the classification is estimated using error matrix or confusion matrix or contingency

matrix. Error matrices compare the reference data (represented by the columns of the matrix) with the automated classified data (represented by the rows of the matrix) category-by-category basis. The major diagonal of the error matrix represents the proper land cover categories and nondiagonal elements of the matrix represent errors of omission or commission. The information derived from the error matrix is error of omission (Producer's accuracy) and error of commission (user's accuracy) (Story and Congalton 1986; Lillesand and kiefer 1994; Cambell 2002). The overall accuracy is computed by dividing the total number of correctly classified pixels (sum of the elements along the major diagonal) by the total number of reference pixels. Similarly, the overall accuracy for a particular classified image is calculated by the number of correctly classified pixels in each category by the total number of pixels in the corresponding row or column.

1.8.1.3.1. Producer's accuracy

Producer's accuracy of a particular category is determined by dividing the number of correctly classified pixels in each category (on the major diagonal) by the number of training set (reference) pixels used for the category (the column total). Producer's accuracy measures how well training set pixels of the given cover type are classified. It includes the error of omission, which refers to the proportion of the observed features on the ground that is not classified in the map. The more error of omission leads to lower producer's accuracy.

$$Producer's\ Accuracy = \frac{Number\ of\ correctly\ classified\ pixels\ of\ a\ perticular\ class}{Number\ of\ reference\ pixels\ of\ the\ same\ class} \times 100 \quad (1.8)$$

1.8.1.3.2. User's accuracy

User's accuracy is computed by dividing the number of correctly classified pixels in each category by the total number of pixels that were classified in that category (the row total). User's accuracy measures error of commission and indicates the probability that a pixel classified into a given category actually represents that

category on the ground. The more error of commission indicates lower the user's accuracy.

$$User's\ Accuracy = \frac{Number\ of\ correctly\ classified\ pixels\ of\ a\ particular\ class}{Number\ of\ classified\ pixels\ in\ the\ class} \times 100 \qquad (1.9)$$

1.8.1.3.4. Kappa Coefficient

KAPPA analysis is a discrete multivariate technique used in accuracy assessment (Congalton and Mead 1983) and it yields a K_{hat} statistic (and estimate of KAPPA), is a measure of agreement or accuracy (Congalton 1991). It is a measure of the difference between the actual agreement, between reference data and an automated classifier and the chance agreement, between the reference data and a random classifier (Lillesand et al. 2004). Conceptually, K_{hat} is defined as,

$$K_{hat} = \frac{Observed\ accuracy - Chance\ agreement}{1 - Chance\ agreement} \qquad (1.10)$$

1.9. Scope of the Research Work

Based on the advantages of remotely sensed data, it is widely used in coastal applications to conserve sustainable development of coastal zone management. Monitoring of coastal zones using low contrast satellite images is difficult and loss of information will be the maximum during interpretation of images. To overcome the drawbacks of low contrast satellite images, various contrast enhancement techniques were developed and histogram equalization is an extensively used well-known method. It is possible to improve the quality of the images through histogram equalization based techniques and it can be improved the identification and extraction of features from images for further analysis without loss of information. It is also possible to extract the information of isolated coastal regions from the enhanced images and these enhancement methods offer to develop automatic feature detection from the satellite images. The present study provides the scope to develop contrast

enhancement techniques for accurate study and management of coastal zones using satellite images.

1.10. Objectives of the Study

The main objective of the present study is to develop, HE–based contrast enhancement techniques for remotely sensed satellite images to study coastal applications. Accordingly, the objectives of the present study are;

i. To develop contrast enhancement techniques for satellite images
ii. To apply the developed algorithms for satellite images for
    a. Automatic shoreline detection and analysis
    b. Suspended sediment transport
    c. Land use and land cover assessment

1.11. Study Area

1.11.1. Location of the study area

Mangalore coast, starting from Talapadi in the South to Mulky in the North, in Karnataka State, along the West Coast of India is considered as study area and it lies between 12˚45'-13˚07'N latitudes and 74˚45'-74˚55'E longitude as shown in Figure1.1. The length of the coastline is 40 km and it is oriented along the NNW-SSE direction, width of 5 Km towards offshore and 15 km towards landward covering an area of 800 Km^2 is considered. The climate is tropical and the mean daily temperature recorded so far is 37˚C. The average annual rainfall is 3954 mm of which 87% is received during the southwest monsoon (June to September) (Murthy et al. 1988). In the study area, Netravati and Gurpur rivers join together at Mangalore, whereas Mulky and Pavanje rivers join together at Hejamadi Kodi, before joining the Arabian Sea (Dwarakish

2001). In the study area, strong winds are observed from Southwest and West direction during Southwest monsoon period. Rest of the year winds are mainly from North and East in the forenoons and Westerly or Northwesterly in the afternoons (Dwarakish 2001). The average wind velocity during non-monsoon season varies from 0 to 18 Kmph and 8 to 26 Kmph during monsoon season (Vishwanath 1993). The major rock type is the granite gneiss which is popularly known as peninsular gneiss. Laterities are abundant in the coastal regions and exposed laterites develop a hard crust and are devoid of vegetation as they do not retain any moisture. About 13 km of total length of Mangalore coast have been protected by constructing the seawalls at the places of severe erosion (Dwarakish et al. 2010). The beaches of the coast are low open sandy beaches which are 25 to 100 m in width. The material of the beach is mainly detrital sand and the mean size of it varies from place to place and, the beach material is well sorted sand. For detailed analysis, this study area is further divided into three segments as described in the next sections.

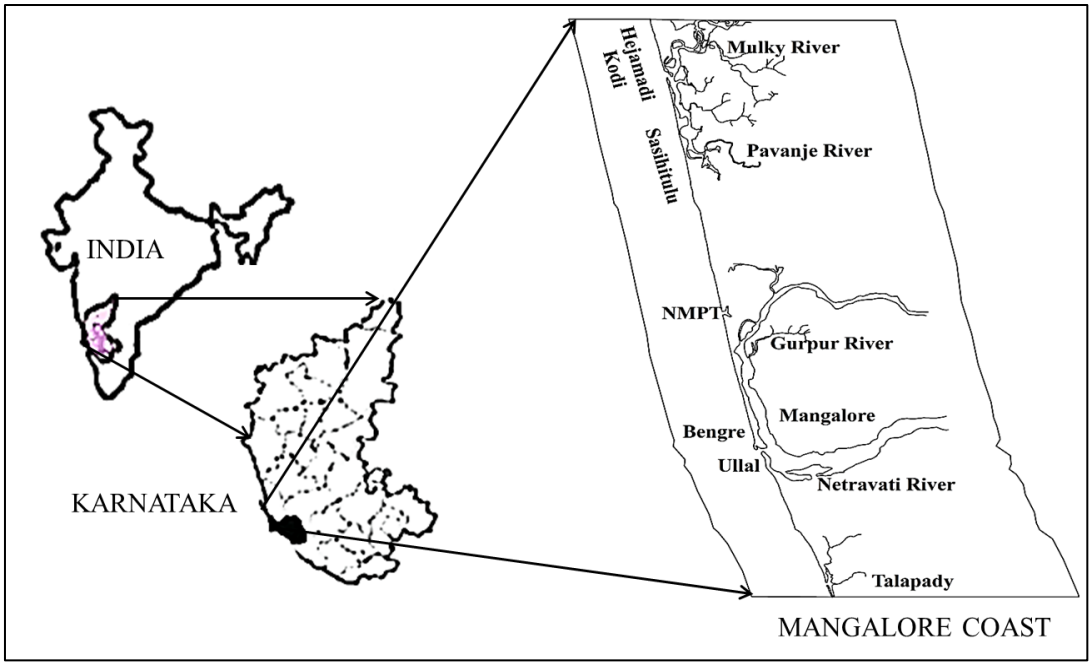

Fig.1.1. Location map of Mangalore Coast

1.11.1.1. Mulky-Pavanje rivermouth area

Mulky-Pavanje rivermouth area is a stretch from Sasihitulu in the South and Hejamadi Kodi in the North along Mangalore Coast, West Coast of India. The rivermouth is located 30 km North of Mangalore, headquarter of Dakshina Kannada district, Karnataka and it lies between 13˚03'00" – 13˚06'00" North latitude and 74˚46'00" - 74˚48'00" East longitude as shown in Figure 1.2. The rivermouth is formed by Mulky and Pavanje rivers, which originate from foot hills of the Western Ghats, flows westward takes almost 90˚ bend near the coast then runs parallel to the coast either northward or southward, before joining the Arabian Sea and the total stretch is 5400 m and 1850 m respectively. Sasihitulu at South and Hejamadi Kodi at North are two active submerged sand spits attached to mainland developing infront of the confluence of rivermouth, which is approximately 200 m. The annual discharge from Mulky and Pavanje rivers is 1253 Mm^3 and 619 Mm^3 respectively (Nagaraj and Dwarakish 2011).

Total 6 km length of coastline including rivermouth and 5 km width (1 km offshore and 4 km landward from shoreline) covering an area of 30 km^2 is considered as a study area to predict shoreline changes in and around the rivermouth. The rivermouth is unstable because of strong longshore sediment transport, high monsoonal river flow and sediment transported from the shelf region. The position of the rivermouth is shifted towards South during 1973 and 1988, resulted in increase in length of Hejamadi Kodi Sand Spit and reduction in length of Sasihitulu Sand Spit.

1.11.1.2. Netravati-Gurpur rivermouth area

Netravati-Gurpur rivermouth area is a stretch from Talapady in the South and Thannirbhavi beach in the North along Mangalore Coast, West Coast of India. The study area lies between 12˚45'26"–12˚53'25" North latitude and 74˚47'00"-74˚53'00" East longitude as shown in Figure 1.3. Netravati and Gurpur rivers are also originate in the Western Ghats, flows westward, takes almost 90˚ turn near the cost and then

flows parallel to the coast either southward or northward, before joining the Arabian Sea at Mangalore (Dwarakish 2001). Bengre at North and Ullal at South are two active submerged sand spits attached to mainland developing infront of the confluence of rivermouth. From the U.S. Naval Oceanographic Charts, it is observed that the current pattern in the West Coast of India is from North to South with velocities ranging from 0.11 to 0.40 m/s during February to September and South to North with velocities of 0.11 to 0.30 m/s for the remaining period. At Netravati-Gurpur river mouth, during the monsoon season, the maximum speed of surface and bottom currents are 98 cm/sec and 104 cm/sec respectively during flood tide and 130 cm/sec and 108 cm/sec respectively during ebb tide. During pre-monsoon season, the flood currents are slightly stronger than the ebb currents.

Total 16 km length of coastline including rivermouth and 5 km width (1 km offshore and 4 km landward from shoreline) covering an area of 80 km^2 is considered as a study area to predict shoreline changes in and around the rivermouth. Netravati river discharges lot of sediments compared to Gurpur river into Arabian Sea. The Ullal sand spit was decreased by 0.19 km^2 between 1988 to 1993, whereas an increase of 0.02 km^2 was observed between 1993 to 1998. The Bengre spit was also decreased by 0.04 km^2 between 1998 to 1993 and then increased by 0.03 km^2 between 1993 to 1998 (Dwarakish 2001). The Netravati-Gurpur rivermouth was shifting from South to North (1905 to 1979; 1953 to 1968) and North to South (1949 to 1953). After constructing the two breakwaters at Netravati-Gurpur rivermouth during 1994, the shifting rivermouth is now arrested.

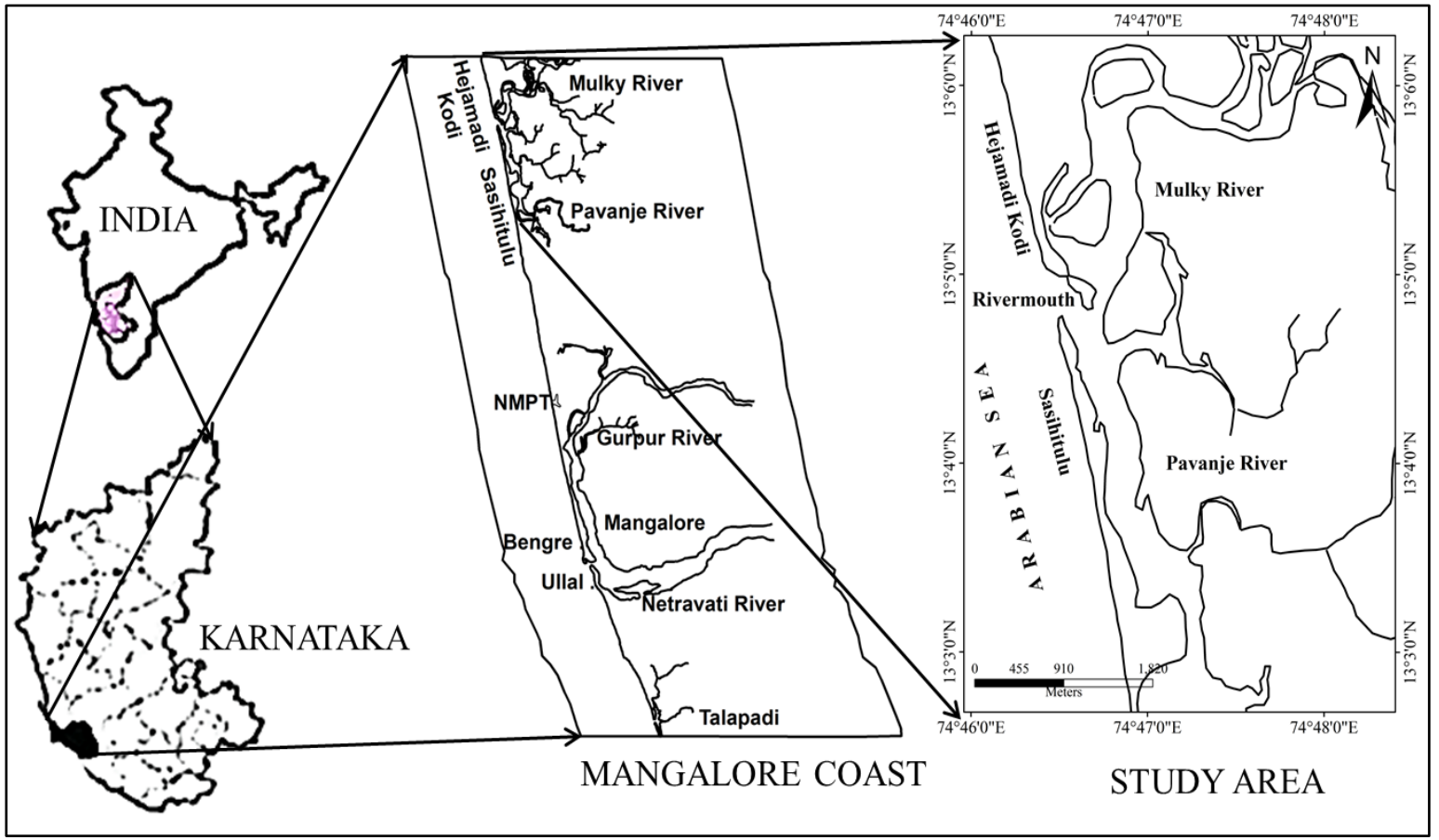

Fig.1.2. Location map of Mulky-Pavanje rivermouth area

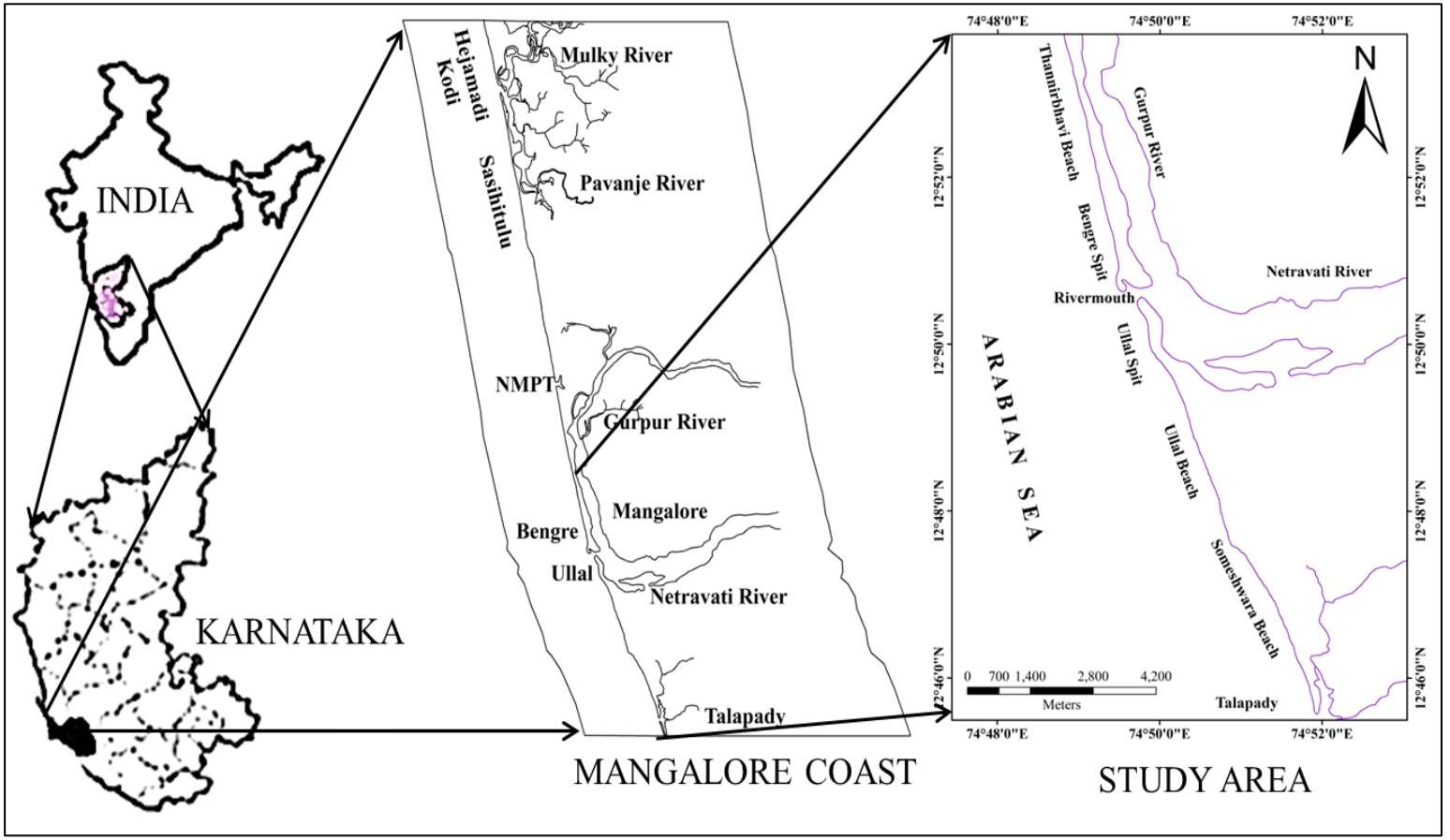

Fig.1.3. Location map of Netravati-Gurpur rivermouth area

1.11.1.3. New Mangalore Port Trust (NMPT)

New Mangalore Port Trust (NMPT) is all weather port, situated at about 10 km North of Mangalore. The study area lies between 12˚53'50"–13˚02'00" North latitude and 74˚45'00"-74˚55'00" East longitude as shown in Figure 1.4. NMPT is having two breakwaters on either side of approach channel with length of 770 m and extended up to -6 m contour. Approach channel has a length of 7.5 km and a base width of 245 m with a depth of -15.4 m below the chart datum (Dwarakish 2001). It is a lagoon type of harbor artificially created by dredging. Sedimentation in the approach channel is more than that in the lagoon (Dattatri and Kamath 1997). New Mangalore Port is one of the eleventh major ports of India started its operations on 11th January 1975. Being India's ninth largest cargo handling port, Mangalore port is well connected with other parts of the country by all means of transportation. Maximum hinterland of NMPT is covered with various industries, such as Mangalore Chemicals and Fertilizers (MCF), Kudremukh Iron Ore Company Limited (KIOCL), Kudremukh Iron & Steel Company Limited (KISCO), Mangalore Refinery and Petrochemicals Limited (MRPL), BASF India Limited and Udupi Power Corporation Limited (UPCL) etc.

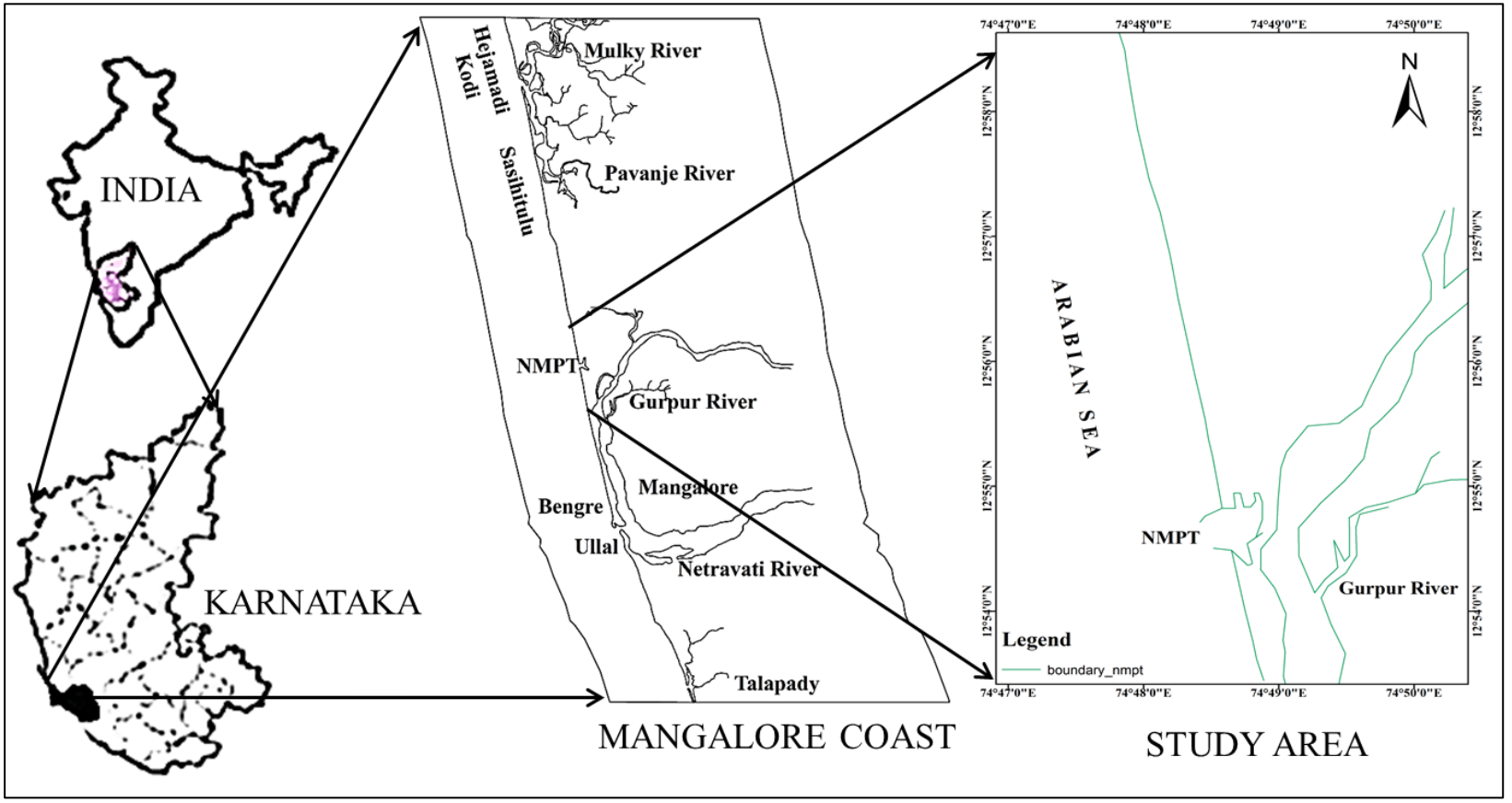

Fig.1.4. Location map of New Mangalore Port Trust (NMPT) area

1.12. Organization of the thesis

The present thesis report is organized in six chapters. Chapter 1 provides brief introduction of remote sensing, digital image processing and image enhancement techniques. It also covers coastal processes, sediment transport and land use and land cover mapping. In addition to these, objectives of the present study and description of selected study area are also briefed. A detailed literature review of all the aspects of identified objectives for the present study is presented in Chapter 2. Chapter 3 demonstrates the comparative analysis of histogram equalization based contrast enhancement techniques through image quality measures. Chapter 4 describes the methodology and data products, which includes the procedure of developed algorithms and their analysis using various data products. Chapter 5 demonstrates the results obtained from developed algorithms and corresponding discussion as per the objectives of the present study. Finally, the concluding technical remarks of the research and recommendations for the future work are summarized in Chapter 6.

CHAPTER 2
LITERATURE REVIEW

2.1. General

Coast, the dynamic junction of ocean, atmosphere and land, undergoes continuous geomorphologic changes in response to natural forces and human activities (Komar 1976; Bruun 1985; Horikawa 1978). Coastal zones are most complex ecosystems with a large number of biotic and abiotic resources and it is a transition zone of the sea and the land with frequent human activities. These are exposed to a series of dynamic natural processes like coastal erosion, sediment transport, environmental pollution, and coastal development that usually causes changes in long and short-term spans. Coastal zones are major socio-economic environment in worldwide and these coastal changes impacts on loss of life and property, security of harbors, change of the coastal socio-economic environment, and decrease of coastal land resources. So, coastal zone monitoring is an important task in national development and environmental protection, in which, extraction of shoreline to estimate shoreline erosion and accretion, sediment transport, flooding and sea level changes which continuously modify the shoreline are some of the prominent activities of coastal zone management. Both conventional and remotely sensed data can be used to study coastal processes and advancements in remote sensing and geographical information system (GIS) techniques are improving the quality of the coastal geographical studies. Many digital image processing techniques were developed to get efficient results using satellite images. Contrast enhancement techniques were providing good contrast between spectral information of one object to another object, which is helpful in identifying the features from satellite images. Several histogram equalization, edge detection, principal component analysis, classification based methods were developed to study coastal processes. In this chapter, various digital image processing techniques

related to automatic shoreline detection, sediment transport and land use and land cover mapping are discussed in detail.

2.2. Contrast Enhancement Techniques

Contrast enhancement is an important phase in image processing for both human interpretation and computer vision. It is widely used as a pre-processing step in speech recognition, texture synthesis, and many other image/video processing applications (Wahad et al. 1998; Pizer 2003; Pei et al. 2004; Torre et al. 2005). Generally, remote sensors record reflected and emitted radiant flux exiting from the Earth's surface materials. Ideally, one material would reflect a tremendous amount of energy in a certain wavelength, while another material would reflect much less energy in the same wavelength. This would result in low contrast between the two types of materials when recorded by a remote sensing satellite sensor system. Unfortunately, different materials often reflect similar amounts of radiant flux throughout the visible, near-infrared, and mid-infrared portion of the electromagnetic spectrum, resulting in a relatively low contrast image (Jensen 1996). The low sensitivity of the detectors also creates low-contrast image because of insufficient radiometric sensitivity of a detector to record the full range of intensities of reflected or emitted energy originating from the earth surface. Contrast enhancement is essential to overcome these drawbacks from remotely sensed images for further usage in applications. Histogram Equalization (HE) is commonly used non-linear contrast enhancement technique.

2.2.1. Histogram Equalization

Histogram Equalization (HE) is a well-known, simple and an effective indirect contrast enhancement technique which distributes the pixel values uniformly. It is a global operation and hence, it doesn't preserve the brightness preservation. HE has significant drawback of changing the brightness globally, which resulted in either

under-saturation or over-saturation of important regions in the image. HE stretched the contrast of high histogram regions and compressed the contrast of low histogram regions, and introduced unwanted artefacts in the image (Sengee and Choi 2008). As a consequence, when the object of interest in an image, occupies only a small portion of the image, the object was not be successfully enhanced by histogram equalization. HE method also extremely pushed the intensities towards the right or the left side of the histogram, causes level saturation effects. It does not preserved the brightness of the input, where preserving the input brightness was essential to avoid the generation of non-existing artefacts in the output image. Narrow or small range sections were not enhanced significantly by HE method (Ibrahim and Kong 2007). Due to these reasons, for the implementation of contrast enhancement, it was advised that the loss of intensity values by the histogram processing should be minimized in the output image. To overcome these drawbacks several HE based contrast enhancement techniques were developed. Based on modification of histogram, the HE-based techniques were categorized into Bi-Histogram Equalization (Bi-HE) and HE-based methods, Multi-Histogram Equalization (Multi-HE) methods and Clipped Histogram Equalization (CHE) methods.

2.2.1.1. Bi-Histogram Equalization based methods

Bi-Histogram Equalization method separate the input image histogram into two sub-histograms based on statistical functions and each sub-histogram is equalized independently. Equalized sub-histograms are transformed using transformation function based on cumulative density function of histograms.

Brightness Preserving Bi-Histogram Equalization (BBHE), first mean based separation of histogram was proposed by Kim (1997) to preserve the mean brightness of the input image. BBHE decomposed the input image histogram into two sub-histograms based on its mean value. While the contrast of the image was enhanced, it

preserved the brightness of an image to some extent and showed better results than HE. Similar to BBHE, Wang et al. (1999) presented Dualistic Sub-Image Histogram Equalization (DSIHE), using median value instead of mean value to separate the input histogram and got better brightness preservation than BBHE and HE. BBHE and DSIHE were not much suitable for images, which required higher degree of brightness preservation to avoid annoying artefacts.

Chen and Ramli (2003) proposed Minimum Mean Brightness Error Bi-Histogram Equalization (MMBEBHE), an extended method of BBHE technique. In MMBEBHE, the input histogram was divided based on threshold value, which was derived from minimum Absolute Mean Brightness Error (AMBE). This method was allowed maximum level of brightness preserving in Bi-Histogram Equalization to avoid annoying artefacts and unnatural enhancement due to excessive equalization. But, MMBEBHE showed poor brightness preserving and enhancement, where the images that required far more brightness preservation and it failed to control the over enhancement of the image. Bi-Histogram Equalization with Neighbourhood Metric (BHENM) was introduced by Sengee et al. (2010), which divided the large histogram bins that cause washout artefacts into sub-bins using neighbourhood metrics, and the histogram of the original image was separated into two sub-histograms based on the mean of the histogram. Then, sub-histograms were equalized independently using refined histogram equalization. Zuo et al. (2012) proposed Range Limited Bi-Histogram Equalization (RLBHE), which divided the input histogram into two independent sub-histograms by a threshold value that minimizes the intra-class variance. This was carried out to effectively separate the objects from the background and achieved fair contrast enhancement and brightness preservation. RLBHE was easy to implement in real-time processing applications. Bi-Histogram Equalization (Bi-HE) methods enhanced the image contrast significantly and preserved the brightness to some extent, but it introduced undesirable artefacts (Khan et al. 2012).

2.2.1.2. Histogram Equalization based methods

Wang and Ye (2005) introduced Brightness Preserving Histogram Equalization with Maximum Entropy (BPHEME), a novel extension of HE method, to maximize the target histogram's entropy, under the constraints of brightness using histogram transformation by maximizing the probability densities subject to constraints. Jyoti and Rawat (2007) applied BPHEME to enhance and brightness preservation of underwater, ground, aerial satellite images. Sengee and Choi (2008) introduced Brightness Preserving Weight Clustering Histogram Equalization (BPWCHE) to enhance image visualization and brightness preservation by assigning each non-zero bin in the original image's histogram to a unique cluster, and computed the weight of each cluster. Cluster weight, weight ratio and the width of two neighbouring clusters were used to merge pairs of neighbouring clusters to reduce the number of clusters. Transformation function for each cluster's sub-histogram was computed using Global Histogram Equalization (GHE) method and sub-histogram's gray levels were mapped to the output image.

To eliminate the domination of higher histogram components on lower histogram components and to control the amount of grey level stretching for significant enhancement of the image features, Demirel et al. (2010) proposed Satellite Image Contrast Enhancement using Discrete Wavelet Transform (DWT) and Singular Value Decomposition (SVD). SVD of the LL sub-band was improved the contrast of the image, but this method tends to distort the image details in low and high intensity regions. The algorithm Two-Dimensional Histogram Equalization (2DHE), which utilized contextual information around each pixel to enhance the contrast of an input image was proposed by Celik (2012) and it was based on the observation that contrast in an image can be improved by increasing the gray-level differences between each pixel and its neighbouring pixels. Grey-level differences were equally distributed over the entire input image for equalization and the final mapping between input grey-

levels and output grey-levels was achieved by considering 2D input and target histograms. Humied et al. (2012) proposed automatic contrast enhancement method by combining two techniques, HE and Fast Gray-Level Grouping (FGLG). The original histogram of a low contrast image was segmented into two sub-histograms according to the location of the highest amplitude of the histogram components, and achieved contrast enhancement by equalizing the left segment of histogram components using HE and right segment was equalized using FGLG. This method was fully automated and showed superior contrast enhancement.

2.2.1.3. Multi-Histogram Equalization

In order to enhance contrast, brightness preservation and improve natural quality of the images, multi-histogram equalization techniques was used to decompose the input image histogram into several sub-histograms, and then applied the traditional histogram equalization process to each of the sub-histogram.

Wongsritong et al. (1998) proposed Multi-Peak Histogram Equalization with Brightness Preserving (MPHEBP) to improve the brightness preservation of the image. The input histogram was smoothened and divided based on the local maxima. MPHEBP was preserved brightness better than BBHE. Recursive Mean-Separate Histogram Equalization (RMSHE) proposed by Chen and Ramli (2003) divided the input histogram into two sub-histograms, based on its mean before equalizing them independently. This separation was done one time in BBHE, but in this technique new histograms (separated) were further divided based on their mean value. It was analyzed mathematically that, mean brightness value of the output image would meet to the mean brightness value of the input image as the number of recursive mean separations increases. In order to achieve higher brightness preservation, this model was proposed to perform the mean separation recursively and separated the resulted histograms again based on their respective means. Similar to RMSHE, Recursive Sub-Image Histogram Equalization (RSIHE) was proposed by Sim et al. (2007) to

separate the input histogram based on a gray level with median, but RMSHE used mean-separation and both the methods shared the same characteristics in equalizing the sub-histograms. Both methods were provided good brightness preserving because of multi separation of histogram, but for bright images these methods lead to over enhancement.

Wadud et al. (2007) introduced Dynamic Histogram Equalization (DHE) similar to Multi-peak Histogram Equalization with Brightness Preserving (MPHEBP) method. DHE smoothened the input histogram using one dimension smoothing filter and divided histogram based on the local minimum values. Each section was mapped into a new dynamic range before equalizing the sub-histograms. An extension method of MPHEBP and DHE, Brightness Preserving Dynamic Histogram Equalization (BPDHE) was proposed by Ibrahim and Kong (2007). BPDHE identified the local maximum values from filtered histogram by Gaussian filter and mapped each partition into a new dynamic range based on local maximums. Each partition was equalized independently and normalized for image brightness. Recursively Separated and Weighted Histogram Equalization (RSWHE) introduced by Kim and Chung (2008) to enhance the image contrast and preserved the brightness using three modules, such as, histogram segmentation, histogram weighting and histogram equalization modules. There were two different versions of the RSWHE. RSWHE-M performed the mean-based segmentation and RSWHE-D performed the median-based segmentation. RSWHE-M method was found to be better than the RSWHE-D for brightness preserving and contrast enhancement. Wadud et al. (2008) proposed Spatially Controlled Histogram Equalization (SCHE). In spite of processing the whole histogram with the transformation function at a time, it divided the histogram into a number of sub-histograms until it ensured that no dominating portion was presented in any of the newly created sub-histograms. The entire technique was divided into three parts, partitioned histogram, allocated grey level (GL) ranges for

each sub-histogram and applied HE on each of them and it performed better in increasing contrast without introducing any artefacts.

Menotti et al. (2007) proposed Minimum Within-Class Variance Multi-Histogram Equalization (MWCVMHE) and Minimum Middle Level Squared Error Multi Histogram Equalization (MMLSEMHE) techniques to yield images with natural contrast enhancement. MWCVMHE partitioned the input histogram into multiple sub-histograms by minimizing within-class variance and then applied histogram equalization in each sub-histogram separately. MMLSEMHE used Otsu threshold technique to select threshold value and equalized each sub-histogram individually. MMLSEMHE was computationally more complex because it estimated optimal number of sub-histograms from all possible sub-histograms to minimize certain discrepancy functions (Sengee and Choi 2008). Both the methods preserved the brightness to a maximum extent but the contrast enhancement was less intensive. Kim and Chung (2008) introduced Recursively Separated and Weighted Histogram Equalization (RSWHE) to enhance the image contrast as well as to preserve the image brightness. This method segmented the input histogram into two or more sub-histograms recursively based on the mean or median of the image. Also the resulted sub-image histograms were changed through a weighting process based on the power law function. RMSHE and RSIHE were similar to RSWHE in terms of recursive histogram segmentation, but they did not execute the histogram weighting function as in RSWHE. RSWHE-M and RSWHE-D were two different implementations of RSWHE. RSWHE-M performed the mean-based segmentation and RSWHE-D performed the median-based segmentation. RSWHE-M method was better than RSWHE-D for brightness preserving and contrast enhancement. Wadud et al. (2008) presented Spatially Controlled Histogram Equalization (SCHE) by dividing the input histogram into a number of sub-histograms until it ensures that no dominating portion was present in any of the newly created sub-histograms. Then a dynamic gray level (GL) range was allocated for each sub-histogram to which its gray levels were

mapped. This total dynamic range of gray levels of the output image was distributed among the sub-histograms based on their dynamic range in the input image and cumulative distribution function (CDF) of histogram values.

Sheet et al. (2010) introduced Brightness Preserving Dynamic Fuzzy Histogram Equalization (BPDFHE), a modification of BPDHE technique using fuzzy histogram and partitioned the histogram into multiple sub-histograms based on local maxima. Every valley portion between two consecutive local maxima forms a partition. When the dynamic equalization of these partitions was performed, the peaks of the histogram did not get remapped and resulted in a better preservation of the mean image brightness while increasing the contrast. Khan et al. (2012) proposed Weighted Average Multi Segment Histogram Equalization (WAMSHE), which divided the smoothed histogram into multiple segments based on optimal thresholds and equalized each segment by histogram equalization. WAMSHE showed better brightness preserving and contrast enhancement among Multi-histogram equalization methods and also aided to reduce the noise present in the image. Huang and Yeh (2013) introduced contrast enhancement for preserving mean brightness without losing image features by segmenting the histogram with multiple threshold operation and equalized each sub-histogram using HE. Image processed by Multi-HE methods preserved the image brightness and prevented undesirable artefacts but not significantly enhanced the contrast (Khan et al., 2012).

2.2.1.4. Clipped Histogram Equalization

Generally, Histogram equalization stretched the contrast of the high histogram regions, and compressed the contrast of the low histogram regions (Sengee and Choi 2008). As significance, when the object of interest in an image occupied only a small portion of the image, this object was not successfully enhanced by histogram equalization. This method also extremely pushed the intensities towards the right or

the left side of the histogram, caused level saturation effects. Clipped Histogram Equalization (CHE) methods were used to restrict the enhancement rate. Enhancement from the histogram equalization was depended on cumulative density function *c(x)* and the enhancement rate was proportional to the rate of *c(x)*. Clipped Histogram Equalization (CHE) was far more effective for contrast enhancement than the existing HE-based methods.

Yang et al. (2003) proposed Contrast Enhancement using Histogram Equalization with Bin Underflow and Bin Overflow (BUBO), a simple enhancement rate control mechanism for the histogram equalization. The gradient of the mapping function was controlled by putting constraints on the probability density function (PDF) with the bin underflow (BU) and bin overflow (BO). It was provided the rate of enhancement from none to the full HE with a single parameter. With the enhancement rate control mechanism variable, the HE was used to perform image processing tasks such as black/white level stretch or automatic brightness control as well as variable contrast enhancement. Wang et al. (2006) presented a Self-Adaptive Contrast Enhancement algorithm based on Plateau Histogram Equalization (SAPHE) to enhance the main objects and suppress the background for infrared images. SAPHE, the input histogram was filtered by using median filter to remove empty bins. The local maximum and global maximum values were identified from filtered histogram and mean of local and global maximum values were used to calculate plateau threshold value. By eliminating median filter from SAPHE, Kong et al. (2009) proposed modified SAPHE (MSAPHE) to enhance microscopic images. SAPHE was failed to detect any local peaks in the image and MASAPHE was overcome this problem. Gain-Controllable Clipped Histogram Equalization (GC-CHE), a combination of existing bi-histogram equalization (BHE) and recursive mean-separate histogram equalization (RMSHE) methods was developed by Kim and Paik (2008) to overwhelm the limitation of the existing CHE method. GC-CHE controlled noise and preserved the original brightness, but it sacrificed the amount of contrast. In GC-CHE method, first

clipping level was determined and based on this level the input histogram was clipped. The clipped portion was then re-distributed to the entire dynamic range by locally regulated the clipping gain. While enhancing the contrast of a low light-level image adjusted the contrast elevation ration to solve the noise amplification problem according to the input image and compensated contrast using the gain control method. Bi-Histogram Equalization Plateau Limit (BHEPL) as the fusion of the BBHE and clipped histogram equalization was proposed by Ooi et al (2009). Similar to BBHE, the BHEPL decomposed the input image into two independent sub-histograms to maintain the mean brightness and these sub-histograms were clipped by using the plateau limit or clipping limit or threshold limit as the mean of the number of intensity occurrence. The decomposed sub-histograms were equalized independently. This method avoided the excessive enhancement and over amplification of noise in the image. Ooi et al. (2010) introduced clipping based Quadrants Dynamic Histogram Equalization (QDHE), which separated the histogram into four sub-histograms based on the median of the input image. Then, the resultant sub-histograms were clipped according to the mean of intensity occurrence of the input image before new dynamic range was assigned to each sub-histogram and then equalized individually. QDHE was most robust method to extract the details of the low contrast images. Liang et al. (2012) proposed Double Plateaus Histogram Equalization (DPHE), an improvement of plateau histogram equalization for infrared image enhancement. The upper and lower threshold values were calculated by using local maximum values. The upper threshold was utilized in the algorithm for preventing over-enhancement of background noise with typical gray levels, and the lower threshold was set for protecting detailed information with fewer pixels from being combined. Upper and lower thresholds according to local maximum of non-zero histogram and the minimum gray level interval, this algorithm was efficient for enhancing infrared images in various scenes in real time. Singh and Kapoor (2014) introduced Exposure based Sub-Image Histogram Equalization (ESIHE) by clipping the histogram based on threshold value and divided the clipped histogram into two sub-histograms. Sub-

histograms were equalized using HE and equalized sub-histograms were combined into one image.

2.2.1.5. Summary

Bi-HE methods were used to enhance the image contrast considerably and preserve the brightness to some extent by introducing undesirable artefacts. Decomposition of image histogram into several sub-histograms, Multi-HE methods showed better brightness preservation and prevented undesirable artefacts but not showed any significant contrast enhancement. CHE methods provided better brightness preservation without introducing any artefacts by clipping the histograms through threshold values and produced substantial contrast enhancement. CHE methods were also controlled the over-enhancement in the image and provided natural contrast enhancement.

2.3. Automatic-Shoreline Detection and Analysis

The extraction of shoreline is useful for several applications like coastal processes, coastline change detection and coastal zone management, but this task is difficult, time consuming, and sometimes impossible for entire coastal system when using traditional ground survey techniques (Cracknell 1999). Due to the preference and huge effort involved in manual detection, quite a few automatic shoreline detection methods were proposed. Advanced remote sensing and geographical information system (GIS) techniques overcome these difficulties in detecting shoreline position and shoreline change analysis. A number of satellite image processing techniques were developed to extract shoreline and change detection analysis such as, image enhancement, multi-temporal data classification and comparison of two independent land cover classifications, density slice using single or multiple bands, and multi-spectral classification, both supervised and unsupervised (like ISODATA, Principle

Component Analysis (PCA), Tasseled Cap, NDWI) (Mas 1999; Frazier and Page 2000; Ryu et al. 2002; Braud and Feng 1998; Kuleli 2010; Kuleli et al. 2011; Zheng et al. 2011; Bouchahma and Yan 2012). Along with image classification methods, various thresholding based techniques were also proposed (Bayram et al. 2008; Jishuang and Chao 2002; White and Asmar 1999; Yamayo et al. 2006). In addition to these image processing algorithms such as pre-segmentation, segmentation and post-segmentation were proposed for automatic extraction of coastline from remotely sensed images (Liu and Jezek 2004; Mason and Davenport 1996; Di et al. 2003).

Lee and Jurkevich (1990) proposed a continuous shoreline detection method using edge detection supported by an edge-tracking algorithm from SEASAT Synthetic Aperture Radar (SAR) image, but achieved less shoreline positional accuracy. Ryan et al. (1991) employed image segmentation method and tested the method on several small portions (256X256) of scanned US Geological Survey (USGS) aerial photographs. Manson and Davenport (1996) extracted coastline using a speckle sensitive edge detector and contrast ratio filter (Touzi et al. 1988) with an active contour model and applied extracted shoreline to several full scene European Remote Sensing Satellite (ERS)-1 SAR images.

Sohn and Jezek (1999) introduced locally adaptive thresholding based image segmentation approach for automatic coastline mapping and applied to both ERS-1 SAR and Satellite Probatoire d'Observation de la Terre (SPOT) images. By dividing the image into homogeneous regions using mean shift segmentation method Di et al. (2003) extracted shoreline from PAN and XS IKONOS images. Yu and Acton (2004) proposed an automated detection of coastline with polarimetric filtering, Speckle Reducing Anisotropic Diffusion (SRAD), Instantaneous Coefficient of Variation (ICOV) edge detector and watershed segmentation algorithm for polarimetric SAR imagery. This method eliminated undesired boundary segments and delineated true coastlines.

By integrating canny edge detector and locally adaptive thresholding methods, Liu and Jezek (2004) presented an automatic shoreline extraction method from satellite images and applied to SAR and Landsat 7 ETM+ images. High positional accuracy of the coastline was one of the advantages of this method. Kuleli (2010) used band ratio technique for Landsat TM and ETM, and ISODATA classification methods for MSS band to extract coastline of Mediterranean Coast in Turkey. Zheng et al. (2011) extracted shoreline by using Normalized Difference Water Index (NDWI) threshold method and Object-Oriented Methods to study shoreline changes of Bohai Bay West Coast of Tianjin. Object-Oriented Method segmented the image into a set of mean image with certain logic and described the objects with a set of characteristics. An automatic outlining of shoreline using segmentation algorithms that evaluate Top of the Atmosphere (TOA) reflectance of Landsat satellite images was developed by Kuleli et al. (2011).

Bouchahma and Yan (2012) applied threshold segmentation (Otsu 1979) on NDWI images to separate the land from sea and the shoreline was outlined by using canny edge detector (Canny 1986) from the segmented Landsat TM image to study shoreline changes on Djerba Island of Tunisia. With grey level threshold segmentation, edge enhancement and fractal dimension methods, Dan et al. (2012) mapped shoreline changes of Hangzhou Bay from Landsat MSS/TM remote sensing images. Pardo-Pascual et al. (2012) proposed a sub-pixel automatic shoreline extraction algorithm, together with a high-precision image registration method from Landsat TM and ETM+ images.

2.3.1. Automatic-Shoreline Detection using Remote Sensing

A variety of airborne, satellite, and land-based remote sensing techniques are generally available to the coastal researchers, and are classified into three categories, such as ground surveying, modern altimetric technology and image measurement

(Chen and Rau 1998). Ground surveying techniques provide high accuracy, but labour intensive and more time consuming. Altimeter technology which used radar altimeters or laser altimeters had high positional accuracy, but data from these detectors are not available regularly. Image measurement technology, airborne imagery provides ample pictorial information, but, the photogrammetric imagery is costly because, this technology includes cost of data acquisition and data reduction. Satellite remote sensing due to its large ground coverage with a revisit capability, high resolution, synoptic and multi-spectral data availability, is a good alternative for regular shoreline change detection. The applicability of satellite images for coastal zone monitoring becomes more promising because of enhanced spatial and temporal resolutions of satellite images.

Lee and Jurkevich (1990) and Niedermeier et al. (2000) mapped shorelines from SEASAT Synthetic Aperture Radar (SAR) and Kumar et al. 1992; Bhat and Subramanya 1993; Gowda et al. 1995; Prithviraj 1995 and Dwarakish et al. 1998 used Indian Remote Sensing Satellite (IRS)-1A/1B images for shoreline change detection and analysis. Kumar et al. 1992 and Frihy et al. 1994, 1998 mapped shoreline using Landsat MSS and TM data. Mason and Davenport (1996) extracted coastline from first European Remote Sensing Satellite (ERS-1) SAR image and Sohn and Jezek (1999) used ERS-1 SAR and Satellite Probatoire d'Observation de la Terre (SPOT) images to extract shorelines. Di et al. (2003) outlined shoreline from PAN and XS IKONOS and Liu and Jezek (2004) delineated coastline from SAR and Landsat 7 ETM+ images. Yu and Acton (2004) Polarimetric SAR images and Maiti and Bhattacharya (2009) Landsat TM and ETM+ and ASTER images were used to demarcate shorelines. Kuleli (2010) and Kuleli et al. (2011) used Landsat TM and ETM+ images. Dan et al. (2012) mapped shoreline changes of Hangzhou Bay from Landsat MSS/TM remote sensing images and Pardo-Pascual et al. (2012) extracted shorelines from Landsat TM and ETM+ satellite images.

2.3.2. Shoreline Change studies related to Mangalore Coast

The rivermouth changes along Mangalore Coast are natural and cyclic in nature. The sand spits on either side of the rivermouth are in continuous movements and this would result in a deposition and growth of one sand spit and corresponding erosion on the opposite sand spit. Due to heavy discharge from Netravati river compared to Gurpur and waves from Southwest direction during SW monsoon, sand deposited on Bengre spit (Northern sector). Also, the Netravai-Gurpur rivermouth was shifted from South to North during 1905 to 1949 and 1953 to 1968 and from North to South during 1949 to 1953 (Dwarakish 2001). Due to the construction of seawall in 1984 along the Bengre sand spit, the erosion near tip of the spit has ceased and sand started deposited on Bengre spit (Hegde and Ravindra 2000; Bannur et al. 1991). The erosion along the Ullal sand spit prevented due to construction of seawall in 1987 along the shoreline (Hegde and Ravindra 2000). To arrest the shifting tendency of rivermouth, two breakwaters had been constructed at rivermouth during 1991-1994. In the beginning of breakwaters constructed, there were no changes neither on the Ullal side nor on the Bengre side but large amount of sand deposited later on the Bengre spit. Ullal sand spit area was decreased between 1988 and 1993 and increased between 1993 and 1998.

Manavalan et al. (1996) studied shoreline changes of Netravati-Gurpur as well as the Mulky-Pavanje rivermouths using the IRS-IC PAN (1996) and IRS-IA LISS II (1998) and stated that the Bengre spit was more stabilized and widened, while the deposition on the Ullal spit was less. Nagaraj and Dwarakish (2011) stated that during 1998-2003, there was slight erosion on Ullal spit and accretion on Bengre spit, however no appreciable change in confluence width of rivermouth was observed during this period.

Mulky-Pavanje rivermouth shifted towards North during 1973 -1988 and the length of Hejamadi Kodi spit has reduced and the length of Mulky spit has increased (Dwarakish 2001). After 1992, Hejamadi Kodi spit, northern part and Sasihitulu spit, southern part were stabilized due to construction of river bank protection works on Hajamadi Kodi spit. Based on long-term rivermouth study between 1912 and 2011, Nagaraj and Dwarakish (2011) concluded that the Mulky-Pavanje rivermouth almost stabilized and net volume of sand deposition was more than the net erosion and this phenomenon shows cyclic behavior.

2.3.3. Summary

Most of the automatic shoreline detection techniques were based on edge detection, classification of the land and water regions, segmentation and band fractioning. These automatic shoreline extraction methods classified the mixed pixels as sea or land, and these methods are not used to monitor small changes in the shoreline unless high resolution images were used. Edge detection methods or edge template operations were highlight and locate the shoreline using spatial differentiation, and` segmentation was generally partition the image into the land and water regions. In automatic shoreline extraction process, general-purpose edge detection and image segmentation techniques were not adequate, because of lack of consistency in earth surface features and insufficient intensity contrast between the land and water regions. This increases the complexity in separating the shoreline edges from the edges of other objects. Considerable amount of contrast exists between the land and water masses generate continuous and clear shoreline.

2.4. Suspended Sediment Transport using Satellite data

Coastal areas are potential zones of marine resources for a country like India which has around 7500 km of coastline. Oceanic water circulation dynamics along the coast

plays an important role in understanding the numerous physical, chemical and biological processes in nearshore operations (Clark 1995; Tang et al. 2002). The study of suspended sediment is an ecological interest as sediment comprises various inorganic and organic substrates and becomes the main substratum for biogeochemical processes. It also affects the penetration of light, transport of nutrients, shoreline morphology and other coastal processes. Estimating suspended sediment concentration (SSC) over large oceanic areas using in-situ sampling is a lengthy, expensive, and time-consuming process. In contrast, remotely sensed spectral radiant energy measured by satellite sensors provides an alternate, synoptic, speedy, and economic approach for assessing the SSCs in oceans, lakes, rivers and coastal waters (McKim et al. 1984; Curran and Wilkinson 1985). However, efficient algorithms are required to convert radiance or reflectance values to estimate water constituents. In sediment dominated coastal waters, refined algorithms are particularly needed to estimate the suspended particulate concentrations accurately from the remotely sensed ocean color data (Robinson et al. 1998; Moore et al. 1999). The colour of seawater depends on the relative concentrations of optically active water-column constituents, including phytoplankton pigments, non-algal particulate and dissolved organic carbon, and water molecules themselves (Morel and Prieur 1977). The retrieval of SSC in nearshore waters involves three major steps such as atmospheric correction of visible channels to obtain normalized water leaving radiances followed by calculation of remote sensing reflectance *Rrs(k)* and retrieval of SSC.

Empirical algorithms were used to derive information about water constituents (optical properties, particulate concentrations) from the estimated radiance from the water surface. Such information is useful for the management of water quality, monitoring of water pollution, modeling of sediment distribution and transportation, and sediment budget in coastal environments. Algorithms designed to estimate SSCs in open ocean waters as a function of chlorophyll (CHL) concentration in the deep sea

depend on concentrations of plankton and associated organic detrital matter (Morel 1980; Viollier and Sturm 1984). The commonly adopted algorithms for CHL and SSC are reflectance band ratios, characterizing the high absorption of CHL around 440 nm and low absorption at 550 nm.

2.4.1. Remote Sensing and Digital Image Processing

Tides, waves, wind stress, turbidity, currents, river discharge and other coastal processes modulate the transport and distribution of suspended sediments in coastal environment. Remotely sensed satellite data can be used to detect and quantify the total suspended matters successfully (Klemas et al. 1974; Tassan and Strum 1986; Kunte 1994; Chauhan et al. 1996; Kunte et al. 2003; Dwarakish et al. 2010). Ocean Color sensors onboard satellites due to its synoptic view, high repitivity and resolution provide an excellent data to map and monitor sediment patterns, estimate relative changes in sediment concentrations and retrieve sea surface velocities using sediments as a tracer in sequential images (Garcia and Robinson 1989).

Kunte (1994) introduced principal component transform of spectral bands to enhance coastal features and littoral details for studying patterns of near-shore turbidity along the Goa-North Karnataka Coast, West Coast of India using Landsat Multi-Spectral Scanner (MSS) data. Chauhan et al. (1996) used principal component analysis and convolution filtering for enhancing the suspended sediment distribution along the Tamil Nadu Coastal Waters using IRS 1A and 1B satellite images.

Kunte et al. (2002, 2003) presented sediment plume mapping to understand the distribution and dispersion of suspended sediment for Gulf of Kutch area using False Colour Composite (FCC) and Principal Component Analysis (PCA). From IRS-P4 OCM image, first false colour composite image OCM FCC-1 was generated using image processing system. Two FFCs were generated from Principal Component

Analysis (PCs) 2, 3 and 4 (RGB) and 1, 2 and 3 (RGB). Kunte (2008) has been generated FCCs from IRS-1C LISS III to map coastal, near-shore geomorphic features and used IRS-P4 OCM data to study underwater flow-generated bed form structures and suspended sediment dispersal patterns of Gulf of Cambay.

2.4.2. Sediment distribution along Mangalore Coast

Based on reflection, absorption and scattering of light in water and its constituents, Suspended Sediment Concentration (SSC) have been measured in coastal waters (Klemas et al. 1974; Gordon and Morel 1983; Reddy 1993; Nayak 1985; Nayak et al. 2001; Tassan and Strum 1986; Ritchie et al. 1990; Hooker et al., 1992; Forster et al., 1993; Tassan, 1994; Chauhan et al., 1996; Allee and Johnson, 1999; Chauhan 2000; Thiemann and Kaufmann 2000; Dwarakish 2001; Singh et al. 2002; Forget et al. 2001; Santhosh 2002; Selvavinayagam et al. 2003; Menon 2004; Dwarakish, et al. 2010; Avinash et al. 2012; Sravanthi et al. 2013).

Dwarakish et al. (2010) estimated SSC along the Mangalore Coast, West Coast of India using both *in-situ* and IRS-P4 OCM data. Ocean Color Monitor (OCM) data was analysed using OCM Data Analysis Software (OCMDAS), which is based on Tassan's algorithm developed by Space Application Centre (SAC), Ahmedabad, India. Avinash et al. (2012) presented regionally tuned Tassan's algorithm to study the seasonal variations of SSC using IRS-P4 OCM data along Southern Karnataka Coast, West Coast of India. Sravanthi et al. (2013) proposed an empirical algorithm based on a statistical relation between SSC and reflectance *(Rrs)* to estimate SSCs from spectral reflectance for coastal waters of Kerala using IRS-P4 OCM data.

2.4.3. Summary

Image enhancement techniques are required to identify and map various sediment-bearing waters from satellite imagery. Sufficient intensity contrast between coastal waters and various costal geomorphic units is essential for estimation of SSC. The properly enhanced image is highly helpful in mapping of sediment plumes to understand the distribution and dispersion of suspended sediments in nearshore coastal waters.

2.5. Land Use and Land Cover Mapping

The main objective of land use and land cover mapping is to divide the terrain of interest into discrete standardized sections of land, and then to assign a name to each section based on feature classes available on earth surface, that is mapping legend. Spectral information is often used in land use and land cover (LULC) mapping, while some of the classes of interest may not have unique spectral information, because of the imperfections in the information acquisition and extraction processes. The reduction of the spectral differentiation within-class is a significant step of LULC mapping (Rabben 1960). The effectiveness of the reduction in the radiometric resolution of spectral data, i.e histogram quantization, has been demonstrated in digital classification algorithms (Beaubien and Simard 1993; Beaubien 1994; Beaubien et al. 1997). The analyst can increase the accuracy of LULC mapping by enhancing the information extraction process. Many techniques have been developed to improve the accuracy of LULC mapping for various applications in different study areas.

Existing land use and land cover classification techniques for change detection are belongs to broad category of image thresholding, where changes are detected by first analysing multi-temporal images and then thresholding the resultant images.

Techniques of this category include uni-variate comparison methods such as differencing, ratioing, and regression and multi-variate comparison techniques such as change vector analysis as well as data transformation based change detection methods (Singh, 1989). Mathematical transformation techniques such as PCA to analyze multi-temporal images and then threshold the resultant image to identify land cover changes (Byrne et al., 1980; Fung and Ellsworth, 1987). Patel and Kaushal (2010) used PCA to improve the User's accuracy of land cover classification. Aplin and Atkinson (2001) introduced sub-pixel land cover mapping for per-field classification using segmentation of pixels and ranking the segmented pixels. Cihlar et al. (2001) proposed Flexible Histogram Quantization (FHQ) algorithm for land cover mapping. FHQ had a higher efficiency (by 65% to 148%), except for histogram equalization and it also retained more information than histogram equalization. Most importantly, it provided finer resolution in the tails of main histogram peak for infrequent but potentially important land cover types.

Jesus et al. (2012) presented a combined pixel-based and object-based approach for optimizing land cover classification accuracy. Faid and Abdulaziz (2012) used NDVI for mapping vegetation cover, Principal Component Analysis (PCA) for mapping urban land use and land cover and onscreen digitization for extracting irrigation channels to obtain minimum classification errors in land use and land cover changes of Kom Ombo area, South Egypt. Amarsaikhan et al. (2012) introduced image fusion method for land cover classification using multiplicative method, Brovey transform, PCA, Gram-Schmidt fusion, wavelet-based fusion and Elhers fusion methods and results are compared. Sinha and Kumar (2013) proposed 'Independent Two-Step' thresholding approach for optimal threshold value determination for spectrally increased and decreased part using Normalized Difference Vegetation Index (NDVI) difference image. Threshold values were based on the standard deviation (SD) from the mean, assuming the amount of change to be symmetrically distributed on a standard normal curve.

2.5.1. Summary

From the literature review, it is clear that, most of the information is not properly classified with available classification (object-based or pixel-based) techniques due to spectral diversity in within-class of homogeneous land features. Also similar class features may not have same spectral characteristics, because of limitations in data acquisition and extraction processes. Due to difference in amount of energy reflected by different earth surface materials in a certain wavelength creates difference in spectral information. Similar amounts of radiant flux throughout the visible, near-infrared, and mid-infrared portion of the electromagnetic spectrum also cause for more spectral variation. It is possible to improve the accuracy of the LULC mapping by reducing the spectral variation within-class of features. Reduction in the number of digital numbers is a key step in digital classification and it reduces the number of possible classes.

2.6. Reviewer's Points

Review of literature has provided very good insight to the selection of best methods for contrast enhancement, good data sets and other procedures for development of algorithms. Accordingly, the following points are incorporated and considered in the present study.

- To improve the quality of coastal objects, clipped histogram equalization based contrast enhancement technique is developed for automatic shoreline detection from satellite images.

- Region of Interest (ROI) technique is adopted to remove unwanted small objects from segmented land and water regions during automatic shoreline detection process.

- Robert's edge detector is adopted for extraction of automatic shoreline from the satellite images.

- IRS-P6 LISS III (2005, 2007 and 2010) and IRS-R2 LISS III 2013 satellite images are employed to find the shoreline changes.

- Digital Shoreline Analysis System (DSAS), a GIS tool is adopted for shoreline change rate analysis through End Point Rate (EPR) and Linear Regression Rate (LRR) statistical methods.

- To improve the tonal variation of sediments, clipped histogram equalization based contrast enhancement method is developed.

- IRS-P4 OCM data is selected for the preparation of suspended sediment transport distribution map for Mangalore Coast, West Coast of India.

- For qualitative comparison of sediment distribution map developed for Mangalore Coast, Dwarakish et al., 2010 and Avinash et al., 2012 studies are considered. Results of In-situ data analysis by previous researchers, Dwarakish et al. (2010) and Avinash et al. (2012) are used.

- IRS-R2 LISS III 2013 image is selected for Land Use and Land Cover assessment using developed clipped histogram equalization based contrast enhancement algorithm.

- Overall accuracy and Kappa Coefficients are considered to estimate improvement of LULC classification.

CHAPTER 3
COMPARISON OF HE-BASED METHODS

3.1. General

Contrast enhancement techniques increase the contrast between target features and their back grounds. Histogram Equalization (HE) is an eminent active indirect non-linear contrast enhancement method for satellite images, based on the grey level of the data. HE is often used very effective image enhancement technique because it requires very little information to implement it. HE has been widely applied when the image has low contrast and needs enhancement for further processes, such as satellite image processing, medical image processing, radar image processing, texture synthesis, and speech recognition etc. The present chapter describes various HE based methods to overcome the drawbacks of HE and comparative analysis of those techniques using image quality measures such as Peak-Signal to Nosie Ratio (PSNR) and Absolute Mean Brightness Error (AMBE).

3.2. Histogram Equalization

Histogram Equalization (HE) is a simple, standard and most effective technique for contrast enhancement (Gonzalez and Woods, 2008). The HE works on the cumulative distribution function based mapping of intensity levels and it flattens and stretches the dynamic range of the image histogram grey levels to achieve overall contrast enhancement. HE is designed to maximise the entropy of an image by distributing the grey levels uniformly using grey levels probability density function.

3.3. Drawbacks of Histogram Equalization

Remote sensing satellite sensor record dissimilar amount of energy reflected from different earth surface features in certain wavelength, which creates the low-contrast satellite image. HE enhances the low contrast image by globally distributing the brightness values within the histogram, which resulted in either under-saturation or

over-saturation of important regions in the image. HE stretches the contrast of high histogram regions and compresses the contrast of low histogram regions, and introduces unwanted artefacts in the image (Sengee and Choi 2008). As a consequence, when the object of interest in an image occupies only a small portion of the image, the object is not successfully enhanced by histogram equalization. HE method also extremely pushes the intensities towards the right or the left side of the histogram, causes level saturation effects. In HE the data has redistributed to the cumulative frequency of the histogram data. After equalization, some pixels which had originally different DN values are now assigned same DN values. HE also alters the relationship between brightness values and image structure.

HE not preserved the brightness of the input, where preserving the input brightness is essential to avoid the generation of non-existing artefacts in the output image. Narrow or small range sections are not enhanced significantly by HE method (Ibrahim and Kong 2007). Due to these reasons, for the implementation of contrast enhancement, it is advised that the loss of intensity values by the histogram processing should be minimized in the output image.

3.4. Histogram Equalization based Methods

To overcome drawbacks of HE, several HE based techniques were developed. Based on modification of input image histogram, the techniques were categorized as, Bi-Histogram Equalization (Bi-HE) methods, Multi-Histogram Equalization (Multi-HE) Methods and Clipped Histogram Equalization (CHE) methods.

3.4.1. Bi-Histogram Equalization Methods

Bi-Histogram Equalization (Bi-HE) method divides the original input image histogram into two sub-histograms, based on different statistical functions. Then, each sub-histogram was equalized individually based on histogram equalization. Bi-HE methods enhanced the image contrast significantly and preserved the brightness to some extent, but it introduced undesirable artefacts (Khan et al. 2012).

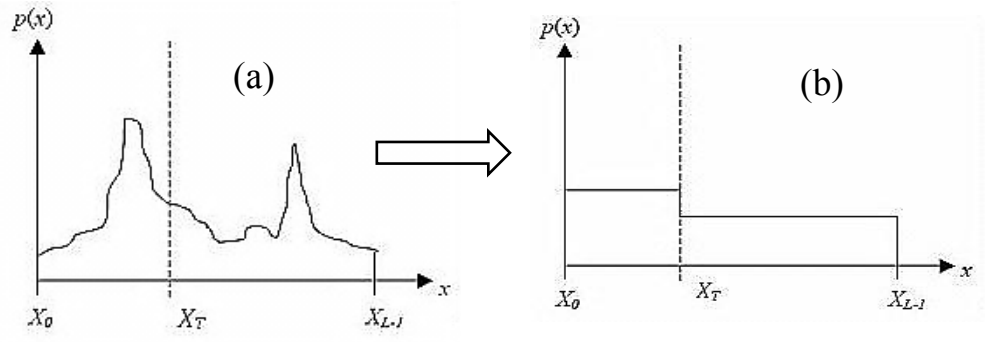

Figure 3.1. Bi-histogram equalization method
(a) Input histogram divided into two sub-histograms (b) Equalized sub-histograms

The main Bi-HE methods are, Brightness Preserving Bi-Histogram Equalization (BBHE), Dualistic Sub-Image Histogram Equalization (DSIHE), Minimum Mean Brightness Error Bi-Histogram Equalization (MMBEBHE), Brightness Preserving Histogram Equalization with Maximum Entropy (BPHEME), Dynamic Histogram Equalization (DHE), Brightness Preserving Dynamic Histogram Equalization (BPDHE), Recursively Separated and Weighted Histogram Equalization (RSWHE), Brightness Preserving Weight Clustering Histogram Equalization (BPWCHE), Spatially Controlled Histogram Equalization (SCHE), Brightness Preserving Dynamic Fuzzy Histogram Equalization (BPDFHE), Bi-Histogram Equalization with Neighbourhood Metric (BHENM), Two-Dimensional Histogram Equalization (2DHE) and Range Limited Bi-Histogram Equalization (RLBHE).

3.4.2. Multi-Histogram Equalization Methods

Multi-Histogram Equalization (Multi-HE) techniques decomposed the input image histogram into several sub-images, and then applied the classical histogram equalization process to each of sub-histogram to enhance contrast, preserving brightness and improved natural looking of the images without artefacts. Due to multiple segments of image histogram, multi-HE methods preserved the image brightness and prevented introduction of undesirable artefacts but not significantly enhanced the contrast.

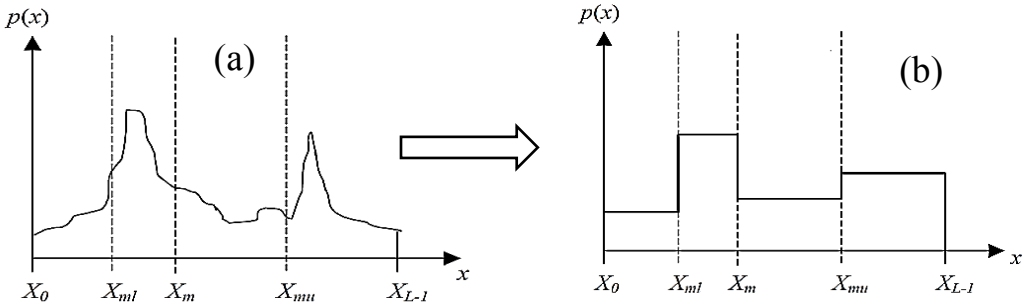

Figure 3.2. Recursive Mean-Separate Histogram Equalization (RMSHE) method (a) Separated histogram (b) Equalized histogram (r=2)

3.4.3. Clipped Histogram Equalization Methods

Clipped Histogram Equalization (CHE) methods clipped the high histogram regions to restrict the enhancement rate. These methods enhanced the objects of interest, which occupied a small portion of the image successfully by equalizing the clipped histograms. CHE methods also controlled the level saturation effects by selecting the proper threshold value to clip the histogram regions. In some cases, where images desired more enhancements, the clipped portion was redistributed back to the histogram and then histogram equalization was carried out. CHE was effective in contrast enhancement than the existing HE-based methods.

3.5. Image Quality Measures

The image quality measurement (IQM) tools are used to evaluate the ability of the histogram equalization based techniques to maintain contrast enhancement and the mean brightness preserving. Absolute Mean Brightness Error (AMBE), Peak Signal-to-Noise Ratio (PSNR) and Entropy are most commonly used IQMs. The available HE-based techniques and IQMs (Chen 2012) used to evaluate them are listed in Table 3.1.

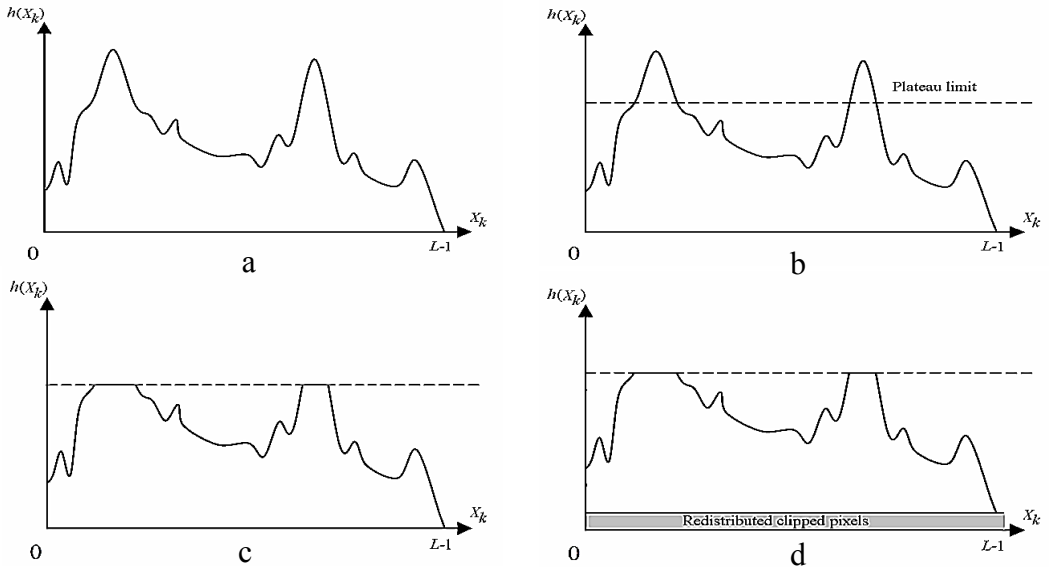

Figure 3.3. Clipped Histogram Equalization (CHE) Method (a). The Original input histogram (b). The settings of the Plateau limit (c). Clipping the histogram based on the plateau limit (d). Redistribution of clipped portion back into the modified histogram

3.5.1. Absolute Mean Brightness Error

Absolute Mean Brightness Error (AMBE) is defined as the absolute difference between the mean of the input and the output images. The objective of AMBE is proposed to rate the performance in preserving the original brightness (AMBE) (Chen and Ramli 2003 and 2004).

$$AMBE = |E(\boldsymbol{X}) - E(\boldsymbol{Y})| \qquad (1)$$

X and Y denotes the input and output image, respectively, and E (.) denotes the expected value, i.e. the statistical mean. Lower AMBE indicates the better brightness preservation of the image. Equation (1) clearly shows that AMBE is designed to detect one of the distortions–excessive brightness changes (Chen 2012).

3.5.2. Peak Signal-to-Noise Ratio

Peak Signal-to-Noise Ratio (PSNR) ratio is often used as a quality measurement between the original and enhanced image. PSNR is the ratio between the maximum possible power of a signal and the power of corrupting noise that affects the reliability of its representation. The Mean Square Error (MSE) and the PSNR are the two error metrics used to compare image compression quality. The MSE represents the cumulative squared error between the compressed and the original image, whereas PSNR represents the measure of the peak error. The lower value of MSE gives lower error in the output image. Similarly, the higher the PSNR better the quality of the enhanced or compressed or reconstructed image.

Let, *X(i,j)* is a source image that contains *M* by *N* pixels and a reconstructed image *Y(i,j)*, where *Y* is reconstructed by decoding the encoded version of *X(i,j)*. In this method, errors are computed only on the luminance signal; so, the pixel values *X(i,j)* range between black (0) and white (255) (Sim et al. 2007). First, the mean squared error (MSE) of the reconstructed image is calculated as;

$$MSE = \frac{\sum_{i=1}^{M}\sum_{j=1}^{N}[X(i,j)-Y(i,j)]^2}{M\times N} \qquad (2)$$

The root mean square error is computed from root of MSE. Then the PSNR in decibels (dB) is computed as;

$$PSNR = 20log_{10}(\frac{Max(Y(i,j))}{RMSE}) \qquad (3)$$

The higher the PSNR better the quality of the enhanced or compressed or reconstructed image.

Table 3.1. List of automatic HE-based techniques and their IQMs

S. No.	Histogram Equalization based Techniques	Image Quality Measure (IQM)
01	Brightness Preserving Bi-HE (BBHE)	AMBE
02	Multi-peak HE (Multi-peak)	AMBE
03	Dualistic Sub-Image HE (DSIHE)	AMBE, Entropy, Background brightness
04	Minimum Mean Brightness Error Bi-HE (MMBEBHE)	AMBE
05	Brightness Preserving HE with Maximum Entropy (BPHEME)	AMBE, Entropy
06	Brightness Preserving Dynamic HE (BPDHE)	AMBE, Entropy
07	Multi-Histogram Equalization Methods for Contrast Enhancement and Brightness Preserving (Multi-HE)	AMBE
08	Recursively Separated and Weighted HE for Brightness Preservation and Contrast Enhancement (RSWHE)	AMBE, Entropy, PSNR
09	Bi-Histogram Equalization with a Plateau Limit for Digital Image Enhancement (BHEPL)	Average AMBE
10	Adaptive Contrast Enhancement Methods with Brightness Preserving (DQHEPL & BHEPL-D)	Average AMBE, Average Entropy, Average PSNR
11	Fusion frame work of HE and Laplacian Pyramid (FFHEPL)	Standard Deviation of AMBE, Enhancement by Entropy
12	Image Contrast Enhancement using Bi-HE with Neighbourhood Metrics (BHENM)	Average AMBE

***(Source:** Chen 2012)*

3.6. Results and Discussion of Comparative Analysis

For comparative analysis, along with HE, widely used HE-based methods from each class are selected and implemented for comparison using various test images. Selected HE-based methods are compared using image quality measures such as

Absolute Mean Brightness Error (AMBE) and Peak-Signal-to-Noise Ratio (PSNR). AMBE value gives the brightness preservation and PSNR value provides contrast enhancement. Lower value of AMBE specifies greater brightness preservation and higher value of PSNR shows good contrast enhancement of the output image. Identified HE-based methods are compared by testing digital images and satellite images and comparative results are discussed separately in the following two sections.

3.6.1. Comparison of Digital Images

Histogram Equalization, Bi-histogram Equalization (BBHE, DSIHE and MMBEBHE), Multi-histogram Equalization (RMSHE, RSIHE, DHE, BPDHE and RSWHE) and Clipped Histogram Equalization (GC-CHE and BHEPL) algorithm codes were prepared individually using MATLAB R2013a and compared with different test images (.tiff format). Total of 30 test images were used to assess the performance of techniques and 10 selected images results are presented in this study. The results of test images *tire* and *random_matches* are shown in Figure 3.4 and Figure 3.5 and the image quality assessment measures such as AMBE and PSNR values are formulated in Table 3.2 and Table 3.3.

Brightness Preserving Bi-Histogram Equalization (BBHE) produced better brightness preservation than HE and not showed any significant contrast enhancement [Figure 3.4(c) and Figure 3.5(c)]. Individual equalization of two histogram segments, BBHE has given good brightness preservation AMBE (*10.59 tire* and *9.80 random_matches*) than HE, AMBE (*73.98 tire* and *23.75 random_matches*). But, it has not showed considerable contrast enhancement [PSNR (*26.94 tire* and *28.37 random_matches*)] compared to HE, [PSNR (*24.38 tire* and *26.53 random_matches*)] as shown in Table 3.2 and Table 3.3.

Dualistic Sub-Image Histogram Equalization (DSIHE) has shown all most the same AMBE and PSNR values for all test images. DSIHE and BBHE were presented better brightness preservation and contrast enhancement than HE.

Minimum Mean Brightness Error Bi-Histogram Equalization (MMBEBHE) technique has shown better brightness preservation and there is no much variation in contrast enhancement, compared to BBHE and DSIHE. MMBEBHE is an extended method of BBHE and given better brightness preserving (*AMBE 0.87; bottom_left*) and contrast enhancement (*PSNR 43.93; bottom_left*) than BBHE (*AMBE 1.36, PSNR 41.41; bottom_left*). However, it is not controlled over-enhancement as presented in Figure 3.4(e) and revealed less brightness preserving for bright images like *Cygnusloop* (AMBE is *14.83*) from Table 1.

Multi-HE based methods have shown very good brightness preserving except recursive based techniques, due to repetition of histogram segmentation based on mean or median value of the histogram. Recursive Mean-Separate Histogram Equalization (RMSHE), Recursive Sub-Image Histogram Equalization (RSIHE) and Recursively Separated and Weighted Histogram Equalization (RSWHE) techniques have shown less brightness preservation and contrast enhancement because of recursive separation of histogram. The output images of these recursive methods are presented over-enhancement without brightness preservation, which is the cause of noise amplification and washout effect in the images. Consequently, more background information has lost in the output image. For *tire* image RMSHE has given *10.59* (AMBE) and *26.94* (PSNR); RSIHE has given *14.39* (AMBE) and *26.51* (PSNR); and RSWHE has shown *87.32 (*AMBE) and *24.18* (PSNR).

Multi-HE based methods, DHE and BPDHE have shown good brightness preservation, but not shown significant contrast enhancement. DHE has given good brightness preserving values for *Cameraman* (*AMBE 4.27*) and *Pirate* (*AMBE 5.50*) and it has shown poor contrast enhancement for *Cameraman* (*PSNR 7.12*), *bottom_left* (*PSNR 7.82*) and *Cygnusloop* (*PSNR 9.30*). DHE has shown better smoothed enhancement of the image and tends to introduce saturation artefacts. BPDHE has presented very good brightness preservation for *Face* (*AMBE 0.01*), *bottom_left* (*AMBE 0.01*), *Pirate* (*AMBE 0.01*) and contrast enhancement for *tire* (*PSNR 28.68*), *Pirate* (*PSNR 33.34*), *Lenna* (*PSNR 33.37*) and *random_matches*

(*PSNR 27.78*). DHE and BPDHE have introduced unwanted artefacts in the output images.

Clipped histogram equalization (CHE) methods have controlled the enhancement rate by clipping the high intensity of the histogram regions using proper threshold value. Bi-Histogram Equalization Plateau Limit (BHEPL) method has shown good brightness preserving (low AMBE value) like *0.44* for *random_matches* image and *0.51* for *bottom left* image. The bright images like *face*, *pirate*, *lenna* and *Cygnusloop* have shown AMBE values as *10.19, 18.47, 18.04* and *10.58* respectively. CHE methods also presented good contrast enhancement (high PSNR value) for *bottom_left* (*50.70*) and *random_matches* (*42.67*). BHEPL has controlled the over-enhancement and over amplification of noise in the output images.

Gain-Controllable Clipped Histogram Equalization (GC-CHE) method has shown excellent brightness preserving and contrast enhancement for all test images. It has presented vey less AMBE values, which are close to zero for *Cygnusloop* and *crabpulsar-ratio* (i.e. 0.00). It has also given good PSNR values for *tire* (*61.61*) and *bottom_left* (*46.63*). GC-CHE has controlled the over-enhancement by clipping the high histogram regions and controlled noise amplification by adjusting contrast elevation ratio. By re-distributing the clipped portion of the histogram, GC-CHE preserved more brightness in the output image.

All the above methods have overcome the drawbacks of histogram equalization and enhanced the contrast and also preserved the brightness of the image, as given in Table 3.2 and Table 3.3 and also shown in Figure 3.4 and Figure 3.5. From the present analysis, it is clear that the Brightness Preserving Dynamic Histogram Equalization (BPDHE) and Gain-Controllable Clipped Histogram Equalization (GC-CHE) methods are more suitable for both brightness preservation and contrast enhancement of the images as well.

Table 3.2. Assessment of the Brightness Preservation based on AMBE (Absolute Mean Brightness Error)

Methods / Test Images	Bi-HE based methods				Multi-HE based methods					CHE based methods	
	HE	**BBHE**	**DSIHE**	**MMBEBHE**	**RMSHE**	**RSIHE**	**RSWHE**	**DHE**	**BPDHE**	**BHEPL**	**GC-CHE**
Tire	73.98	10.59	10.59	7.93	10.59	14.39	87.32	13.23	0.01	11.41	0.02
bottom_left	89.12	1.36	1.30	0.87	1.35	0.12	33.55	92.32	0.01	0.51	0.01
Cameraman	16.32	6.28	6.28	6.45	51.46	0.54	81.54	4.27	0.02	32.78	0.15
Face	34.62	5.32	5.32	5.65	15.32	3.87	81.10	60.27	0.01	10.19	0.14
Hurricane Andrew	46.83	12.56	12.56	2.09	34.79	4.53	86.90	25.37	0.02	23.17	0.15
Pirate	21.08	10.72	10.72	7.40	29.63	12.60	90.02	5.50	0.01	18.47	0.18
Lenna	25.76	13.43	13.43	11.98	34.84	3.87	93.88	57.01	0.05	18.04	0.10
Cygnusloop	73.66	17.01	17.01	14.83	17.01	17.13	72.18	15.86	0.07	10.58	0.00
random_matches	23.75	9.80	9.80	7.40	9.80	14.65	91.14	57.43	0.01	0.44	0.31
crabpulsar-radio	95.16	22.91	22.91	19.10	22.91	19.19	79.43	15.86	0.09	28.64	0.00

Table 3.3. Assessment of the Contrast Enhancement based on PSNR (Peak Signal-to-Noise Ratio)

Methods / Test Images	Bi-HE based methods				Multi-HE based methods					CHE based methods	
	HE	**BBHE**	**DSIHE**	**MMBEBHE**	**RMSHE**	**RSIHE**	**RSWHE**	**DHE**	**BPDHE**	**BHEPL**	**GC-CHE**
Tire	24.38	26.94	26.94	27.98	26.94	26.51	24.18	12.45	28.68	27.86	61.61
bottom_left	24.60	41.41	41.41	43.93	31.25	44.24	24.06	7.82	20.65	50.70	46.63
Cameraman	27.46	12.38	12.38	12.53	12.38	12.40	24.19	7.12	30.02	25.89	45.14
Face	25.18	16.95	30.04	29.91	29.07	29.32	24.08	11.11	31.61	27.11	44.63
Hurricane Andrew	25.03	14.42	14.42	14.12	14.41	14.73	24.07	15.80	31.28	27.93	37.22
Pirate	27.01	16.95	16.95	15.72	15.94	15.78	24.06	13.88	33.34	26.84	39.44
Lenna	26.50	15.50	15.50	14.81	14.56	14.57	24.06	11.42	33.37	26.88	40.08
Cygnusloop	24.06	26.85	26.85	27.13	26.47	26.53	25.60	9.30	25.05	28.60	----------
random_matches	26.53	28.37	28.37	30.38	28.37	25.90	24.18	10.62	27.78	42.67	34.15
crabpulsar-radio	24.06	26.93	26.93	27.07	26.90	27.02	26.01	9.30	26.81	27.23	----------

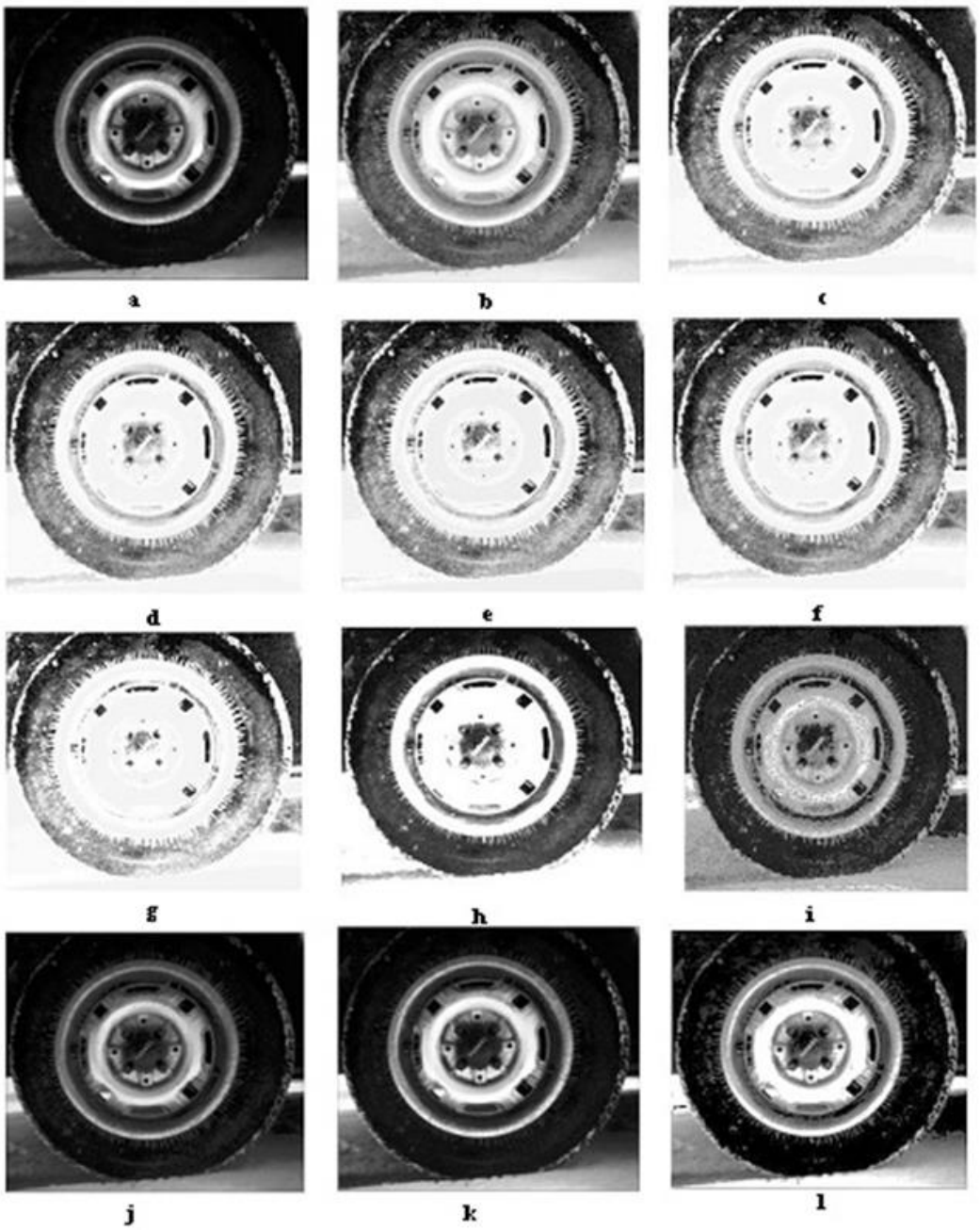

Figure 3.4. Performance comparison using *tire* image

(a). Original Image (b). Histogram Equalization, (c). Brightness Preserving Bi-Histogram Equalization (BBHE), (d). Dualistic Sub-Image Histogram Equalization (DSIHE), (e). Minimum Mean Brightness Error Bi-Histogram Equalization (MMBEBHE), (f). Recursive Mean-Separate Histogram Equalization (RMSHE) (r=2), (g). Recursive Sub-Image Histogram Equalization (RSIHE), (h). Recursively Separated and Weighted Histogram Equalization (RSWHE), (i). Dynamic Histogram Equalization (DHE), (j). Brightness Preserving Dynamic Histogram Equalization (BPDHE), (k). Bi-Histogram Equalization with Plateau Limit (BHEPL) and (l). Gain-Controllable Clipped Histogram Equalization (GC-CHE).

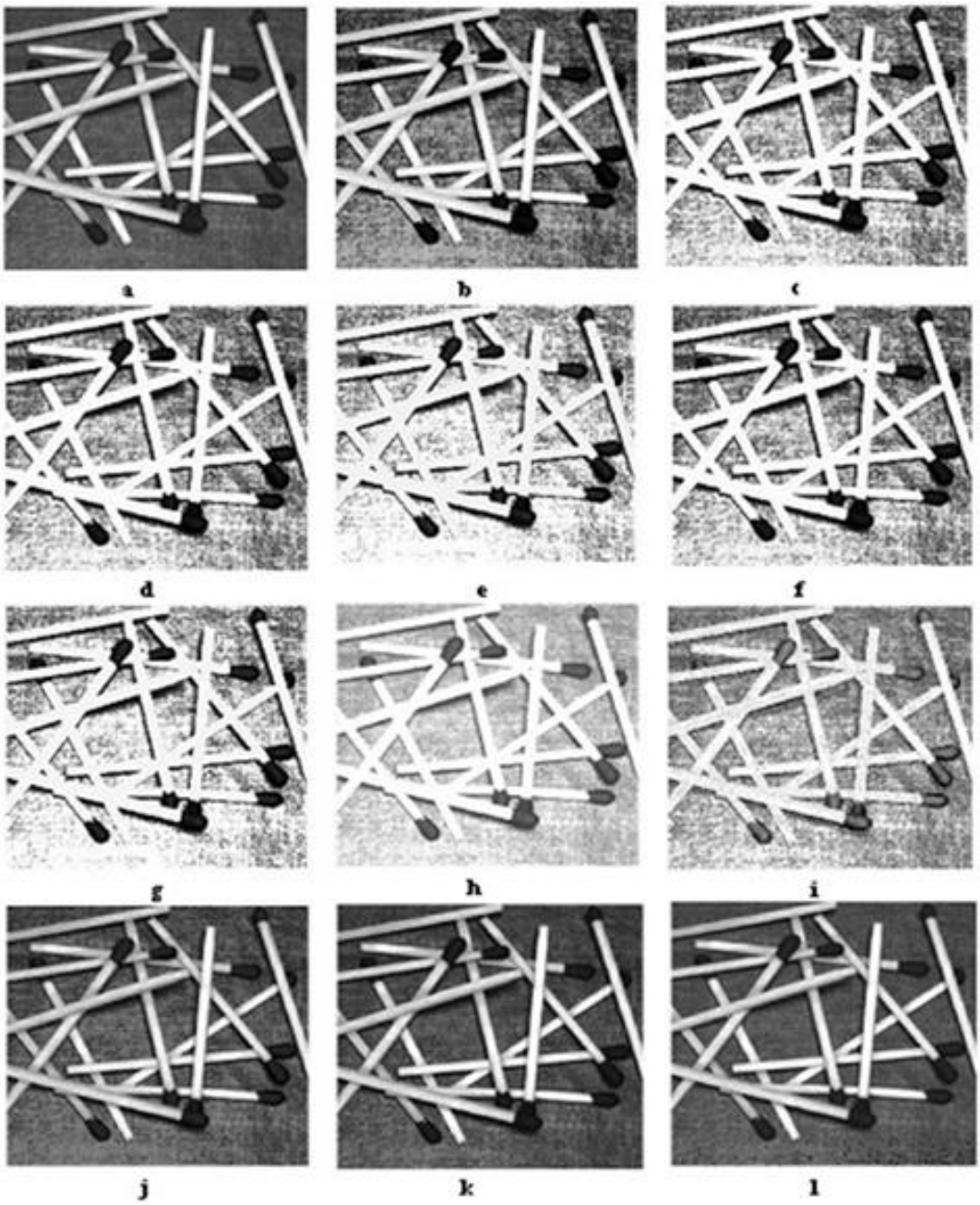

Figure 3.5. Performance comparison using *random_matches* image

(a). Original Image (b). Histogram Equalization, (c). Brightness Preserving Bi-Histogram Equalization (BBHE), (d). Dualistic Sub-Image Histogram Equalization (DSIHE), (e). Minimum Mean Brightness Error Bi-Histogram Equalization (MMBEBHE), (f). Recursive Mean-Separate Histogram Equalization (RMSHE) (r=2), (g). Recursive Sub-Image Histogram Equalization (RSIHE), (h). Recursively Separated and Weighted Histogram Equalization (RSWHE), (i). Dynamic Histogram Equalization (DHE), (j). Brightness Preserving Dynamic Histogram Equalization (BPDHE), (k). Bi-Histogram Equalization with Plateau Limit (BHEPL) and (l). Gain-Controllable Clipped Histogram Equalization (GC-CHE).

3.6.2. Comparison of Satellite Images

Histogram Equalization based contrast enhancement techniques are also compared with satellite images for detection of shoreline and coastal features along with basic Histogram Equalization (HE) methods, such as Brightness Preserving Bi-Histogram Equalization (BBHE), Dualistic Sub-Image Histogram Equalization (DSIHE), Minimum Mean Brightness Error Bi-histogram Equalization (MMBEBHE), Dynamic Histogram Equalization (DHE), Brightness Preserving Dynamic Histogram Equalization (BPDHE), Bi-histogram Equalization with Plateau Limit (BHEPL) and Gain-Controllable Clipped Histogram Equalization (GC-CHE). For comparative analysis, HE-based methods are implemented on MATLAB R2013a and compared the enhanced satellite (*IRS-P6 LISS III_band4.tif, 23.5 m resolution*) and *IRS-P6 LISS IV_band4.tif, 5.8 m resolution*) images using image quality measures such as Peak-Signal to Noise Ratio (PSNR), and Absolute Mean Brightness Error (AMBE), which represents the amount of contrast enhancement and brightness preserving of the image. The results (PSNR and AMBE values) of test images *IRS LISS III_band4.tif* and *IRS LISS IV_band4.tif* are tabulated in Table 3.4. and final output images of *IRS LISS IV_band4.tif* are shown in Figure 3.6.

Gain-Controllable Clipped Histogram Equalization (GC-CHE), Bi-histogram Equalization with Plateau Limit (BHEPL) and Brightness Preserving Dynamic Histogram Equalization (BPDHE) has shown very good brightness preservation and contrast enhancement for both the test images. Due to re-distribution of clipped portion of histogram, GC-CHE has given better AMBE and PSNR values *LISS IV_band4.tif* (*PSNR* 56.87*; AMBE 2.97*) and *LISS III_band4.tif (PSNR 57.65; AMBE 1.98).* BHEPL has shown more contrast enhancement and brightness preservation for both test images, *LISS IV_band4.tif* (*PSNR 32.27; AMBE 4.50*) and *LISS III_band4.tif (PSNR 34.39; AMBE 3.49).* BHEPL has shown natural enhancement without introducing unwanted noise and also presented good brightness preservation. BHEPL has given *32.27* (PSNR) and *4.50* (AMBE) for *LISS IV_band4.tif* image, signifying good contrast enhancement without additional artefacts.

BPDHE, a Multi-HE technique, has also presented better brightness preservation because of multiple segmentation of input histogram and equalize each segment individually and it has shown significant contrast enhancement, but introduced unwanted artefacts, which affects the natural enhancement. DHE, has shown less PSNR (*13.22*) and more AMBE (*16.81*) values and PSNR (*8.26)* and AMBE (*88.77)* for *LISS IV_band4.tif* and *LISS III_band4.tif* respectively, due to the nature of neglecting mean brightness preservation, it tends to intensity saturation artefacts.

Bi-HE methods such as BBHE, DSIHE and MMBEBHE have not shown significant contrast enhancement and brightness preservation and also introduced annoying artefacts in the output image. These techniques also not controlled the over-enhancement; so, most of the information has lost in the output image. MMBEBHE has given very less AMBE value *0.69* for *LISS IV_band4.tif* and marginally greater to BHEPL (*3.49*) for *LISS III_band4.tif*. BBHE and DSIHE have presented normal contrast enhancement and brightness preservation, and also shown over-enhancement causing noise in the output image as shown in Figure 3.6. From Table 3.4, one can observe that, for *LISS IV_band4.tif*, BBHE and DSIHE have given less PSNR (*28.45*) and AMBE (*8.73*) and for *LISS III_band4.tif* also these methods produced less PSNR *(28.62)* and AMBE *(7.62).*

Table 3.4: Assessment of contrast enhancement (PSNR) and brightness preserving (AMBE)

Image / Method	LISS IV_band4.tif		LISS III_band4.tif	
	PSNR	AMBE	PSNR	AMBE
HE	24.06	105.42	18.61	84.71
BBHE	28.45	8.73	28.62	7.62
DSIHE	28.45	8.73	28.62	7.62
MMBEBHE	46.68	0.69	30.87	5.87
DHE	13.22	16.81	8.26	88.77
BPDHE	53.81	5.64	49.67	6.71
BHEPL	32.27	4.50	34.39	3.49
GC-CHE	56.87	2.97	57.65	1.98

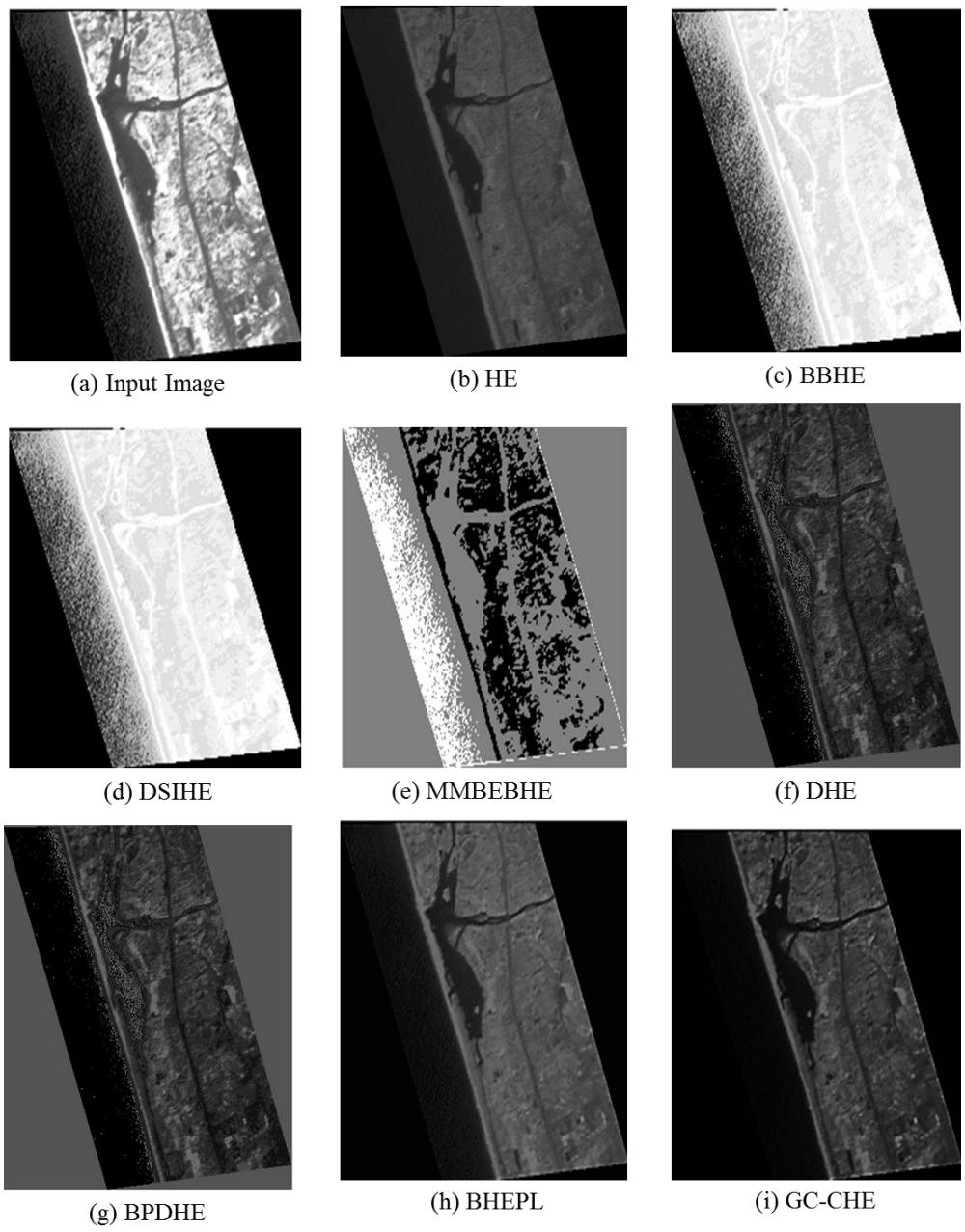

Figure 3.6. Performance comparison using *LISS IV_band4.tif* image

(a). Input Image, (b). Histogram Equalization (HE), (c). Brightness Preserving Bi-Histogram Equalization (BBHE), (d). Dualistic Sub-Image Histogram Equalization (DSIHE) (e). Minimum Mean Brightness Error Bi-Histogram Equalization (MMBEBHE) (f). Dynamic Histogram Equalization (DHE), (g). Brightness Preserving Dynamic Histogram Equalization (BPDHE) (h). Bi-Histogram Equalization with Plateau Limit (BHEPL) and (i). Gain-Controllable Clipped Histogram Equalization (GC-CHE).

3.7. Summary

BBHE, DSIHE, MMBEBHE, RMSHE, RSIHE and RSWHE methods have shown better contrast enhancement and brightness preservation than HE. However, these methods are not presented considerable contrast enhancement and not preserved the brightness in the output image. MMBEBHE, the extension method of BBHE has shown a better brightness preserving. But it could not control over-enhancement of the image. Due to over-enhancement in MMBEBHE, RMSHE and RSIHE, there is a loss of information in the output image. RSIHE technique has also shown more over-enhancement than MMBEBHE and RMSHE. RSWHE and DHE methods have shown good brightness preserving as well as a controlled over-enhancement, but introduced annoying noise in the output image. BHEPL technique has also presented good brightness preserving.

BPDHE technique has given very less value of AMBE indicating good brightness preserving and high values of PSNR shows better contrast enhancement. GC-CHE method has also shown good brightness preserving and contrast enhancement. The output images of GC-CHE are very clear without any noise and there is no loss of information. BPDHE and GC-CHE techniques are more suitable for digital images and satellite images, where contrast enhancement and preservation of the original brightness is essential.

From the above comparative analysis, one can see that, Clipped Histogram Equalization (CHE) based methods are more suitable for contrast enhancement and brightness preservation of digital images and satellite images, when compared to all other methods. Hence, in the present study, CHE-based methods are adopted and CHE based contrast enhancement algorithms have been developed for Automatic shoreline detection, Suspended sediment transport and Land Use and Land Cover (LULC) assessment.

CHAPTER 4
MATERIALS AND METHODOLOGY

4.1. General

Coastal zone monitoring is an essential component in national development and environmental protection, in which extraction of shoreline, sediment transport and coastal land use and land cover mapping are some of the prominent activities. Many conventional and remote sensing techniques are available for effective study of coastal zone management. Conventional methods provides more accurate and site specific, but data collection is time consuming, expensive, requires more manpower and may not be extrapolated to larger area. Due to the advantage of repetitive and synoptic coverage of the larger and inaccessible areas, efficient, quick and economical remote sensing data is now regularly being used for coastal applications. This chapter describes the data used and methodologies developed to address the identified objectives for the present study.

4.2. Data Products

Coastal zone represents wide-range and extremely dynamic ecosystems and due to globalization these ecosystems are now under pressure. It is necessary to develop precise, up-to-date and comprehensive scientific database on coastal ecosystems to ensure sustainable development. The remotely sensed satellite images, geographical information system (GIS) and global positioning system (GPS) are extremely valuable in development of database for coastal ecosystems. These tools are also accurate to analyse them in the integrated manner and derive management action plans to protect the coastal zone.

4.2.1. Remote Sensing Data

Indian Remote Sensing (IRS) data having moderate (23-36 m) to high spatial resolution (1 m) are used to generate database on numerous components of coastal zone. Monitoring of periodical change is possible due to availability of repetitive, synoptic and multispectral remote sensing data. In the present study, IRS-P6 LISS III (2005, 2007 and 2010) data and IRS-R2 LISS III (2013) data were used for the shoreline extraction and Land Use and Land Cover (LULC) mapping.

IRS-P4 OCEANSAT-2 OCM (2013) data was used for identification of sediment movement and distribution. IRS-P6 LISS III (2005, 2007 and 2010), IRS-R2 LISS III (2013) and IRS-P4 OCEANSAT-2 OCM (2013) data were obtained from National Remote Sensing Centre (NRSC), Hyderabad, India. In addition, Boundary and study area maps were prepared by merging two Survey of India (SOI) toposheets No. 48 K/16 (1969) and 48 L/13 (1973) with scale 1:50000 and these toposheets were obtained from SOI, Bangalore, India. The details of SOI toposheets and the specifications of satellite data used in the present study are given in the Table 4.1. and Table 4.2 respectively.

Table 4.1. SOI toposheets used in the present study

Sl No.	Data	Source	Year	Scale	Sheet No.
01	Toposheet	Survey of India (SOI)	1969	1:50,000	48 K/16
02	Toposheet	Survey of India (SOI)	1973	1:50,000	48 L/13

Table 4.2. Satellite images used in the present study

Sl No	Satellite & Sensor	Date of Acquisition	Path and row	Resolution (m)	Purpose
1	IRS-P6 LISS-III	05/01/2005	97 and 64	23.5	Shoreline extraction and LULC mapping
2		21/12/2007			
3		03/01/2010			
4	IRS-R2 LISS-III	23/01/2013	97 and 64	23.5	
5	IRS-P4 Oceansat-2 OCM	12/12/2013	09 and 14	360	Sediment distribution

The Ocean Color Monitor (OCM) sensor is optimally designed to estimate/monitor the coastal and oceanic parameters such as suspended sediments (Santosh et al. 2002, Surendran et al. 2006), chlorophyll (Chauhan et al. 2002), phytoplankton blooms (Sarangi et al. 2008) and atmospheric aerosols (Das et al. 2002, Mishra et al. 2008). The optical sensor, OCM onboard IRS-P4 has eight spectral bands, out of which six bands are belongs to visible region of electromagnetic spectrum and the remaining two are belongs to near infrared (NIR) region. Together they are in the range of 404–887 nm with spectral resolution of 20 nm in the visible bands and 40 nm in NIR bands, and the spatial resolution of 360 m with 2 days of repetivity.

The specifications of the IRS-P4 OCM sensor (Mishra et al. 2008) and acquisition date of the data product are given in Table 4.3. The spectral bands of OCM sensor and sensitiveness to various ocean parameters are presented in Table 4.4.

Table 4.3. Technical characteristics of IRS-P4 OCM sensor (Mishra et al. 2008)

Spectral range	404–882 nm
No. of channels	8
Wavelength (nm)	Channel 1:404–424 Channel 2: 432–452 Channel 3: 479–499 Channel 4: 502–522 Channel 5: 547–567 Channel 6: 660–680 Channel 7: 778–788 Channel 8: 847–887
Satellite altitude (km)	720
Spatial resolution (m)	360X236
Swath (km)	1420
Repetivity	2 days
Quantization	12 bits
Equatorial crossing time	12 noon
Along-track steering (to avoid sunglint)	20˚
Path and Row	09 and 14
Date of data acquisition	December 12, 2013

Table 4.4. The spectral bands OCM sensor and sensitiveness to different ocean parameters

Bands	Wavelength (nm)	Applications
C1	402 – 422	Yellow substance and turbidity
C2	433 – 453	Chlorophyll absorption maxima
C3	480 – 500	Chlorophyll and other pigments ($\leq$1.5 mg m^{-3})
C4	500 – 520	Chlorophyll and other pigments ($\geq$1.5 mg m^{-3})
C5	**545 – 565**	**Suspended sediments (away from chlorophyll and Gelbstoff)**
C6	**660 – 680**	**Second chlorophyll absorption, maxima**
C7	**745 – 785**	**O_2 absorption R-branch**
C8	845 - 885	Aero optical thickness

4.2.2. Software used

In order to develop the contrast enhancement algorithms for automatic shoreline detection, suspended sediment transport and Land Use and Land Cover (LULC) assessment, the present study used Earth Resources Data Analysis System (ERDAS) Imagine 9.2, a digital image processing software, ArcGIS 9.3, a GIS software and Digital Shoreline Analysis System (DSAS) 4.2, a GIS tool for shoreline change rate analysis and MATLAB R2013a used for develop program codes for contrast enhancement algorithms.

ERDAS IMAGINE is the image processing software, which is designed for the purpose of accessing, interpreting, and analyzing multispectral satellite imagery. It has a wide range of features for enhancing and manipulating large number of image files. It also enables to develop new models for satellite image processing based on earth applications. ERDAS Imagine includes an innovative set of tools for extraction of earth surface features and allows geospatial data layers to be created and maintained through the use of remotely sensed imagery. In ERDAS Imagine, satellite remotely sensed imagery and geospatial data of all categories' Earth application can be analyzed to produce GIS-ready mapping.

GIS is an information system that used to store, retrieve, manipulate and analyse geographically referenced or geospatial data. DSAS is a GIS software tool, used to calculate the rate-of-change statistics from multiple significant shoreline positions (Thieler et al. 2005). DSAS computes the shoreline movement and its changes through statistical methods such as End Point Rate (EPR), Linear Regression Rate (LRR), Net Shoreline Movement (NSM), Weighted Linear Regression Rate (WLR), Shoreline Change Envelope (SCE), Least Median of Squares (LMS) and Jackknife (J). The SCE and NSM reports a distance not a rate. The SCE represents the total change in shoreline movement for all available shoreline positions and is not related

to their dates. The NSM is associated with the dates of only two shorelines. The NSM represents the total distance between the oldest and youngest shorelines. The EPR is calculated by dividing the distance of shoreline movement by the time elapsed between the oldest and the most recent shoreline. A LRR can be determined by fitting a least-squares regression line to all shoreline points for a particular transects. WLR, more reliable data are given greater emphasis or weight towards determining a best-fit line. In the LMS method the median value of the squared residuals is used instead of the mean to determine the best-fit equation for the line.

4.3. Automatic Shoreline Detection and Analysis

The present study was carried out with a view to develop an automatic shoreline detection algorithm using clipped histogram equalization (CHE) for enhancing coastal objects and edges and thresholding techniques to separate water and land regions. Geometrically corrected and orthorectified band 4 (NIR) grey scale 8-bit (intensity value range between 0 and 255) IRS P6 LISS–III (2005, 2007, 2010) and IRS R2 LISS–III (2013) pre-monsoon (January to May) remotely sensed satellite data sets were considered for shoreline detection and analysis. At near infrared (NIR) wavelength region water appears dark because of its strong absorbance and areas with mainly vegetative or exposed soil appear brighter in the image because of their strong reflectance. The complete algorithm of automatic shoreline detection is shown as flow chart in Figure. 4.1.

4.3.1. CHE-based Contrast Enhancement Method

To improve the sufficient intensity contrast between the land and water regions and to avoid the complexity in detecting shoreline edges form satellite images a CHE-based contrast enhancement has been developed. CHE-based techniques were more suitable and efficient for contrast enhancement and brightness preservation of the satellite images, as discussed earlier in section 3.6.2.

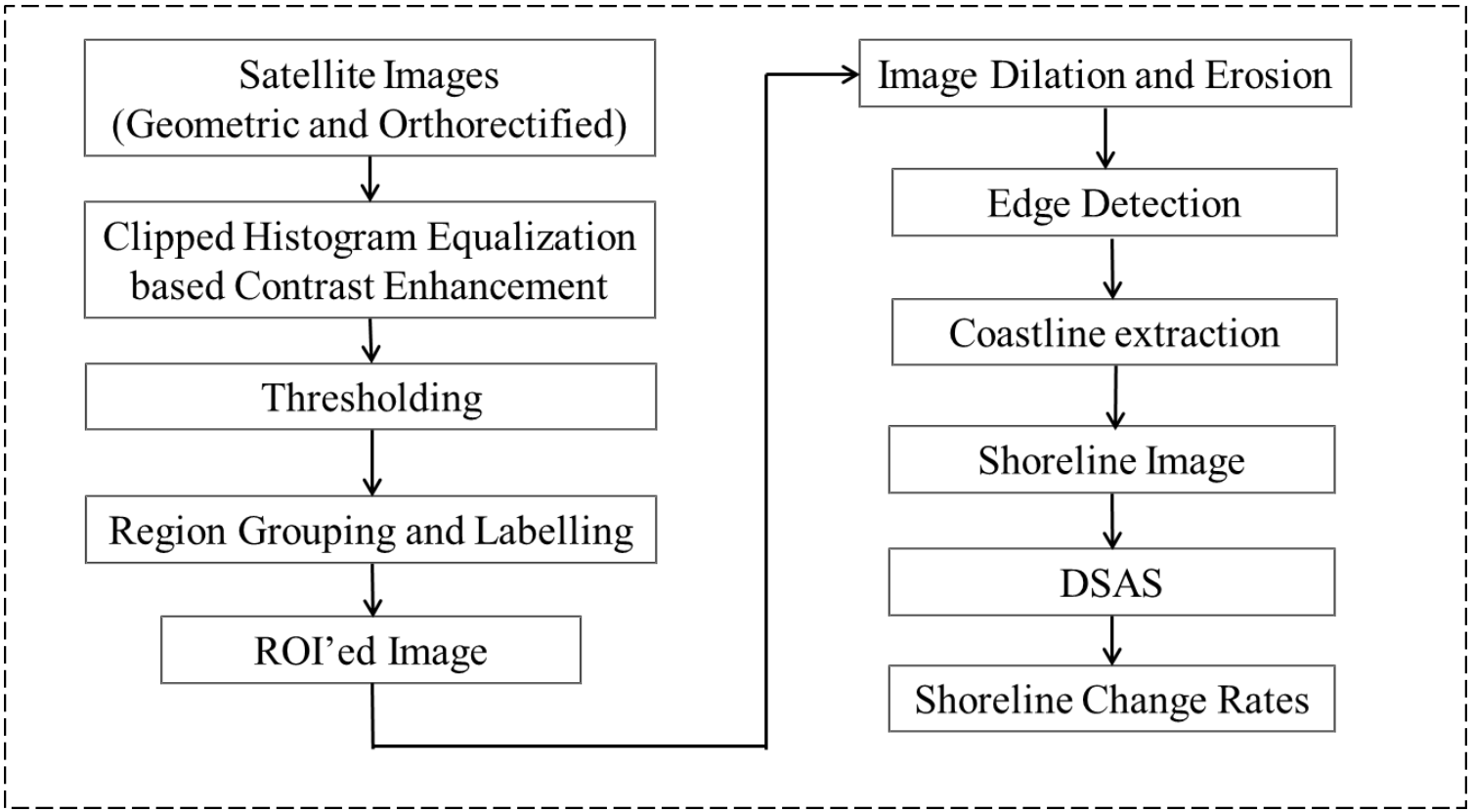

Figure 4.1. Flow chart of automated shoreline extraction algorithm from satellite image

4.3.1.1. Clipped Histogram Equalization

Generally, in histogram equalization (HE) methods, the enhancement rate was proportional to rate of cumulative density function *c(x)*. Control the enhancement rate by limiting the value of *p(x)* or *h(x)* (Pizer et al. 1990) as shown in equation (4.1).

$$\frac{d\ c(x)}{dx} = p(x) \qquad (4.1)$$

Here, *p(x)* and *h(x)* are probability density function and histogram of intensity '*x'*, respectively for a given image 'X'. A CHE method restricted the enhancement rate to overcome the drawbacks of HE method by reducing or increasing the value in histogram's bins based on a threshold limit before equalization of the histogram. The histogram was clipped with threshold or plateau or clipping limit and in the cases of dark images; the clipped portion was redistributed back into the histogram where brightness preservation was more essential. In CHE method, the threshold operation was performed based on selected threshold value '*T*', if the value of histogram of an image *P(K)* greater than *T*, then it shifted to equal *T* (Pratt 1978), otherwise the value of histogram was unchanged. The plateau histogram of an image $P_T(k)$ was computed as;

$$P_T(k)\begin{cases} P(k) & P(k) \le T, \\ T, & P(k) > T, \end{cases} \qquad (4.2)$$

Where, '*k*' represents the gray level of an image, *0≤ k ≤ 255* for 8-bit data. Then, the cumulative histogram of an image $F_T(k)$ was calculated as given in equation 4.3 and 4.4;

$$F_T(k) = \sum_{j=0}^{k} P_T(j) \qquad 0 \le k \le 255 \qquad (4.3)$$

$$D_T(k) = \left\lfloor \frac{255.F_T(k)}{F_T(255)} \right\rfloor \qquad (4.4)$$

Where, $D_T(k)$ was the value of '*k'* after enhancement, and ⌞⌟ represents truncation to the next lower integer. While *T* equals to 1, the enhancement algorithm was histogram projection, and while *T* equals to $P_{max}(k)$, it was histogram equalization.

4.3.1.2. CHE-based Contrast Enhancement Method

The histogram *h(x)* of single band (8-bit) remotely sensed satellite image *X(i,j*), was obtained, for $0 \leq x \leq L-1$. Histogram *h(x)* of the input image, filtered by using a median filter of 3-neighbour (i.e. a median filter of size 1X7 pixels), to reduce the fluctuation and also to remove the empty bins inside the histogram. A new congregation histogram $\{h(x) \mid 0 \leq x \leq J\}$ was found based on non-empty bins of filtered histogram. Where, *J* is the number of non-zero units. The filtered histogram was fragmented into two sub-histograms, X_L and X_U using mean of filtered histogram intensity, X_m, according to equation 4.6 and 4.7;

$$X = X_L \cup X_U \qquad (4.5)$$

Where,

$$X_L = \{X(i,j) | X(i,j) \leq X_m, \forall X(i,j) \in X\} \qquad (4.6)$$

and

$$X_U = \{X(i,j) | X(i,j) > X_m, \forall X(i,j) \in X\} \qquad (4.7)$$

The sub-histograms created from X_L and X_U were denoted as h_L and h_U respectively

Local maximum values of $h_L(x)$ *and* $h_U(x)$ were identified by applying differential operation to $h_L(x)$ *and* $h_U(x)$ as given in equation (4.8) and (4.9);

$$h'_L(x)=h_L(x)-h_L(x-1), \quad for \ \ 1 \le x \le J \tag{4.8}$$

$$h'_U(x)=h_U(x)-h_U(x-1), \quad for \ \ 1 \le x \le J \tag{4.9}$$

A sub-congregation $\{h_L(x_i)\}$ or histogram local maximum values $h_L(x_i)$, were found by using the equations (4.10) and (4.11);

$$|h'_L(x)|<min\{|h'_L(x-1)|,|h'_L(x+1)|\} \tag{4.10}$$

$$h'_L(x-1)>0,\ h'_L(x+1)<0 \tag{4.11}$$

Where, $0 \le x \le J,\ 1 \le i \le N_{Lmax}$ and N_{Lmax} is the number of local maximum values. Mean $h_{Lk,}$ was derived from sub-congregation $\{h_L(x_i) |\ k \le i \le N_{Lmax}\}$. Then, the evaluated $h_{Lk,}$ was the plateau threshold value (i.e. T_L) for first sub-histogram and same procedure followed for another sub-histogram and found T_U. The threshold values of sub-histograms h_L and h_U were T_L and T_U respectively.

The sub-histograms were modified using threshold operation as shown in equation (4.12) and (4.13). The modified histogram $h_{mod}(x)$ with the threshold value is,

$$h_{Lmod}(x) = \begin{cases} h_L(x), & for \ \ h_L(x) \le T_L \\ T_L, & otherwise \end{cases} \tag{4.12}$$

$$h_{Umod}(x) = \begin{cases} h_U(x), & for \ \ h_U(x) \le T_U \\ T_U, & otherwise \end{cases} \tag{4.13}$$

Probability Density Functions (PDF's) of $h_{Lmod}(x)$ *and* $h_{Umod}(x)$ were calculated and then cumulative density functions (CDF), $c_L(x)$ and $c_U(x)$, were determined from the PDFs. From the transformation function, $f(x)$, the output contrast enhanced image was obtained according to the equations (4.14) and (4.15);

$$f_L(x) = \left\lfloor \frac{(L-1).cL(x)}{cL(L-1)} \right\rfloor \quad (4.14)$$

$$f_U(x) = \left\lfloor \frac{(L-1).cU(x)}{cU(L-1)} \right\rfloor \quad (4.15)$$

The segmented sub-histograms were independently equalized based on corresponding transform functions. The output image (Y), was expressed as shown in equation (4.16), (4.17) and (4.18).

$$Y=\{Y(i,j)\}= f_L(X_L) \cup f_U(X_U) \quad (4.16)$$

Where

$$f_L(X_L) = \{f_L(X(i,j))|\forall X(i,j) \in X_L\} \quad (4.17)$$

$$f_U(X_U) = \{f_U(X(i,j))|\forall X(i,j) \in X_U\} \quad (4.18)$$

In order to maintain brightness preservation, the image brightness was normalized by calculating mean brightness of the input image M_i and the mean brightness of the output image $M_{o,}$ using equation as shown in (4.19).

$$g(x,y) = \left(\frac{M_i}{M_o}\right) f(x,y) \quad (4.19)$$

Where, *g(x,y)* was the final output image and *f(x,y)* was the output after the equalization process. The developed contrast enhancement method for satellite images is given in Figure 4.2.

4.3.2. Thresholding

Histogram of the contrast enhanced satellite image by using developed clipped histogram equalization method was obtained. Local maximum and local minimum values of this histogram were found using equations 4.8 to 4.11 and calculated the mean (μ) and standard deviation (σ) of local maximum and local minimum values. The combination of mean and standard deviations, (μ+2σ) and (μ-2σ) were treated as maximum threshold value (T_{MAX}) and minimum threshold value (T_{MIN}) respectively. If *f(i,j)* was intensity value of the image pixel at *(i,j)*, and T_{MAX} and T_{MIN} were locally adaptive maximum and minimum threshold values, the output image *g(i,j)* after thresholding operation (equation 4.20) is;

$$g(i,j) = \begin{cases} 0 & \text{if } f(i,j) > T_{MAX} \\ 255 & \text{if } T_{MIN} < f(i,j) > T_{MAX} \\ 0 & \text{if } f(i,j) < T_{MIN} \end{cases} \qquad (4.20)$$

The pixels with intensity value higher than the maximum threshold value were coded as '0' (land), the pixels intensity between the minimum and maximum threshold values were coded as '255' (sand) and the pixels with intensity value lower than minimum threshold value were coded as '0' (water).

4.3.3. Region Grouping and Labelling

After the thresholding operation, only land (255) and water (0) pixels were presented in the image and all contiguous land and water regions were grouped using region grouping. Based on size, position and geometric shape of each image object was labelled.

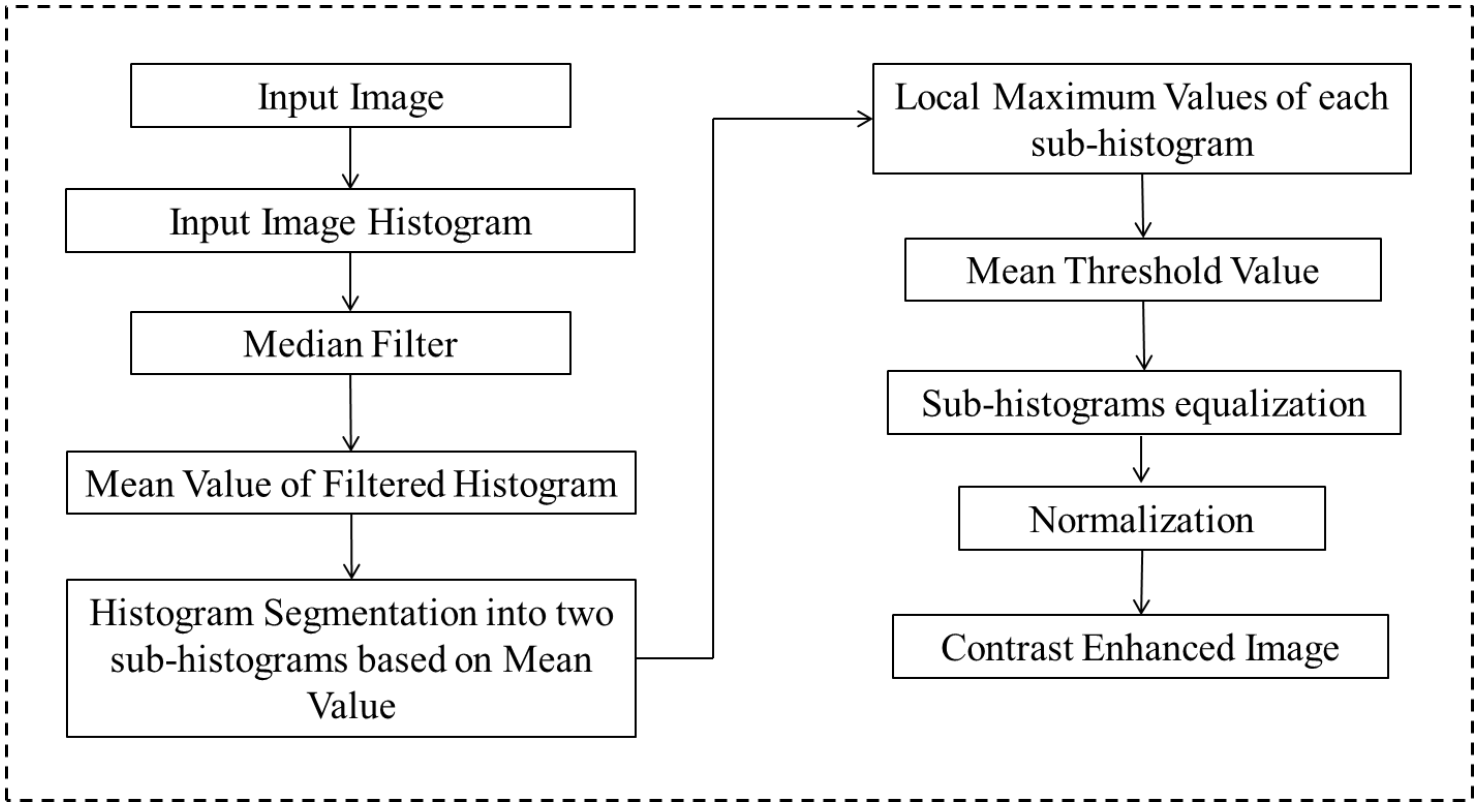

Figure 4.2. Flow chart of Contrast Enhancement method based on Clipped Histogram Equalization (Raju et al. 2014)

Region grouping and labeling was performed based on a ‘grass fire’ concept, where the image was scanned in a row-wise manner, and a ‘fire’ was set at the first pixel of an image object. The ‘fire’ spreads to all pixels to four or eight-neighborhood of the current pixel. The propagation of fire was continued repetitively until all pixels of the image were labelled and fire was turned off after all the objects in the image were labelled. After region grouping and labelling, the water pixels coded as 0s were grouped and labelled as individual image objects and similarly, the land pixels coded as 255s were also grouped and labelled as individual image objects.

4.3.4. Region of Interest

After thresholding and region groping and labelling processes, only two large continuous land and ocean objects were appeared in the image. The small image objects (wetlands, lakes, stream, shadows or image noise), which do not belong to true shoreline were presented on the land areas were removed by Region of Interest (ROI) method and these objects were merged into land region. Due to floating ice, ships, ocean facilities and image noise, small objects were identified on the ocean areas, which were not fit in to ocean areas, were removed by using ROI and dissolved into ocean region.

4.3.5. Image Dilation and Erosion

The most widely used morphological image processing operations for the binary image includes image erosion and dilation (Serra 1982, Parker 1997). Morphological operations add or remove the pixels based on the pattern of neighboring pixels from the binary image. Every operation was performed on each pixel in the input image using the original pattern of pixels. Erosion operation removed the pixels from objects in an image, which should not belong to that objects. Due to thresholding operation, pixels fall into the brightness range of interest, but because of noise few pixels may

not lie within large regions with that brightness values. Erosion operation entirely removed extraneous pixels representing point noise or line defects because these defects were normally only 1 or 2 pixels wide.

In place of removed pixels from objects, a balancing operation called as dilation used to add pixels. The standard dilation operation, similar to image erosion, was to add background pixel which touched another pixel that was already part of a foreground region. Image dilation increased dimensions of objects and merged features because of adding a layer of pixels around the boundary of image features and regions. Erosion operation reduced the size of image regions, because of removing the pixels from the regions or objects and dilation increased the size of regions, by adding the pixels to the edges of features or regions. Unwanted pixels removed by erosion caused a decreasing of the features and followed the erosion with dilation, added pixels around the feature margin, so that the dimensions of the features were restored. Dilation immediately followed by erosion operation was used to make the shoreline morphologically smoother by generalizing the jagged boundaries of the image objects.

4.3.6. Edge Detection

The Robert's edge detector is one of the oldest, simple, quick to compute and efficient edge detectors in digital image processing. It computes 2-D spatial gradient on the image and it highlights regions of high spatial frequency, which frequently correspond to the edges. Input and output images to this operator are gray scale images. Pixel values at each point in the output image signify the assessed absolute magnitude of the spatial gradient of the input image at that point. The smoothed shoreline after image erosion and dilation operations was detected with Robert's edge detector, and finally, continuous and smoothed shoreline was highlighted.

The detected continuous shoreline was outlined and converted into vector map. The shoreline vector maps of IRS-P6 LISS III (2005, 2007 and 2010) and IRS-R2 LISS III (2013) were generated and transferred to GIS environment as a shape file for further processing and shoreline change analysis. Digital Shoreline Analysis System (DSAS), A GIS software tool was used to calculate the rate of shoreline movement and changes. For efficient and detailed shoreline change rate analysis, the study area was divided into two regions namely, Mulky-Pavanje rivermouth area and Netravati-Gurpur rivermouth area.

4.3.7. Digital Shoreline Analysis System

DSAS was the predominant analytical tool used to analyze platform changes of shoreline position and it computes the rate of change statistics for a time series of shoreline vector data (Himmelstoss 2009). Delineated shorelines were transferred to DSAS to calculate the rate of shoreline movement and its changes from 2005 to 2013.

In Mulky-Pavanje rivermouth area, baseline was constructed 400 m distance on landward side by taking 2013 shoreline as a reference and total 318 transects were generated with 20 m spacing along 6 km stretch of the study area. In Netravati-Gurpur rivermouth area, baseline was drawn on landward side with 300 m distance from 2013 shoreline and total 800 transects were generated along 16 km stretch with an interval of 20 m.

Shoreline change rates were estimated using two statistical approaches namely, End Point Rate (EPR) and Linear Regression Rate (LRR). The EPR was calculated by dividing the distance of shoreline movement by the time elapsed between the earliest and latest measurements at each transect and LRR was used to express the long-term shoreline change rates.

4.4. Suspended Sediment Transport

The knowledge of sediment transport and the distribution of sediments along the coast is essential for coastal zone management due to the adverse effects like siltation of harbours, accumulation of sand bars to create navigational hazards, seasonal blockage of estuaries or degradation of coastal environment. Regular study of sediment dynamics by conventional point measurements using ships or boats are limited due to extremely poor spatial coverage that too for a particular time and very high cost of conducting such surveys. Ocean colour sensors onboard satellites provide synoptic view, high repetitive and are excellent tools to map and monitor sediment patterns, assess relative changes in sediment concentrations and retrieve sea surface velocities using multi-temporal remotely sensed satellite images (IOCCG 2000, Garcia and Robinson 1989).

In coastal applications, it is very difficult to study turbidity pattern and sediment plumes along the coast using low resolution remote sensing images. Digital Image enhancement techniques enhance contrast among features for better detection of costal geomorphic units, underwater bed flow structures and mapping of sediment plumes to understand the distribution and concentration of suspended and settled sediments.

In the present study, an image enhancement technique was developed using Clipped Histogram Equalization (CHE) based contrast enhancement and Principle Component Analysis (PCA) methods to map suspended sediment transport and its distribution along Mangalore Coast, West Coast of India. The complete methodology of developed algorithm for sediment transport is shown as flow chart in Figure 4.3.

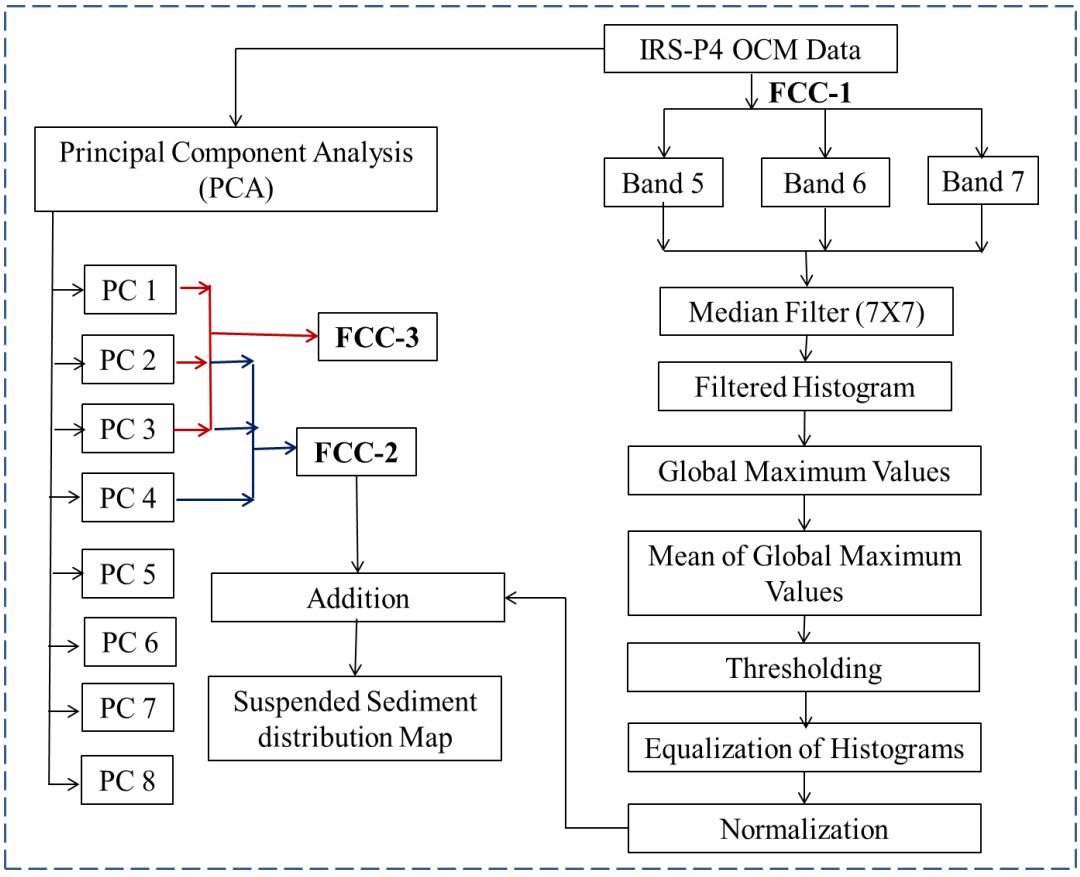

Figure 4.3 Flow chart of contrast enhancement technique developed for suspended sediment distribution in the study area

4.4.1. Clipped Histogram Equalization based Contrast Enhancement

The digital satellite data in all the 8 bands of IRS-P4 Oceansat-2 OCM were acquired for 2013 from the National Remote Sensing Centre (NRSC), Hyderabad, India, to map sediment transport along the study area. Clipped histogram equalization based contrast enhancement algorithm was developed to control over-enhancement of satellite image and to detect coastal features to map sediment plumes without introducing any additional noise.

4.4.1.1. False Colour Composition

False Colour Composition (FCC)-1 of IRS-P4 OCM 2013 image with band 5(R), band 6(G) and band 7(B) was generated. Band 5, band 6 and band 7 were selected based on the specifications of OCM sensor in recording suspended sediments as presented in Table 4.4. The grey scale images of all three bands (5, 6 and 7) histograms were produced individually and filtered using median filter (7X7) to reduce the fluctuation and also to remove the empty bins from the histograms. The filtered histograms were produced without zero bins, which creates noise in the image and the filtered histograms were further processed for identification of threshold value.

4.4.1.2. Identification of Threshold Value

Global maximum values of filtered histograms *f(i,j)* of three bands (5, 6 and 7) were identified. Means of the set of global maximum values of each band were calculated and then, the measured mean values were treated as threshold values (*T*) or clipped values. The threshold value 'T_1' of *band 5*, 'T_2' of *band 6 and* 'T_3' of *band 7* were considered for thresholding operation.

4.4.1.3. Thresholding

If the value of the filtered histogram of the image *f(i,j)* was greater than threshold value 'T_X' then it would be shifted to T_X, otherwise it would be unchanged. The clipped histogram of an image *g(i,j)* was computed through thresholding operation according to the equation (4.21);

$$g(i,j) = \begin{cases} T_X & if\ f(i,j) > T_X \\ f(i,j) & if\ f(i,j) < T_X \end{cases} \qquad (4.21)$$

Thresholding operations of filtered histograms of three bands (5, 6 and 7) are given in equations 4.22, 4.23 and 4.24 respectively.

$$g_5(i,j) = \begin{cases} T_1 & if\ f_5(i,j) > T_1 \\ f_5(i,j) & if\ f_5(i,j) < T_1 \end{cases} \quad (4.22)$$

$$g_6(i,j) = \begin{cases} T_2 & if\ f_6(i,j) > T_2 \\ f_6(i,j) & if\ f_6(i,j) < T_2 \end{cases} \quad (4.23)$$

$$g_7(i,j) = \begin{cases} T_3 & if\ f_7(i,j) > T_3 \\ f_7(i,j) & if\ f_7(i,j) < T_3 \end{cases} \quad (4.24)$$

If, $f_5(i, j)$, $f_6(i, j)$ and $f_7(i, j)$ were filtered histogram of satellite image $X(I,j)$, then, $g_5(i, j)$, $g_6(i, j)$ and $g_7(i, j)$ were modified histograms of three bands (5, 6 an d7) respectively. T_1, T_2 and T_3 were threshold values of band 5, band 6 and band 7 filtered histograms respectively.

4.4.1.4. Equalization

The Probability Density Functions (PDFs) of $g_5(i, j)$, $g_6(i, j)$ and $g_7(i, j)$ were found and then Cumulative Density Functions (CDFs) ($c(x)$) were determined from these PDFs. The transformation function, $y(x)$ was obtained for the contrast enhanced satellite image from the equation (4.25);

$$y(x) = \frac{(L-1).c(x)}{C(L-1)} \quad (4.25)$$

4.4.1.5. Normalization

In order to maintain brightness preservation in the contrast enhanced image, the image brightness was normalized by calculating mean brightness of the input image

'*Mi'* and the mean brightness of the output image '*Mo'*, using equation as shown in (4.26);

$$g(x,y) = \left(\frac{M_i}{M_o}\right) f(x,y) \qquad (4.26)$$

Where, *g(x,y)* was the final output image and *f(x,y)* was the output contrast enhanced image after the equalization process.

4.4.2. Principal Component Analysis

Principal Component Analysis (PCA) was also computed for IRS-P4 OCM data to reduce the dimensions of data without loss of information and to achieve enhancement of the image. Based on principal of PCA, most of the information was quantified in the first three components of PCA including PC1, PC2 and PC3. PC5, PC6, PC7 and PC8 were not indicated any information of the coastal objects and presented noise in the image. Principal Components PC1, PC2, PC3 and PC4 were considered for identification of sediment distribution and PC5, PC6, PC7 and PC8 were not considered because of significant noise. PC1 image shown maximum variance contained features like islands, creeks, spits etc. and PC2 image mainly highlighted dispersion and distribution of suspended sediments along the coast. The PC3 image displayed bedload features, current movements, mangroves etc. and PC4 image presented coastal geomorphic features. The principal component images of IRS-P4 OCM data are shown in Figure 4.4.

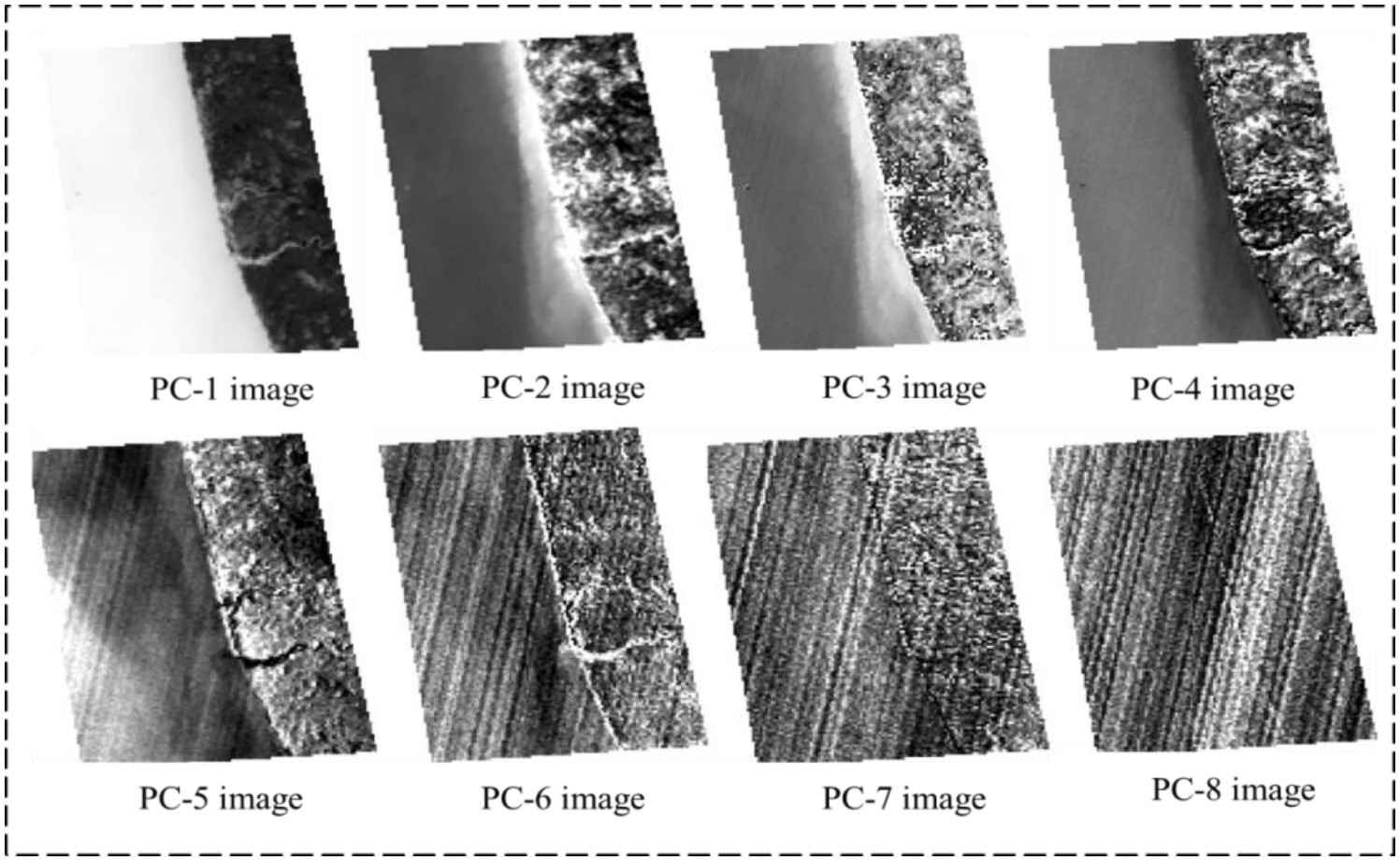

Figure 4.4. Principal component images of IRS-P4 OCM data of the study area

4.4.2.1. False Colour Composite Images

From the principal component images, PC1, PC2, PC3 and PC4 two False Colour Composite (FCC) images were produced for mapping sediment distribution. FCC-2 was generated using PC2, PC3 and PC4 images and FCC-3 was created using PC1, PC2 and PC3. FCC-3 did not show any significant distribution of sediment in the study area because of maximum variance in PC1 image. FCC-2 had shown substantial changes in sediment movement and hence, considered for further analysis.

FCC-2 image was highlighted sediment movements clearly and improved the contrast of image. FCC-2 image was added with normalized contrast enhanced image for better mapping of sediment movements and coastal features in the study area. The directions of sediment distribution were mapped on output image generated from FCC-2 and normalized contrast enhanced image.

For qualitative analysis of SSC, previous results of *in-situ* and satellite data analysis by Dwarakish et al., 2010 and Avinash et al., 2012 for Mangalore Coast, West Coast of India were considered. The sampling stations of these data sets are presented in Table 4.5.

Table 4.5. *In-situ* and OCM retrieved SSC data during Post-Monsoon

Date of In-situ data collection and satellite over pass	**Station**	**Measured SSC (mg/l)**	**OCM retrieved SSC (mg/l)**	**Author**
Netravati – Gurpur Rivermouth				
November 11, 1999 (Post-Monsoon)	2	20	15	Dwarakish et al. 2010
	4	28	28	
	5	28	28	
	6	31	24	
	7	27	24	
	10	16	14	
	11	18	15	
	16	38	29	
October 7, 2003 (Post-Monsoon)	1	35.44	37.12	Avinash et al. 2012
	6	24.15	25.87	
	11	11.14	11.52	
February 5, 2003 (Summer)	1	6.77	6.32	
	6	4.44	4.87	
	11	312	3.06	
Mulky-Pavanje Rivermouth				
October 7, 2003 (Post-Monsoon)	2	29.12	31.04	Avinash et al. 2012
	7	17.13	17.89	
	12	8.82	7.99	
February 5, 2003 (Summer)	2	7.1	7.01	
	7	4.04	4.36	
	12	2.84	3.14	

4.5. Land Use and Land Cover Assessment

Land use and land cover monitoring scenarios using remotely sensed satellite data are becoming more prevalent in remote sensing applications. LULC mapping from multi-spectral satellite image data was based on spectral differences in land cover categories. Since only a limited number of land cover types are desired in most cases, the images contain redundant information which is unnecessarily complicates the digital mapping process. To improve the accuracy assessment of LULC classification and to avoid the complexity in classifying the mixed pixel, the present study developed a new clipped histogram equalization based algorithm for LULC classification.

Monitoring of LULC changes along Mangalore Coast is essential due to increase in trend on industrialization and urbanization, because of its rich ocean resources and favorable conditions for harbor and ports. Continuous expansion of NMPT port creates setting up major industries like MRPL, MCF, BASF India Limited, KIOCl, industrial estate at Baikampagy and improved transportation facilities are the major driving forces for the rapid urbanization along Mangalore Coast. Rapid urbanization and industrialization leads environmental consequences and changes in land use and land cover. For proper urban planning, land and water resources management, LULC monitoring is required.

4.5.1. Clipped Histogram Equalization based Contrast Enhancement

In the present study, a clipped histogram equalization based contrast enhancement method was employed for LULC mapping from satellite images and to improve accuracy of classification of LULC mapping. Indian Remote Sensing- Resourcesat-2 (IRS-R2) LISS III 2013 23.5 m resolution image was considered for LULC mapping and assessment.

4.5.1.1. Principal Component Analysis

PCA performed to geometrically correct and orthorectified IRS-R2 LISS III 2013 image and based on number of bands (4 band) of LISS III 2013 image, four principal component images viz., PC1, PC2, PC3 and PC4 were generated. The histograms of each principal component (PC1, PC2, PC3 and PC4) were obtained individually. The global means of each histogram were calculated and these global means were treated as threshold values of histograms for clipping operation.

Thresholding operation was performed to histogram of each principal component based on the global mean values. If the histogram value was less than the global mean value, then histogram grey level was clipped to global mean value else no change in the histogram grey-value according to the equation 4.21. The modified histogram, after the thresholding operation was produced. The modified histogram was equalized using Probability Density Functions (PDFs) and Cumulative Density Functions (CDFs) of this modified histogram. PDFs of modified histogram were calculated and then, CDFs (*c(x)*) were determined from these PDFs. The transformation function *y(x)* based on CDFs was executed to obtain contrast enhanced image from equation 4.26.

The contrast enhanced images of three principal component images (PC1, PC2, PC3 and PC4) were layer stacked and False Colour Composite (FCC) image was generated for better visual interpretation, mapping and classification of earth surface features presented in the image. From FCC image, LULC was mapped using supervised classification with Maximum Likelihood Classifier (MLC).

4.5.1.2. General Classification Method

A FCC image was generated from geometrically corrected and orthorectified IRS-R2 LISS III 2013 4 band satellite image and classified using supervised classification

with Maximum Likelihood Classifier (MLC) method, which was called as general method. The complete methodology of LULC assessment is presented in Figure 4.5.

After the classification of images from developed and general methods, the accuracy assessment was performed to find the accuracy of classification. The output of the developed contrast enhancement method was compared with the results obtained from the general method through accuracy assessment and Kappa coefficient values.

Six types of features were identified in the study area and classified the features accordingly using satellite images. For better and efficient analysis, the study area of Mangalore Coast, West Coast of India was divided into three regions namely, Mulky-Pavanje (M-P) rivermouth area, New Mangalore Port Trust (NMPT) area and Netravti-Gurpur (N-G) rivermouth area.

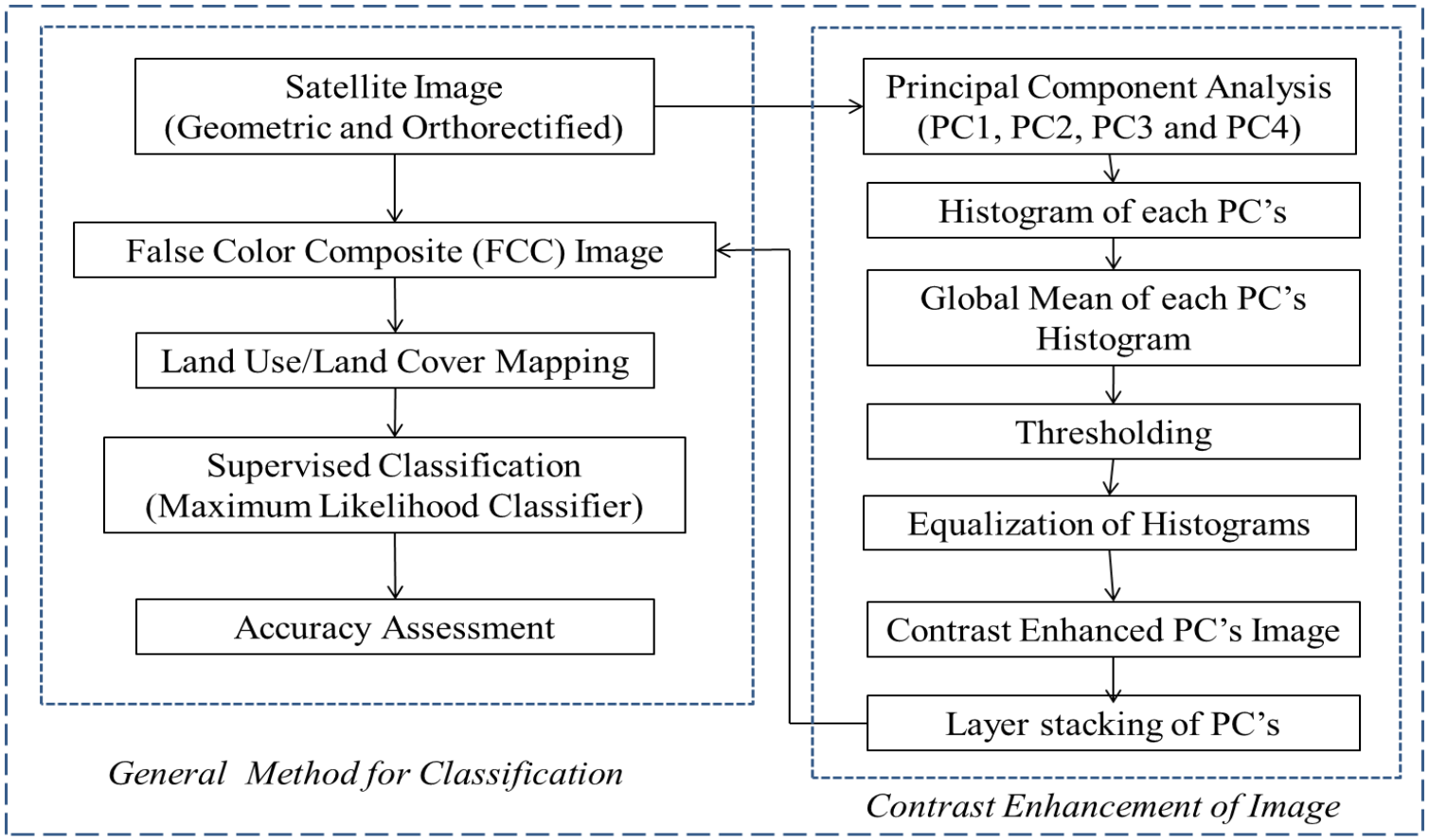

Figure 4.5. Flowchart of Land Use and Land Cover assessment algorithm from the satellite image

CHAPTER 5
RESULTS AND DISCUSSION

5.1. General

Monitoring of coastal processes like, shoreline change, suspended sediment transport and land use and land cover changes in coastal region is necessary for the understanding and management of the coastal environment in sustainable manner. Conventional investigation involves hard field work to study coastal processes for large study areas. Though conventional approach provides accurate measurement, it is costly, time consuming and involves additional manpower. The image processing techniques of remotely sensed data provides efficient results which are cost effective and faster, and also useful for continuous and efficient study of coastal regions in regular interval, resulted in accurate planning and management of coastal zones. The coastal processes including shoreline detection and change analysis, suspended sediment transport and land use and land cover assessment are studied using satellite image by adopting image processing techniques and the results of the same are discussed in this chapter.

5.2. Automatic Shoreline Detection and Analysis

The developed Clipped Histogram Equalization (CHE) based contrast enhancement and thresholding based automatic shoreline detection has been used to extract the shorelines from IRS-P6 LISS III (2005, 2007 and 2010) and IRS-R2 LISS III (2013) satellite images. Shoreline change rates are analysed using Digital Shoreline Analysis System (DSAS) through End Point Rate (EPR) and Linear Regression Rate (LRR) statistical methods. The present study concentrated on shoreline changes in and around of two rivermouth areas within the study area namely Mulky-Pavanje

rivermouth area and Netravati-Gurpur rivermouth area, for better and efficient analysis (Section 1.11.1.1 and section 1.11.1.2).

5.2.1. CHE-based Contrast Enhancement Method

Clipped histogram equalization methods control the enhancement rate and provide good contrast enhancement and brightness preservation, by clipping the high intensity of the histogram regions using properly selected threshold value. The developed CHE method has regulated noise, due to filtering the input image histogram using median filter and removed the empty bins from the histogram. The mean threshold value calculated from local maximum values of two sub-histograms has shown good contrast enhancement. Normalization of the equalized histogram has provided good brightness preservation in the output image.

The experimental results of developed CHE method has compared with existing methods such as HE, BBHE, MMBEBHE, DHE, BHEPL and SAPHE using image quality measures. The image quality measures including Peak-Signal to Noise Ratio (PSNR) and Absolute Mean Brightness Error (AMBE) are obtained for two different test satellite images IRS-P6 LISS III (2005 and 2010). The contrast enhanced 2005 and 2010 images for above methods are shown in Figure 5.1 and Figure 5.2 respectively and the PSNR and AMBE values are provided in Table 5.1.

For both satellite images, Histogram Equalization (HE) has shown over enhancement due to uniform distribution of intensity values and less brightness preservation (AMBE: *86.29, 93.14*) and low contrast enhancement (PSNR: *24.43, 25.01*). Brightness Preserving Bi-Histogram Equalization (BBHE) has introduced additional noise due to over-enhancement and shown low contrast enhancement and brightness preservation as presented in Figure 5.1(c) and Figure 5.2(c). More loss of information in the output images and the PSNR and AMBE values are *50.65, 42.25* for 2005

image and *59.71, 34.06* for 2010 image respectively has been observed. Minimum Mean Brightness Error Bi-Histogram Equalization (MMBEBHE) method also produced low contrast enhancement and brightness preservation as seen in Figure 5.1(d) and Figure 5.2(d) and corresponding PSNR and AMBE values are *50.28, 49.30* for 2005 image and *58.22*, *39.09* for 2010 image respectively.

Dynamic Histogram Equalization (DHE) has not shown proper contrast enhancement and introduced annoying noise in the image and resulted in less brightness preservation and huge information loss in the image as shown in Figure 5.1(e) and Figure 5.2(e). DHE has controlled over-enhancement in the image due to multi segmentation of input image histogram, but introduced more unwanted noise. The PSNR and AMBE values of 2005 image are 26.84 and 58.85 and, 2010 image are 17.58 and 32.69 respectively, shows good contrast enhancement and less brightness preservation.

Bi-Histogram Equalization Plateau Limit (BHEPL) have shown better contrast enhancement (PSNR: *39.53* and *47.09*) and brightness preservation (AMBE: *16.22* and *13.79*) for both the images, compared to HE, BBHE, MMBEBHE and DHE methods as presented in Figure 5.1(f) and Figure 5.2(f). Self-Adaptive Plateau Histogram Equalization (SAPHE) has given better PSNR and low AMBE values, indicates good contrast enhancement and brightness preservation in the images as dipicted in Figure 5.1(g) and Figure 5.2(g). The PSNR and AMBE vales of 2005 image are 37.81 and 11.64 and, for 2010 image are 43.19 and 9.57. SAPHE has a drawback in detecting local and global maximum values for identifying the median threshold value. Sometimes if it identifies only one local maximum, it will be the global maximum of that histogram.

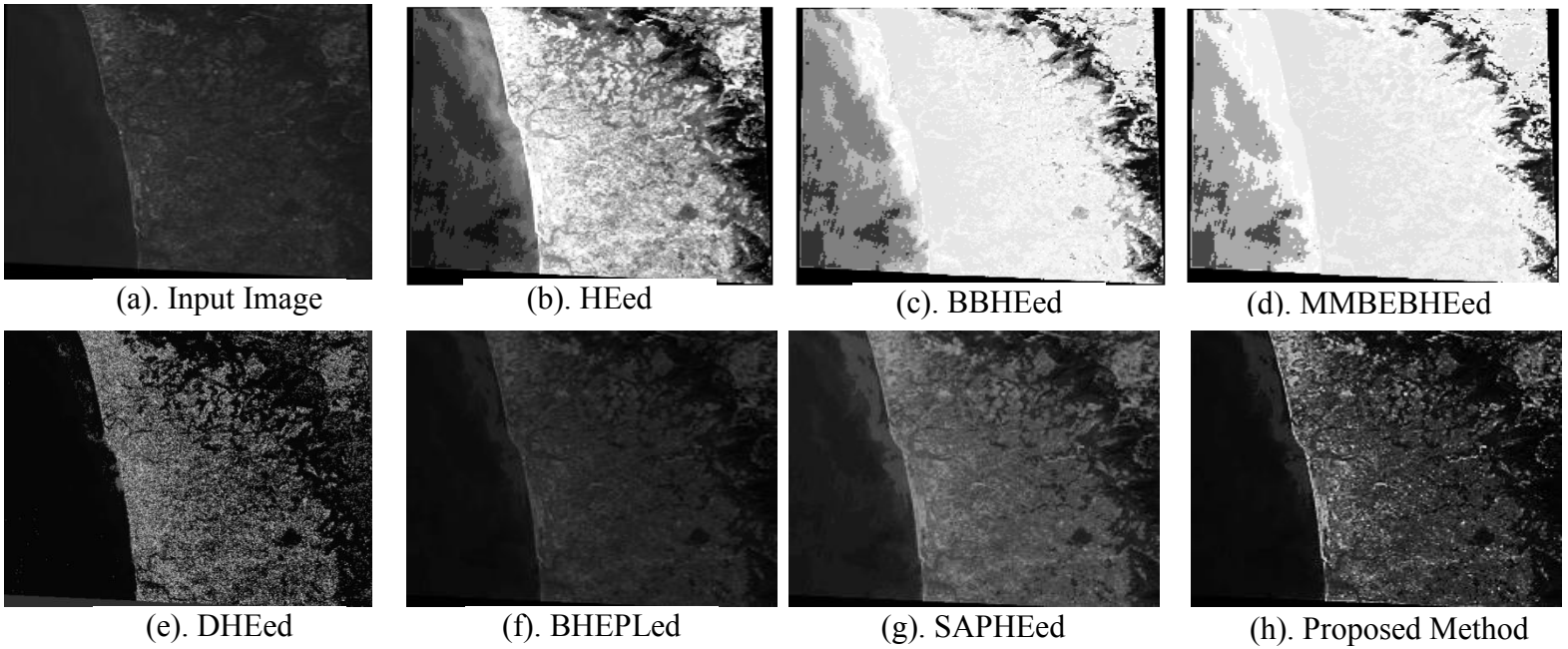

Figure 5.1. Performance comparison of IRS-P6 LISS III 2005 Satellite (single band) image

(a). Original Image, (b). Histogram Equalization (HE), (c). Brightness Preserving Bi-Histogram Equalization (BBHE), (d). Minimum Mean Brightness Error Bi-Histogram Equalization (MMBEBHE), (e). Dynamic Histogram Equalization (DHE), (f). Bi-Histogram Equalization with Plateau Limit (BHEPL), (g). Self-Adaptive Plateau Histogram Equalization (SAPHE) and (h).Proposed Method

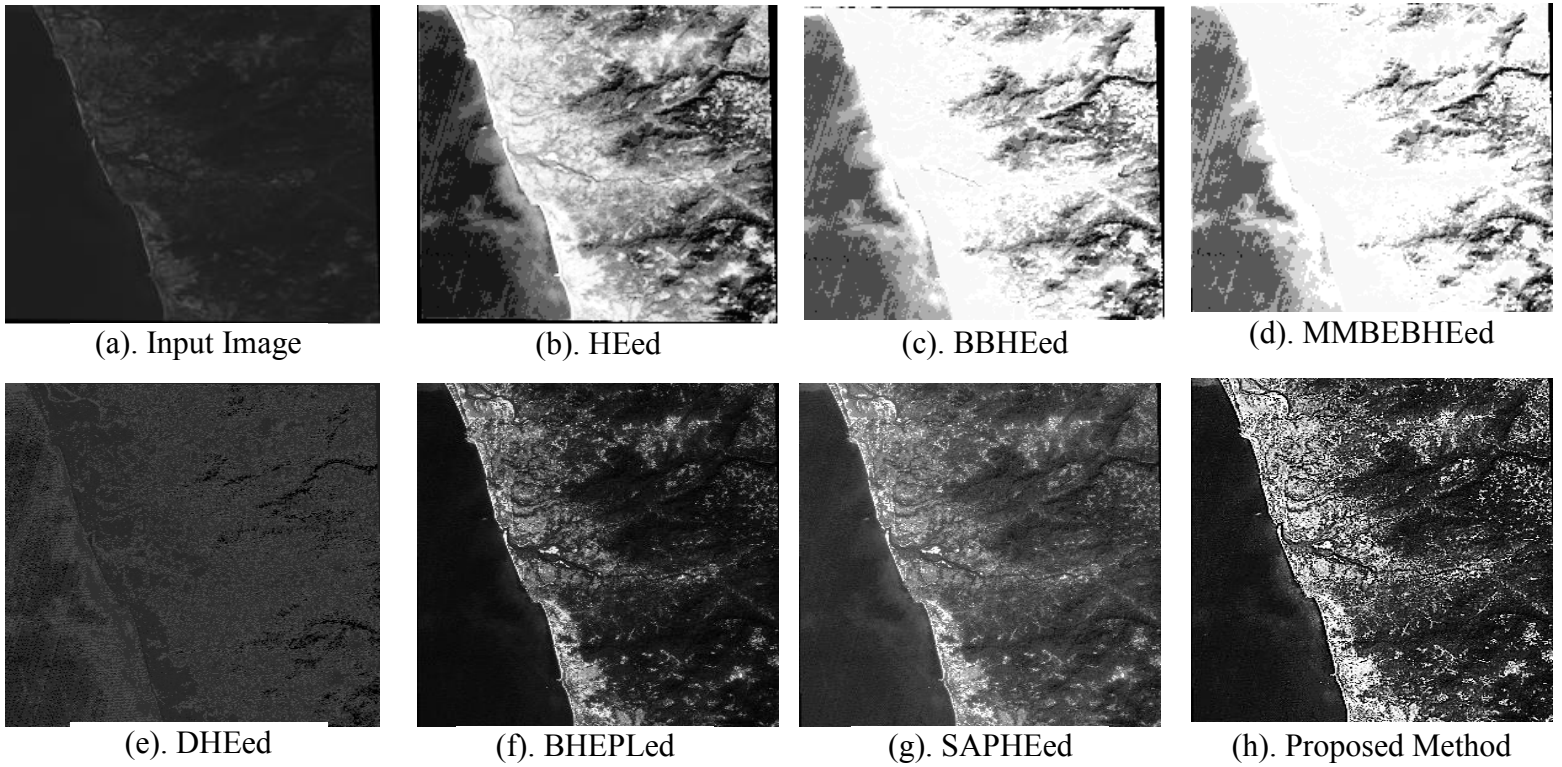

Figure 5.2. Performance comparison of IRS-P6 LISS III 2010 Satellite (single band) image

(a). Original Image, (b). Histogram Equalization (HE), (c). Brightness Preserving Bi-Histogram Equalization (BBHE), (d). Minimum Mean Brightness Error Bi-Histogram Equalization (MMBEBHE), (e). Dynamic Histogram Equalization (DHE), (f). Bi-Histogram Equalization with Plateau Limit (BHEPL), (g). Self-Adaptive Plateau Histogram Equalization (SAPHE) and (h).Proposed Method.

Clipping histogram equalization methods (BHEPL and SAPHE) are shown natural contrast enhancement without over-enhancement and also shown better brightness preservation compared to HE, BBHE, MMBEBHE and DHE. CHE methods are mainly highlighted the bright regions like beach sand, open land without introducing noise and loss of information in the output images. The highlighted bright regions in the image are easy to extract using appropriate thresholding operation. These images are suitable for further extraction of shorelines from the satellite images.

Table 5.1. Assessment of Contrast Enhancement Using PSNR and Brightness Preserving Using AMBE

IQMs / Methods		2005 Image		2010 Image	
		PSNR	*AMBE*	*PSNR*	*AMBE*
Bi-HE	HE	24.43	86.29	25.01	93.14
	BBHE	50.65	42.25	59.71	34.06
	MMBEBHE	50.28	49.30	58.22	39.09
Multi-HE	DHE	26.84	58.85	17.58	32.69
CHE	BHEPL	39.53	16.22	47.09	13.79
	SAPHE	37.81	11.64	43.19	9.57
	Proposed Method	73.92	7.31	68.35	5.91

5.2.2. Automatic Shoreline Detection

The developed automatic shoreline extraction algorithm using clipped histogram equalization and thresholding operation is applied to IRS-P6 LISS-III 2010 (band 4) 23.5 m resolution, of Mangalore Coast, West Coast of India. The complete methodology of automatic shoreline detection process using IRS-P6 LISS III 2010 satellite image is presented in Figure 5.3.

The contrast enhanced image using clipped histogram equalization based method (section 5.1.1) is used for shoreline extraction by thresholding opeartion. The threshold values, in combination of mean (μ) and standard deviation (σ) derived from

local maximum and local minimum values of contrast enhanced image improved efficiency of coastline extraction process. The maximum ($\mu+2\sigma$) and minimum ($\mu-2\sigma$) threshold values are segmented the land and water regions by considering the mixed pixels. The aim of the study is to obtain the maximum positional accuracy of the shoreline and it mainly concentrated on mixed pixels or wet pixels, treated as edge pixels based on their immediate neighbourhood. Image region and labeling, grouped all individual land and water objects into the land and water regions as shown in Figure 5.3(e). Region of Interest (ROI), efficiently removed unwanted objects, which appeared in ocean and land regions and the final image has only black (0) and white (255) regions as seen in Figure 5.3(f). Image dilation and erosion operations are smoothened the boundary lines as shown in Figure 5.3(g). Roberts' edge operator has extracted smooth and continous shoreline and this delineated shoreline is converted into vector-based coastline as shown in Figure 5.3(h).

Automatic shoreline extraction from IRS-P6 LISS III 2010 image of (A) Mulky-Pavanje rivermouth area and (B) Netravati-Gurpur rivermouth areas is shown in Figure 5.4. The extracted shoreline from the developed algorithm is compared with Global Positioning System (GPS) survey values collected during the field visit, synchronized with the day of satellite overpass, i.e. on January 23, 2013 and achieved 96% positional accuracy.

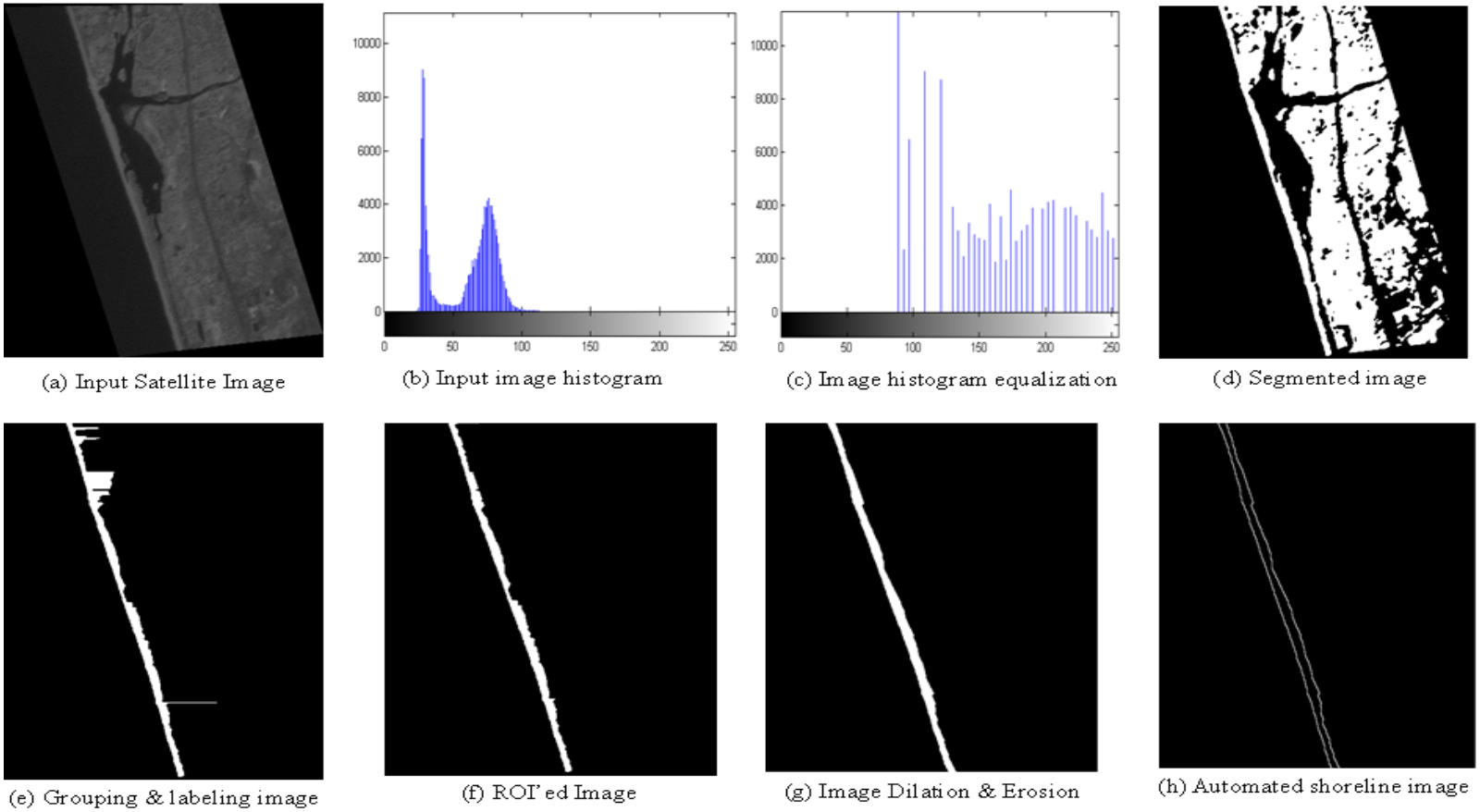

Figure 5.3. The complete methodology of automatic shoreline detection process using IRS-P6 LISS III 2010 satellite image

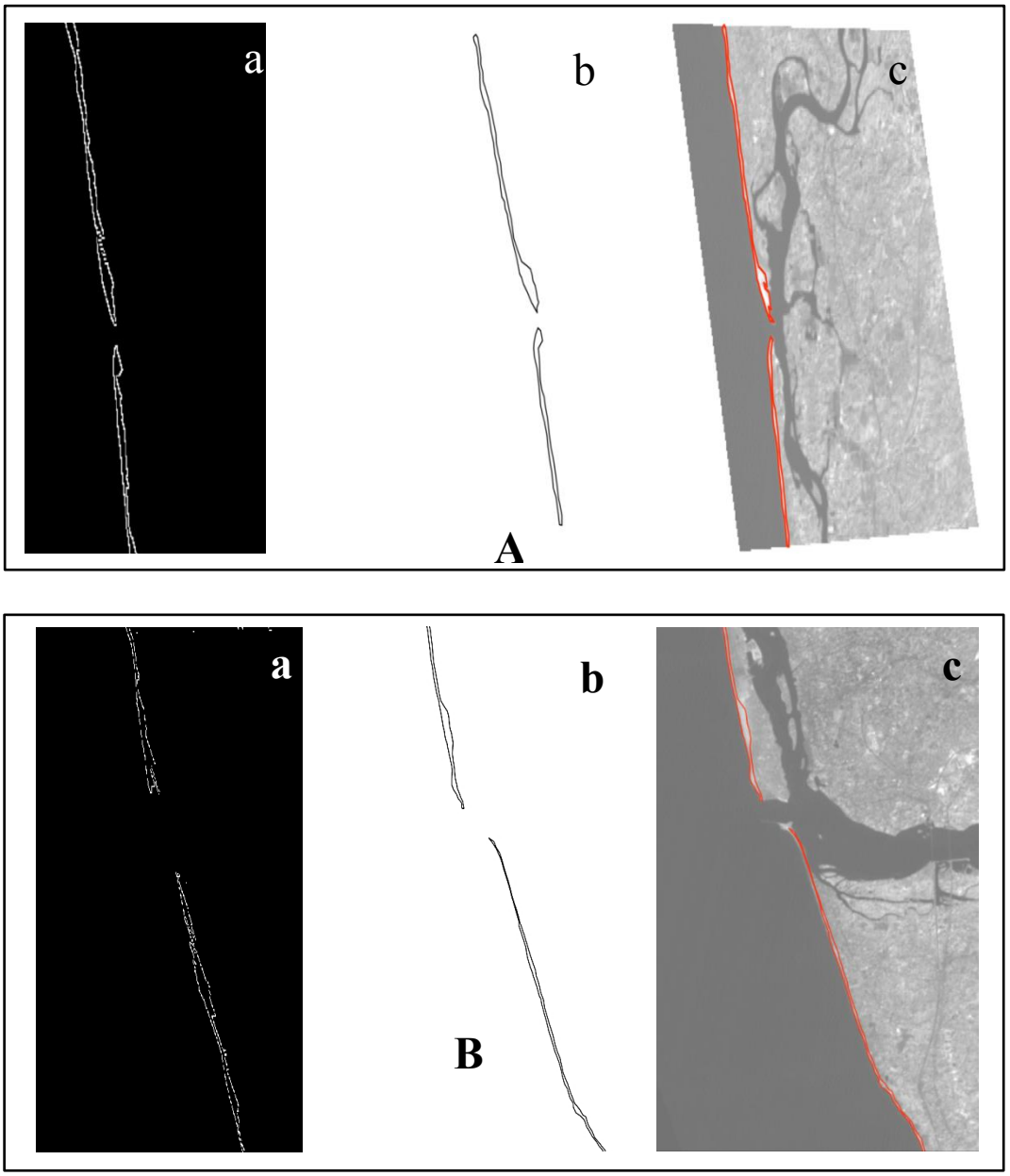

Figure 5.4. Automatic shoreline extraction from IRS-P6 LISS III 2010 satellite image of (A). Mulky-Pavanje and (B). Netravati-Gurpur rivermouth areas. (a). Automatic delineated shoreline, (b). Automatic delineated shoreline vector map, (c). Overlaying extracted shoreline on satellite image

5.2.3. Automatic Shoreline Change Analysis

For the shoreline change analysis, the study area is divided into two regions namely, Mulky-Pavanje rivermouth area (Northern sector of the study area) and Netravati-Gurpur rivermouth area (Southern sector of the study area). The extracted shoreline vector maps of multi-temporal IRS-P6 LISS III (2005, 2007 and 2010) and IRS-R2 LISS III (2013) data are prepared and carried into DSAS software for shoreline change rate analysis of Mulky-Pavanje rivermouth area and Netravati-Gurpur rivermouth area. The shoreline change rates are analysed using two different statistical techniques namely, End Point Rate (EPR) and Linear Regression Rate (LRR).

These rivermouths have sand spits on either side, indicating strong tendencies of migration of the rivermouth. The migration of the rivermouth would involve erosion at one sand spit and deposition at the opposite sand spit. Mangalore Coast is under the influence of Southwest (SW) monsoon and most of the shoreline changes caused by severe wave activity during four monsoon months from June to September. Along Mangalore Coast, the littoral drift is negligible and sand mining is not significant and these are not reasons for the coastal erosion (Dattatri and Kamath 1997, Dwarakish 2001). The coastal erosion reported along Mangalore Coast is due to direct wave action and changes at the rivermouths.

5.2.3.1. Mulky-Pavanje Rivermouth Area

Most significant changes have been observed at Mulky-Pavanje rivermouth and Hejamadi Kodi spit, northern segment of Mulky-Pavanje rivermouth is under accretion and southern sector is under erosion. For detailed shoreline change analysis, the Mulky-Pavanje rivermouth area is further divided into 4 regions. Region A, Hejamadi Kodi Beach, northern part of rivermouth covers transects from 1 to 159 and

transects from 160 to 172 in Hejamadi Kodi Sand Spit is named as Region B. Transects from 173 to 179 are covered rivermouth of Mulky and Pavanje rivers. Region C, Sasihitulu Sand Spit, southern part of rivermouth covered by transects from 180 to 210 and finally, transects from 211 to 318 in Sasihitulu Beach, which is designated as Region D. The transect map of Mulky-Pavanje rivermouth is shown in Figure 5.5. The resulted shoreline change rates assessed at each region with respect to transects is plotted for Mulky-Pavanje rivermouth area and shown in Figure 5.6. End Point Rate (EPR) and Linear Regression Rate (LRR) of transects from 150 to 195, which covers Mulky-Pavanje rivermouth area are presented in Figure 5.7 and Figure 5.8 respectively. The detailed transects and shoreline change trends in all the four regions of Mulky-Pavanje rivermouth area are given in Table 5.2.

Region A, Hejamadi Kodi Beach, from transects 1 to 159 do not show much change in shoreline and the average accretion rate is 5.36 m/yr (EPR) and 5.75 m/yr (LRR) from 2005 to 2013. In Hejamadi Kodi Beach, transects from 149 to 159 shows shoreline erosion and calculated mean shoreline erosion rate is -11.27 m/yr (EPR) and -10.86 m/yr (LRR) and the maximum deposition rate is 13.17 m/yr (EPR) and 12.72 m/yr (LRR) at transect 34.

Region B, Hejamadi Kodi Sand Spit, northern part of rivermouth from transects 160 to 172 is under accretion, since, maximum accretion rate is 33.47 m/yr (EPR) and 28.97 m/yr (LRR) at transect 172 with average deposition of shoreline 19.44 m/yr (EPR) and 18 m/yr (LRR). More sand has deposited on Hejamadi Kodi Sand Spit due to the wave action and current direction, which is from South to North during post-monsoon. The sediments discharged from the Mulky and Pavanje rivers move towards North due to the waves approaching to the coast in Southwest direction and currents from South to North. Larger size particles settled at rivermouth and silt and clay particles move towards North and deposit, which creates more accretion at Hejamadi Kodi sand spit.

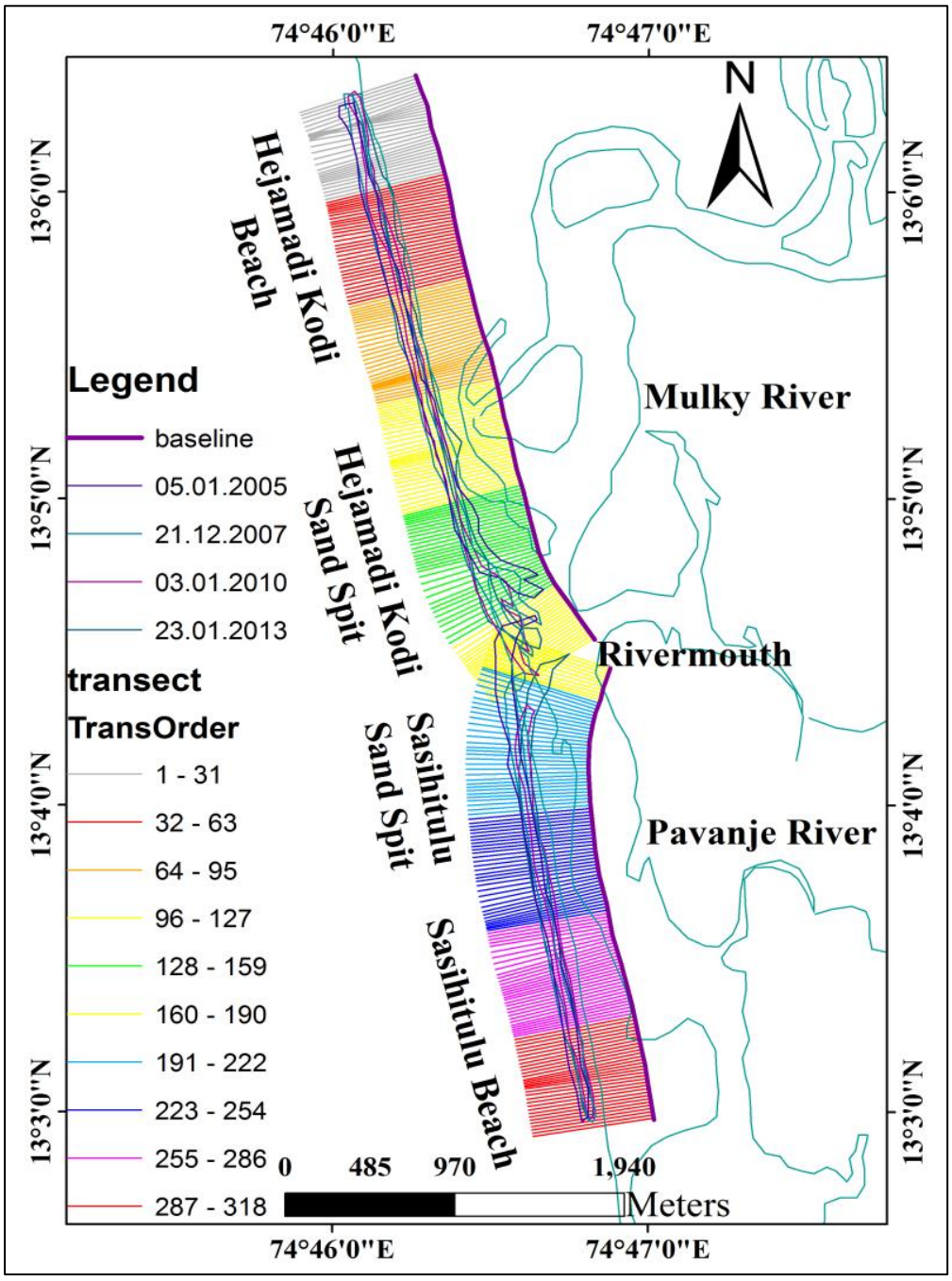

Figure 5.5. The transects (20 m spacing and 700 m length from baseline) map to estimate shoreline change rates (erosion/accretion) in Mulky-Pavanje rivermouth area

Region C, Sasihitulu Sand Spit, the southern sector of Mulky-Pavanje rivermouth shows 18.32 m/yr (EPR) and 17.85 m/yr (LRR) average accretion rate, from transects 180 to 210. Deposition of sand on both the spits of rivermouth, reduce confluence width of the rivermouth from 2005 to 2013. The maximum sand deposition rate observed in Sasihitulu Sand Spit is 49.12 m/yr (EPR) and 43.79 m/yr (LRR) at transect 181 due to wave activity in post-monsoon cause onshore movement of sand and due to less discharge from the rivers, sediments move back into the rivermouth and deposit at tip of both the spits. The shoreline accretion continued towards south up to transect 225 and the mean shoreline change rate is 7.59 m/yr (EPR) and 8.36 m/yr (LRR) from transect 211 to 225. This implies that Sasihitulu sand spit and Hejamadi Kodi sand spits are stabilized and sand deposition is observed on both the spits, due to construction of river bank protection works on Hejamadi Kodi Spit (Dwarakish 2001). By moving towards south of rivermouth, the shoreline change rate in Sasihitulu Sand Spit is reduced and the shoreline rate of 8.55 m/yr from EPR and 8.64 m/yr from LRR is obtained at transect 210 due to onshore movement of sand.

Region D, from transects 211 to 318 covers Sasihitulu Beach shows average accretion rate of 1.25 m/yr (EPR) and 2.01 m/yr (LRR). From transect 226, erosion has started with rate -0.03 m/yr and continued up to transect 268. From transect 269 to 318; coastline accretion is in progress with average shoreline change rate of 2.97 m/yr (EPR) and 3.54 m/yr (LRR) due to transportation of fine sediments towards the beach from nearshore region and deposited on the beaches. From 2005 to 2013, the northern sector of rivermouth is moving towards south due to continuous deposition at Hejamadi Kodi Sand Spit with an average deposition rate of 25.61 m/yr (EPR) and 23.26 m/yr (LRR).

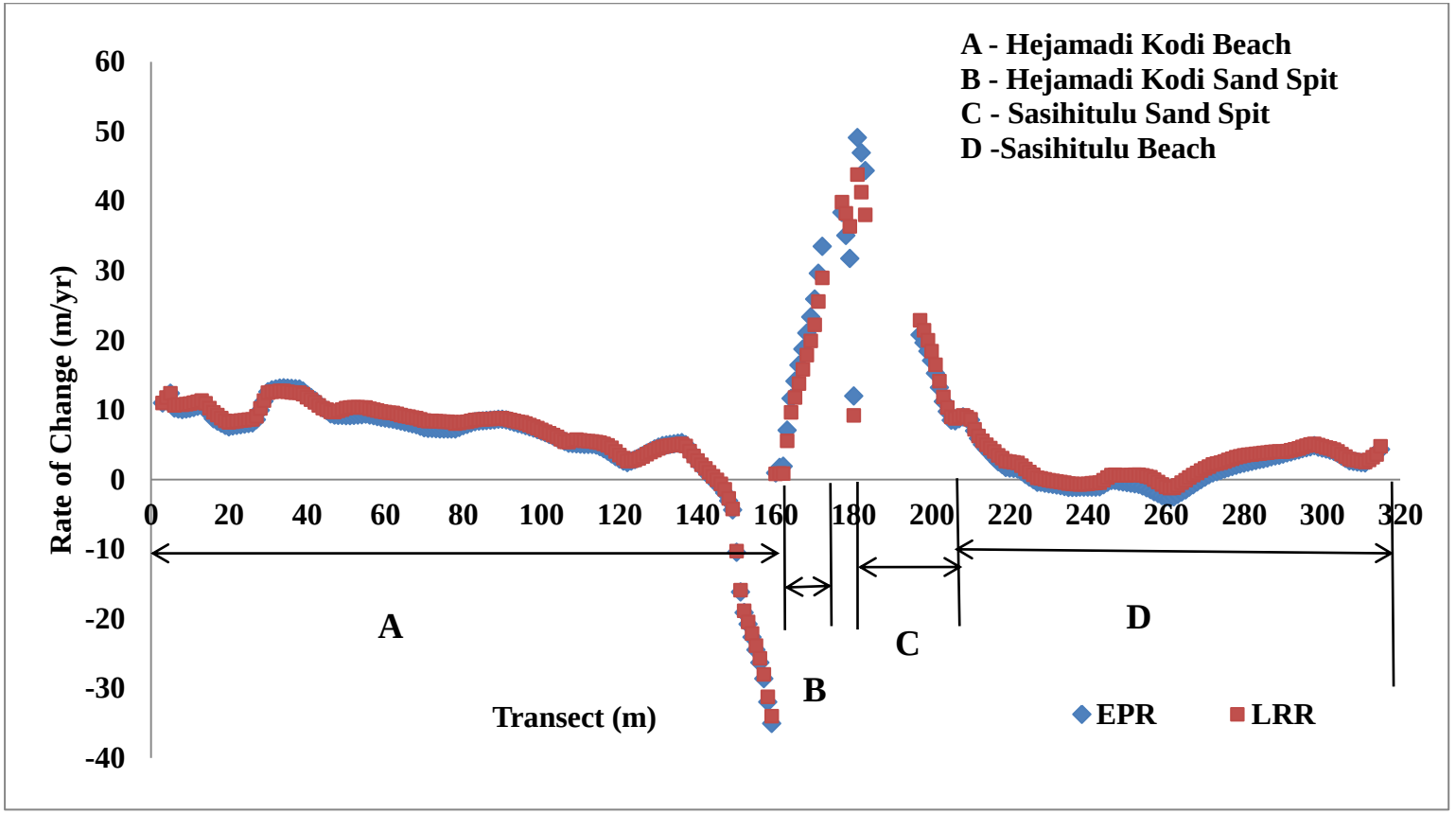

Figure 5.6. Shoreline change rates (erosion/accretion) in Mulky-Pavanje rivermouth area using EPR and LRR

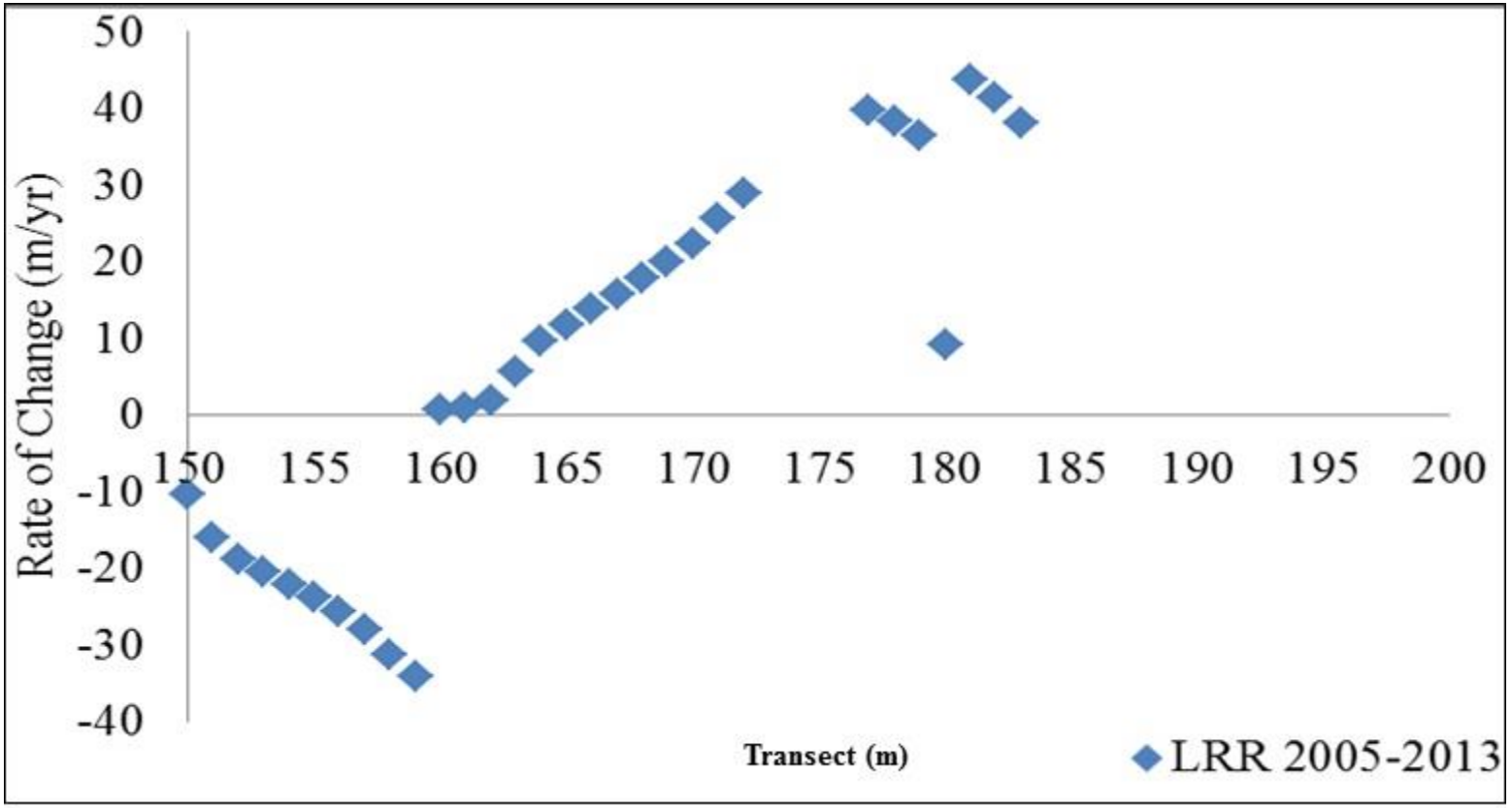

Figure 5.7. Rate of change (erosion/accretion) at Mulky-Pavanje rivermouth using EPR: 2005-2013

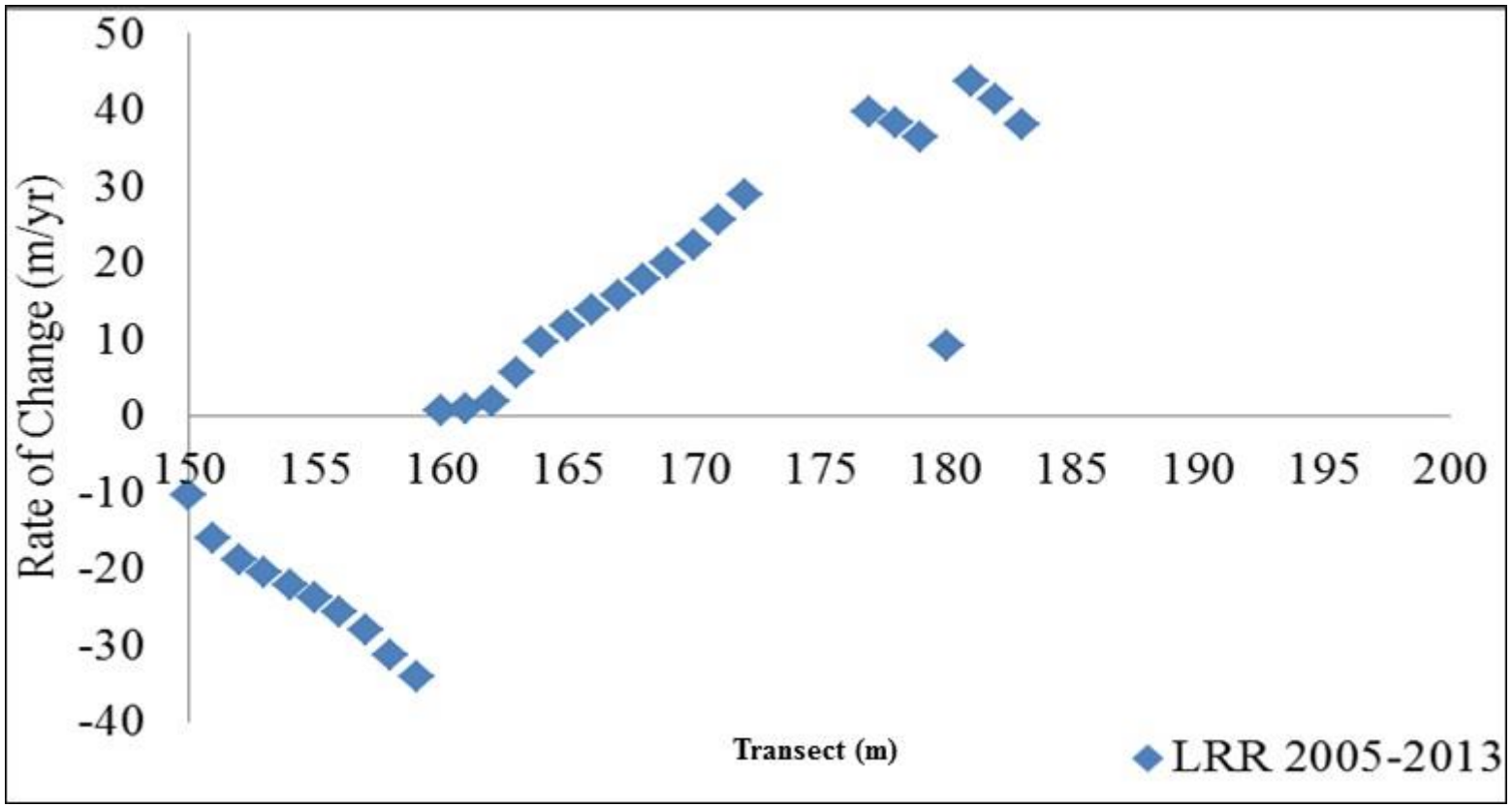

Figure 5.8. Rate of change (erosion/accretion) at Mulky-Pavanje rivermouth using LRR: 2005-2013

Table 5.2 Shoreline change trends of Mulky-Pavanje rivermouth area

Region	A	B	C	D
	Hejamadi Kodi Beach	Hejamadi Kodi Sand Spit	Sasihitulu Sand Spit	Sasihitulu Beach
Transects	1-159	160-172	180-210	211-318
Average Accretion (m/yr)	5.36 (EPR) 5.75 (LRR)	15.84 (EPR) 13.35 (LRR)	4.55 (EPR) 5.18 (LRR)	1.15 (EPR) 1.93 (LRR)
Number of transect	159	13	31	108
Transect length (m)	700	700	700	700
Baseline distance from coastline (m)	400	400	400	400

5.2.3.2. Netravati-Gurpur rivermouth Area

Baseline is constructed 300 m distance from latest 2013 shoreline and total 800 transects are generated with 20 m spacing along 16 km stretch of Netravati-Gurpur rivermouth area. Most substantial changes have been observed at Netravati-Gurpur rivermouth. Bengre spit, northern sector of Netravai-Gurpur rivermouth is under accretion and Ullal spit, southern segment is under erosion. For comprehensive analysis, the Netravati-Gurpur rivermouth area is divided into 5 regions. Region A, Thannirbhavi Beach, northern part of rivermouth covers transects from 1 to 162 and transects from 163 to 234 in Bengre Sand Spit, termed as Region B. Netravati-Gurpur rivermouth is covered by transects from 235 to 264. Region C, Ullal Sand Spit southern part of rivermouth covered by transects from 265 to 300. Ullal Beach from transects 301 to 550 is labeled as Region D and finally, transects from 551 to 800 in Someshwara Beach is considered as Region E. The transect map of Netravati-Gurpur rivermouth area is presented in Figure 5.9. The resulted shoreline change rates calculated at each region with respect to transect is plotted for Netravati-Gurpur rivermouth area is shown in Figure 5.10. The shoreline change rates at Netravati-Gurpur rivermouth area from transect 200 to 300 are shown in Figure 5.11. The detailed transects and shoreline change trends in all the five regions of Netravati-Gurpur rivermouth area are given in Table 5.3.

Region A, Tannirbhavi Beach, from transects 1 to 162 do not show much change in shoreline and average accretion rate is 1.48 m/yr (EPR) and 1.37 m/yr (LRR) from 2005 to 2013 due to the waves in post-monsoon, which cause onshore movement of sand. In Tannirbhavi Beach, transects from 93 to 111 shows shoreline erosion and mean shoreline erosion rate is -1.45 m/yr (EPR) and -1.22 m/yr (LRR). Also from transects 143 to 150 shoreline erosion is observed in Region A and average shoreline erosion rate is -0.69 m/yr (EPR) and -0.7 m/yr (LRR).

Region B, Bengre Sand Spit, northern part of rivermouth from transects 163 to 234 is under accretion and maximum accretion rate is 8.73 m/yr (EPR) and 8.89 m/yr (LRR) at transect 215. The wave action is in southwest direction during monsoon season tends to move the sediments brought in by the rivers into northwest direction. Due to the circulation of water and when the velocity is reduced, calm area is created on the northern sector of rivermouth (Bengre Sand Spit) and more sand is deposited from transects 203 to 218 as shown in Figure 5.11. The average shoreline accretion rate in this area is 5.14 m/yr (EPR) and 5.17 m/yr (LRR). This indicates that predominant movement of sediments from the Netravati-Gurpur rivers is towards North, due to wave action and current direction and the results are matching with Dwarakish (2001).

Region C, Ullal Sand Spit, the southern sector of Netravati-Gurpur rivermouth is undergoing erosion and average shoreline erosion rate is -1.93 m/yr (EPR) and -1.91 m/yr (LRR) from transects 265 to 300. Due to high concentration of wave energy on the Ullal side, indicating the predominant movement of sediments from Netravati-Gurpur rivers towards North and more deposition on Bengre Spit.

Region D, from transects 301 to 550 covers Ullal Beach and shows minimum accretion and erosion rates because of seawall constructed along the coastline. From transects 301 to 310 shows shoreline accretion and average accretion rate is 0.09 m/yr (EPR) and 0.07 m/yr (LRR). From transects 311 to 319, the average shoreline erosion rate is -0.13 m/yr (EPR) and -0.12 m/yr (LRR) and from transects 320 to 338, the mean shoreline accretion rate is 0.09 m/yr (EPR) and 0.07 m/yr (LRR). Similarly, in region D shoreline accretion is seen from transects 348 to 437 and 447 to 488 and, the shoreline erosion is observed from transects 339 to 347; 438 to 446 and 489 to 550.

Someshwara beach, region E from transects 551 to 800 shows minor changes in accretion and erosion rates because of onshore – offshore movement of sediments

caused by the waves during post-monsoon. From transects 551 to 650, average shoreline erosion rate is -2.96 m/yr (EPR) and -2.85 m/yr (LRR) and shoreline average accretion rate from transects 651 to 682 is 1.57 m/yr (EPR) and 1.39 m/yr (LRR). The average shoreline erosion rate is -0.91 m/yr (EPR) and -0.87 m/yr (LRR) from transects 683 to 733 and shoreline accretion rate from transects 734 to 800 is 1.81 m/yr (EPR) and 1.79 m/yr (LRR).

The rivermouth change detection was carried out by Dwarakish (2001) using long-term data from 1905-1968, concluded that, Netravati-Gurpur rivermouth was having the tendency of shifting its position periodically and also beaches at Ullal and Bengre have been undergoing erosion and deposition phases long before the construction of Breackwaters. This implies that, there is no influence of Breakwaters at Netravati-Gurpur rivermouth on the sediment dynamics.

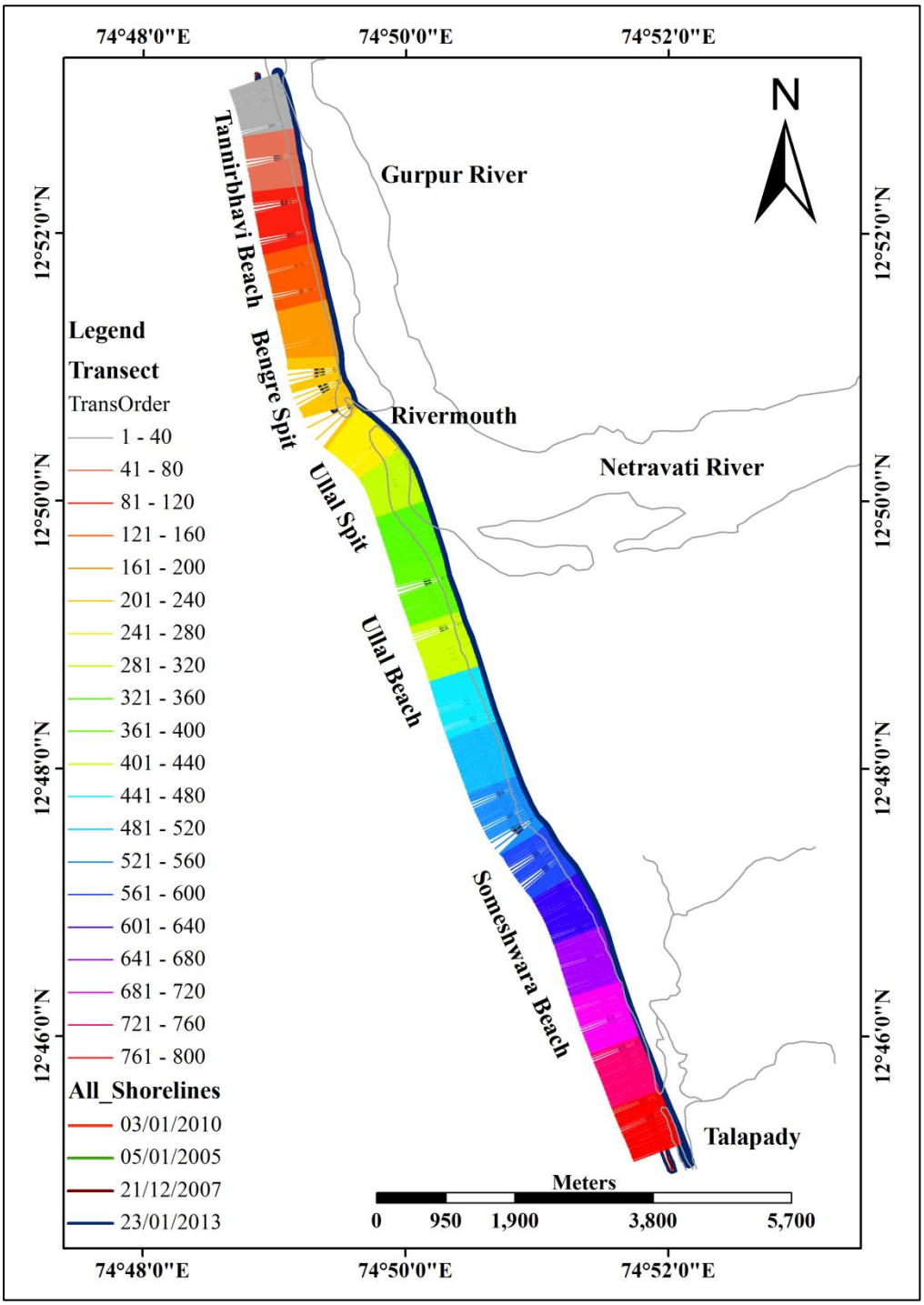

Figure 5.9. The transect (20 m spacing and 700 m length from baseline) map to estimate shoreline change rates (erosion/accretion) in Netravati-Gurpur rivermouth area

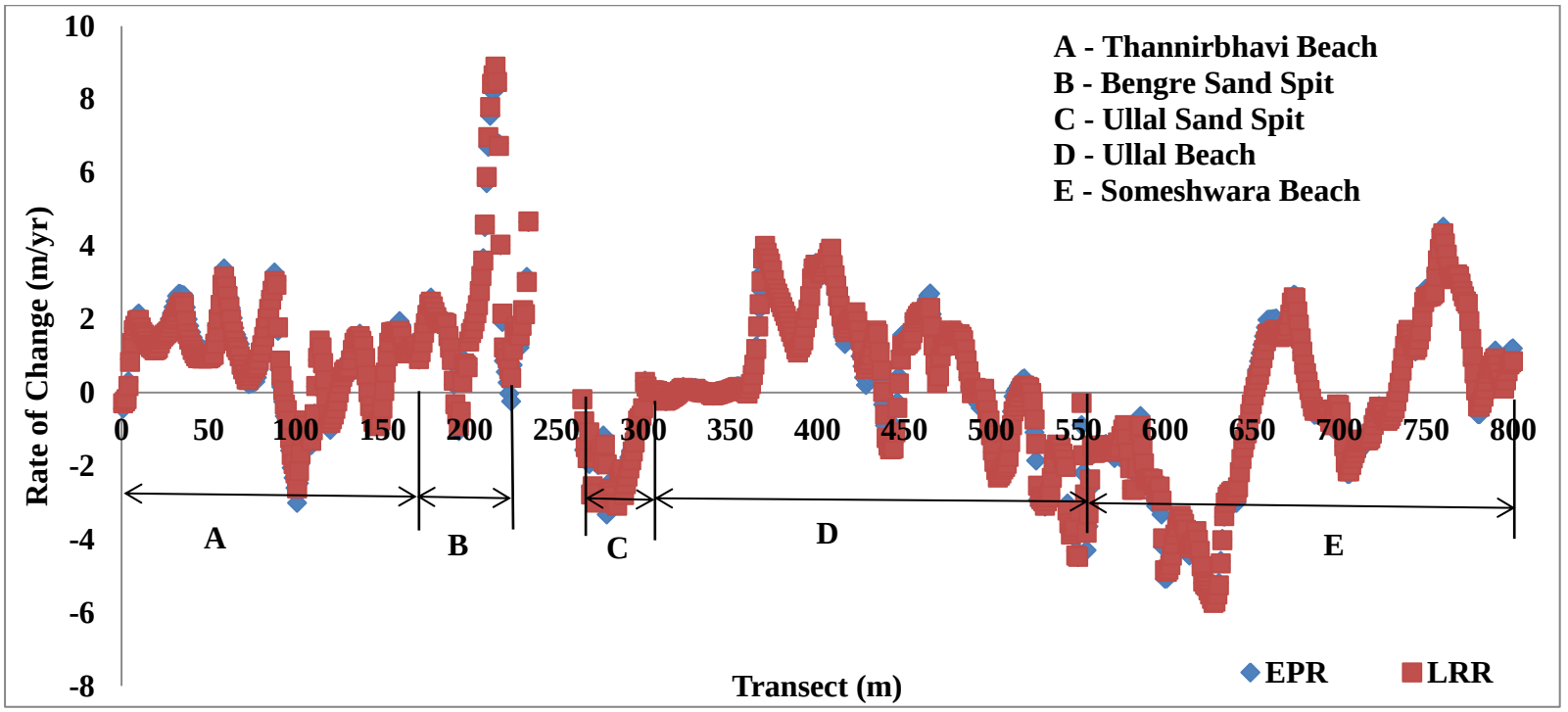

Figure 5.10. Shoreline change rates (erosion/accretion) in Netravati-Gurpur rivermouth area using EPR and LRR

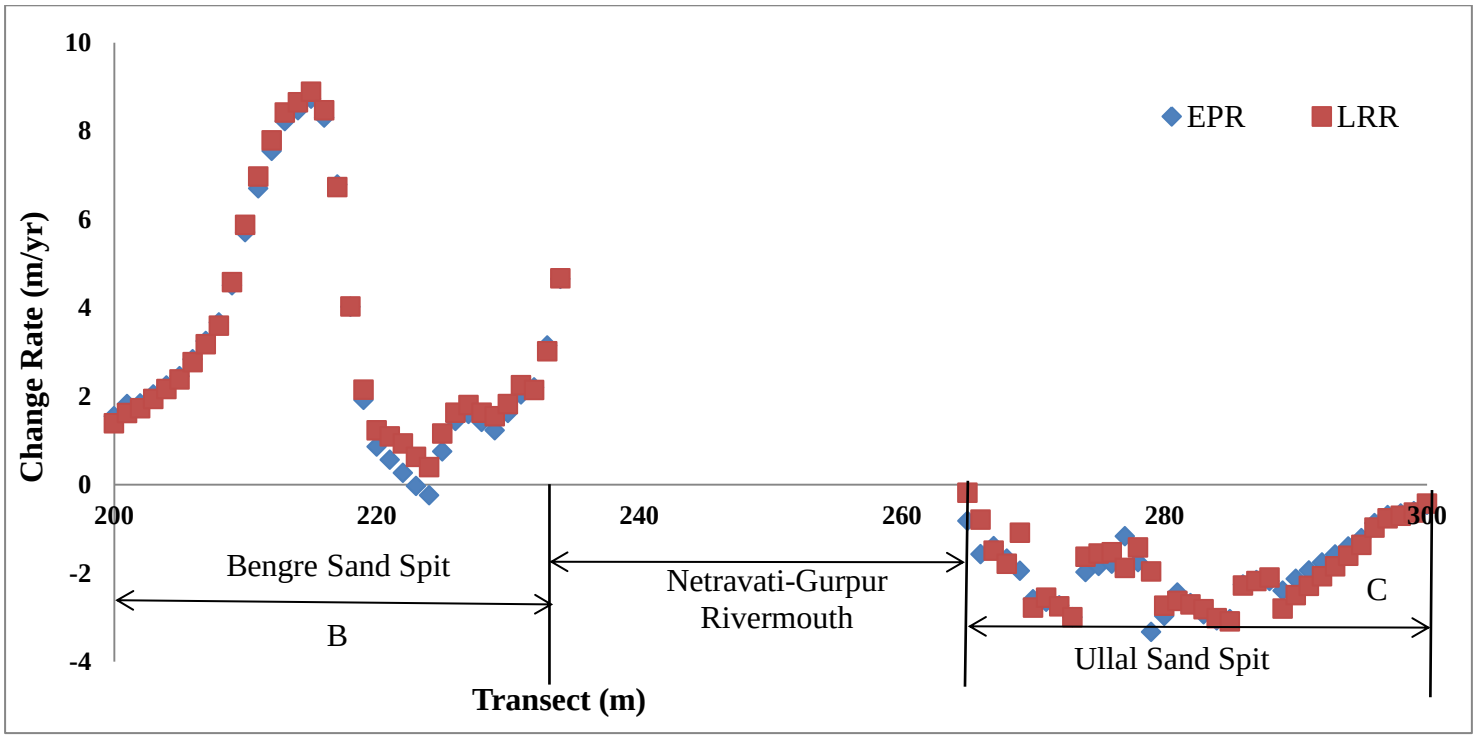

Figure 5.11. Rate of change (erosion/accretion) at Netravati-Gurpur rivermouth using EPR and LRR

Table 5.3. Shoreline change trends of Netravati-Gurpur rivermouth area

Region	A	B	C	D	E
	Tannirbhavi Beach	Bengre Sand Spit	Ullal Sand Spit	Ullal Beach	Someshwara Beach
transect	1-162	163-234	265-300	301-550	551-800
Number of transect	162	72	36	250	250
Transect length (m)	700	700	700	700	700
Baseline distance from coastline (m)	300	300	300	300	300
Average Accretion (m/yr)	1.48 (EPR) 1.37 (LRR)	2.32 (EPR) 2.35 (LRR)	---- ----	3.42 (EPR) 3.43 (LRR)	3.38 (EPR) 3.1 (LRR)
Average Erosion (m/yr)	-1.05 (EPR) -1.01 (LRR)	---- ----	-1.93 (EPR) -1.91 (LRR)	-2.7 (EPR) -2.69 (LRR)	-3.87 (EPR) -3.72 (LRR)
Max. accretion (m/yr) (transect)	3.38 (EPR) 3.16 (LRR) (59)	8.73 (EPR) 8.89 (LRR) (215)	---- ----	3.67 (EPR) 3.82 (LRR) (370)	4.52 (EPR) 4.34 (LRR) (760)
Max. erosion (m/yr) (transect)	-2.60 (EPR) -2.27 (LRR) (100)	---- ----	-3.30 (EPR) -2.96 (LRR) (297)	-4.49 (EPR) -4.48 (LRR) (550)	-5.66 (EPR) -5.74 (LRR) (628)

5.3. Suspended Sediment Transport

The direction and movement of sediments are identified from IRS-P4 OCM (December 12, 2013) satellite image using clipped histogram equalization based contrast enhancement and principal component analysis. After contrast enhancement of satellite image, the sharp contrast between various sediment-laden waters is clear for mapping. Tonal or colour variation is considered as a measure of sediment concentration. Texture and pattern helps in monitoring distribution and dispersion of sediment directions as they became elongated and pointed in the direction of flow. Using these basic principles of image processing and coastal process, movement of sediment is marked on the output image of contrast enhanced and principal component analysis.

The first false colour composite (FCC-1) image is generated from three bands (5, 6 and 7) of IRS-P4 OCM sensor image and it shows all the coastal features and land features adjacent to coast. The histogram thresholding with mean global maximum values shows good contrast between image features without loss of information and additional noise. Normalization of histogram equalized image preserved the brightness in image for identification of coastal objectives.

FCC-3 (PC1, PC2 and PC3) image presents the sediment dispersion and current movement, but due to less contrast enhancement in the image. FCC-2 (PC2, PC3 and PC4) image is highlighted sediment movements clearly and to improve the contrast of FCC-2 image for identification of sediment direction it is merged with normalized image. The resultant image is displayed all the features very clearly and this image is used for mapping the direction and movement of sediments. Based on tonal variation and textural pattern, the sediment movement along Mangalore Coast, West Coast of India is mapped. For comparison of sediment transport along Mangalore Coast, the results obtained by the current method and previous studies (Dwarakish et al. 2010

and Avinash et al. 2012) are employed. Dwarakish et al. (2010) estimated the suspended sediment concentration (SSC) through in-situ data and then compared with satellite data, whereas Avinash et al. (2012), estimated the SSC using satellite data.

The sampling stations of Dwarakish et al., 2010 and Avinash et al., 2012 studies are shown in Figure 5.12. The sediment distribution and transport map is shown in Figure 5.13.

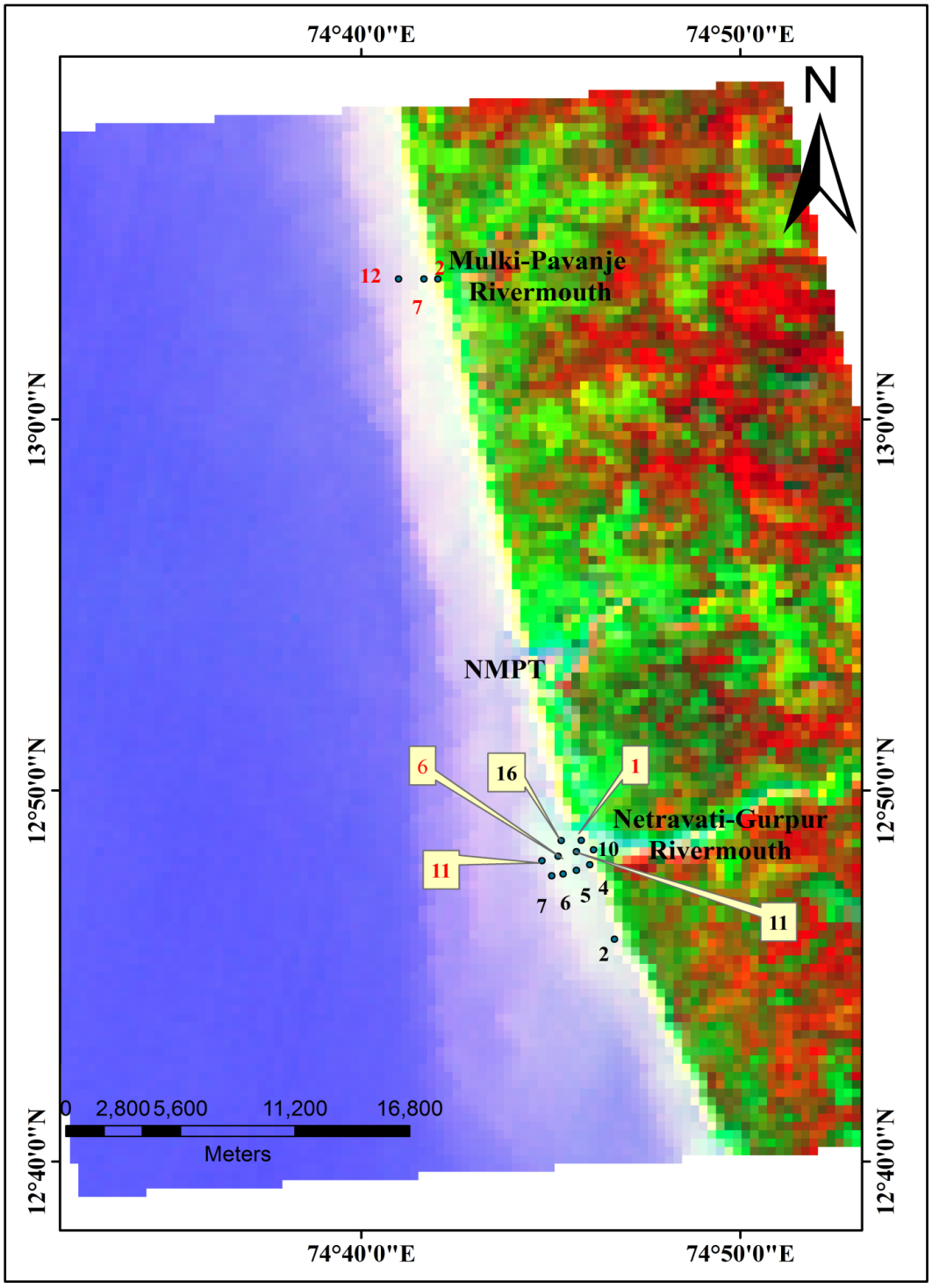

Figure 5.12. Sample stations located on FCC-3 image as per the studies carried out by Dwarakish et al. (2010) and Avinash et al. (2012)

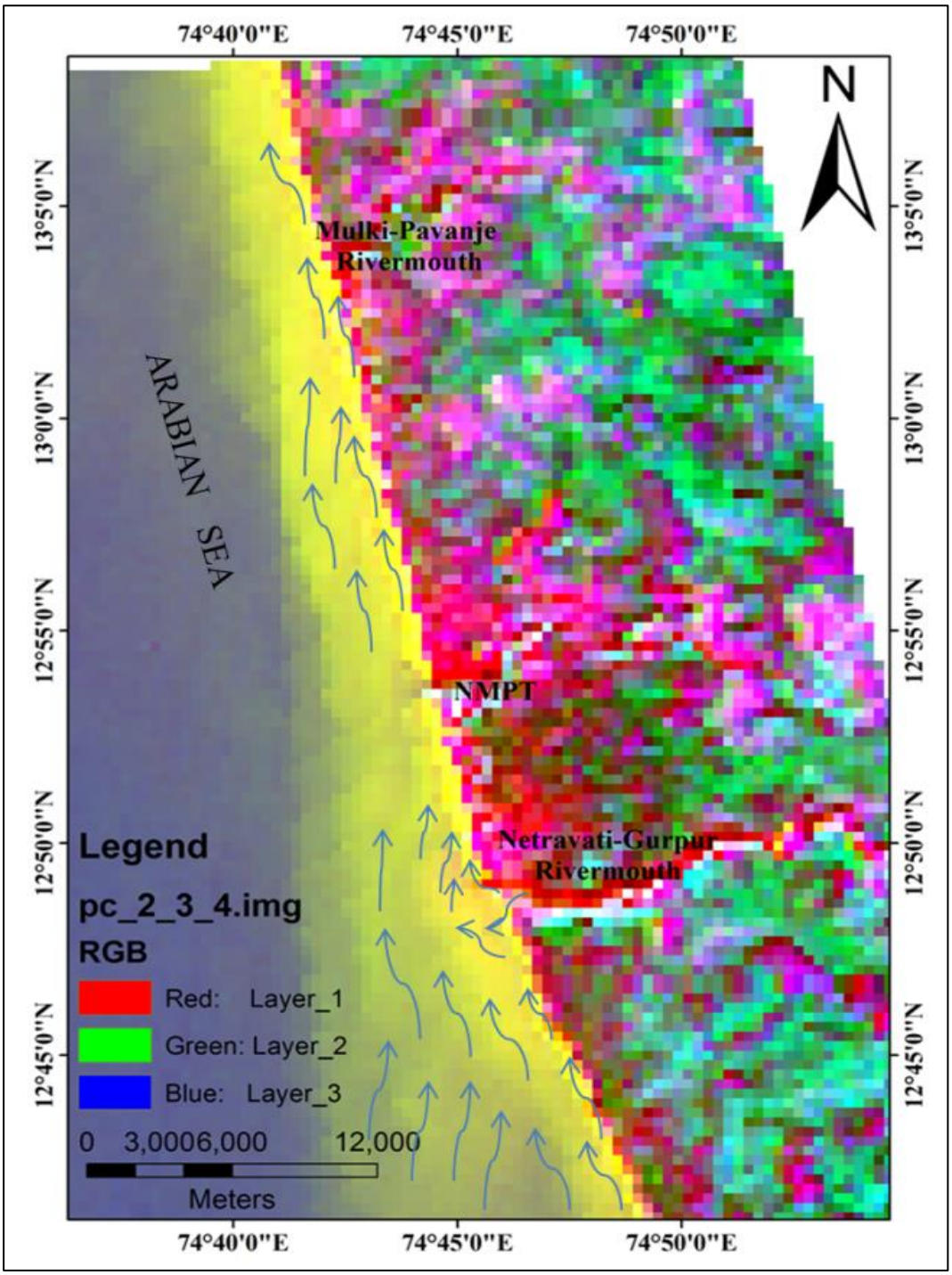

Figure 5.13. Suspended sediment movement on FCC-2 image [PC2(red), PC3(green) and PC4(blue)] of OCM satellite data

Due to heavy rainfall during the southwest monsoon in the catchment area, Netravati and Gurpur rivers bring lot of suspended sediments into the Arabian Sea. Silt and Clay fraction of sediments are taken deep into the Sea and Sand is deposited near the rivermouths. During the post-monsoon period, since the waves are approaching the coast from southwest direction and currents from South to North, the SSC pattern is showing a northward moving tendency. This phenomenon is clearly observed at the Netravati-Gurpur rivermouth from the OCM data as shown in Figure 5.13. The concentration of sediments also reduced from rivermouth to deep sea. Due to the maximum concentration and large amount of sand particles deposited at rivermouth, pinkish yellow colour is observed at Netravati-Gurpur rivermouth and this concentration decreasing towards North, indicating northward movement of sediments. Most of the sediments are deposited on Bengre Spit, northern segment of Netravati-Gurpur rivermouth due to water circulation and calm are is created when, the velocity is reduced, and the deposition at southern sector is almost zero.

Moving towards North of Netravati-Gurpur rivermouth, light colour is observed at sourthern sector of NMPT and light dark colour is observed at northern sector of NMPT, implies the reduced concentration of sediments.

There is no significant colour variations observed at Mulky-Pavanje rivermouth area due to less discharge from Mulky and Pavanje rivers and less confluence width (180-240) of rivermouth. Since, spatial resolution of IRS-P4 OCM data is 360 m, significant changes at Mulky-Pavanje rivermouth area could not be identified.

These suspended sediment transport observations are qualitatively analysed and compared with suspended sediment concentration studies carried out by Dwarakish et al. (2010) and Avinash et al. (2012) for Mangalore Coast. Based on the comparison, it is clear that the sediments discharged from the rivers along Mangalore Coast are moving towards North during post-monsoon due to wave action and current direction,

which is from South to North The sediment transport map prepared from the developed algorithm for Mangalore Coast is satisfactory.

5.3.1. Qualitative Analysis - Post-Monsoon Season

SSC distribution along Mangalore Coast is influenced by heavy rainfall and river discharge during the southwest monsoon. During post-monsoon season, the sediments are moving from South to North due to currents from South to North and the waves from southwest direction along Mangalore Coast. This tendency of sediment transport also qualitatively analysed and compared with the results of sediment concentration studies of Dwarakish et al. (2010) and Avinash et al. (2012).

From Figure 5.12, the sediment concentrations at Netravati-Gurpur rivermouth are 28, 28, 31 and 27 mg/l for sample stations 4, 5, 6 and 7 respectively (Dwarakish et al. 2010) and 35.44 mg/l at station 1 (Avinash et al. 2012) indicating the maximum sediment concentration at rivermouth. Sand particles carried by Netravati and Gurpur rivers are settled at rivermouth and, silt and clay fractions of sediments move into the deep sea water. From the sediment concentrations at sample stations 1, 6 and 11 are 35.44, 24.15 and 11.14 mg/l (Avinash et al. 2012), observed that, sediment concentrations from rivermouth to deep sea region are decreasing. Based on the fluorescent traces study (Shankar and Karbassi 1992) and grain size analysis (KREC Study Team 1994; Dwarakish et al. 1998), it was earlier concluded that catchment area of Netravati-Gurpur rivers is the source of sediments available on Ullal and Bengre beaches. Based on the Sediment Trend Matrix Analysis (STMA) (Dwarakish 2001; Sri Ram 2014), it was concluded that sediments from the Netravati-Gurpur rivermouth were moving predominantly towards North (Bengre sand spit) than South (Ullal sand spit).

The results of present Suspended Sediment Transport study based on IRS-P4 OCM data is augmenting the conclusions of earlier researchers, regarding sediment dynamics at Netravati-Gurpur rivermouth, and hence this methodology can also be utilized to get the information about the sediment transport along the Coast.

The scenario at Mulky-Pavanje rivermouth is entirely different from that of Netravati-Gurpur rivermouth, since, Mulky-Pavanje rivermouth is not protected by any breakwaters. Also, carrying capacity of Mulky-Pavanje rivers is very less compared to Netravati-Gurpur rivermouth (Dwarakish and Natesan 2001) and hence sediment concentration at Mulky-Pavanje rivermouth is less compared to Netravati-Gurpur rivermouth. During the recent field visits to Mulky-Pavanje rivermouth on 08/03/2014, it was observed that area of Hejamadi Kodi Sand spit was relatively higher than Sasihitulu Sand spit and series of offshore block were observed right in front of the rivermouth, which are responsible for reduction in confluence width of the rivermouth. The SSC values at stations 2, 7 and 12 are 29.12, 17.13 and 8.82 mg/l (Avinash et al. 2012), indicating less sediments carrying capacity of Mulky and Pavanje rivers (Dwarakish et al. 2010).

The complete wave hydrodynamics at this rivermouth is controlled by direct wave action, bathymetry and river discharge. Overall it can be concluded that no significant sediment transport at Mulky-Pavanje rivermouth and the net sediment transport is towards North as seen in Figure 5.13.

5.4. Land Use and Land Cover Assessment

The developed Land Use and Land Cover (LULC) Assessment method using clipped histogram equalization based contrast enhancement and principal component analysis techniques improved the accuracy of LULC classification. The clipped histogram equalization algorithm applied to principal components (PC1, PC2, PC3 and PC4) of IRS-R2 LISS III 2013 image has enhanced the contrast of various features presented in the image. Coastal regions generally covered with diversity of species producing most of the image pixels as mixed pixels and hence, the classification of coastal features is difficult with poor resolution images. The developed contrast enhancement algorithm, improved the contrast of mixed pixels without introducing any noise in the image. The pixel based supervised classification using Maximum Likelihood Classifier (MLC) provided better and accurate classification.

The output of the developed model is compared with the results obtained from the general method through accuracy assessment and Kappa coefficient values. The classified images of general and developed methods of Mulky-Pavanje (M-P) rivermouth area, NMPT area and Netravati-Gurpur (N-G) rivermouth area are shown in Figure 5.14, Figure 5.15 and Figure 5.16 respectively. Accuracy Assessment and Kappa Coefficient values of general and developed methods are given in Table 5.4.

The supervised classification was carried out by using MLC method and during the selection of training samples Global Position System (GPS) values and Google Earth maps are considered as references.

Mulky –Pavanje rivermouth, NMPT and Netravati-Gurpur rivermouth areas are connected between terrestrial and marine ecosystems and provide vast coastal habitats. It is difficult to classify the coastal features due to mixed plantation and plantation with urban area and it results as mixed pixels in low resolution satellite

images. The developed contrast enhancement has successfully enhanced the pixels and also highlighted the hidden pixels in all the three regions of study area.

From Table 5.4, it is clear that developed method for M-P rivermouth area has provided an improved accuracy of 85.42% and 0.83 Kappa value when compared to 75% accuracy and 0.70 Kappa coefficient generated by general method.

Similarly for NMPT area, developed method has produced 89.66% accuracy and 0.88 Kappa coefficient, while general method has provided 78.61% accuracy and 0.72 Kappa statistic. Maximum area of NMPT is covered with urban and industries and hidden pixels are enhanced effectively and classified accordingly.

Finally, the accuracy and kappa coefficients for developed method are 86.93% and 0.85, when compared to 76.86% accuracy and 0.71 kappa value provided by general method. The urban areas near to the shore are clearly classified and sea water and river water also successfully classified separately. These results clearly indicates that, the developed method performed very well both in the form of producing better accuracy and kappa coefficient, for all the three segments of the study area. Hence, it can be concluded that the new algorithm developed in the present study can be utilized in assessing the LULC classification.

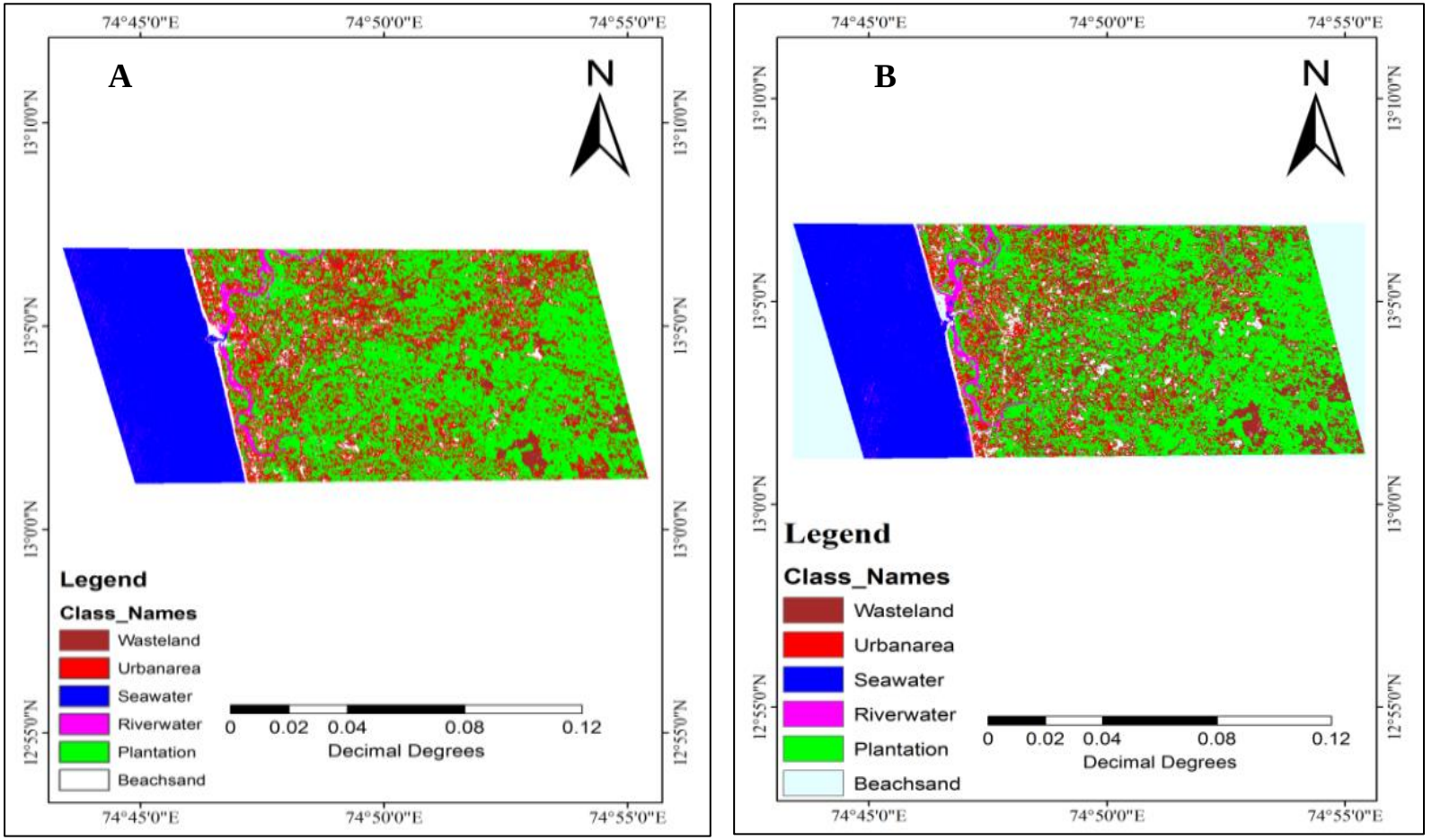

Figure 5.14. Supervised classification images of M-P rivermoth area (A). General (B). Developed

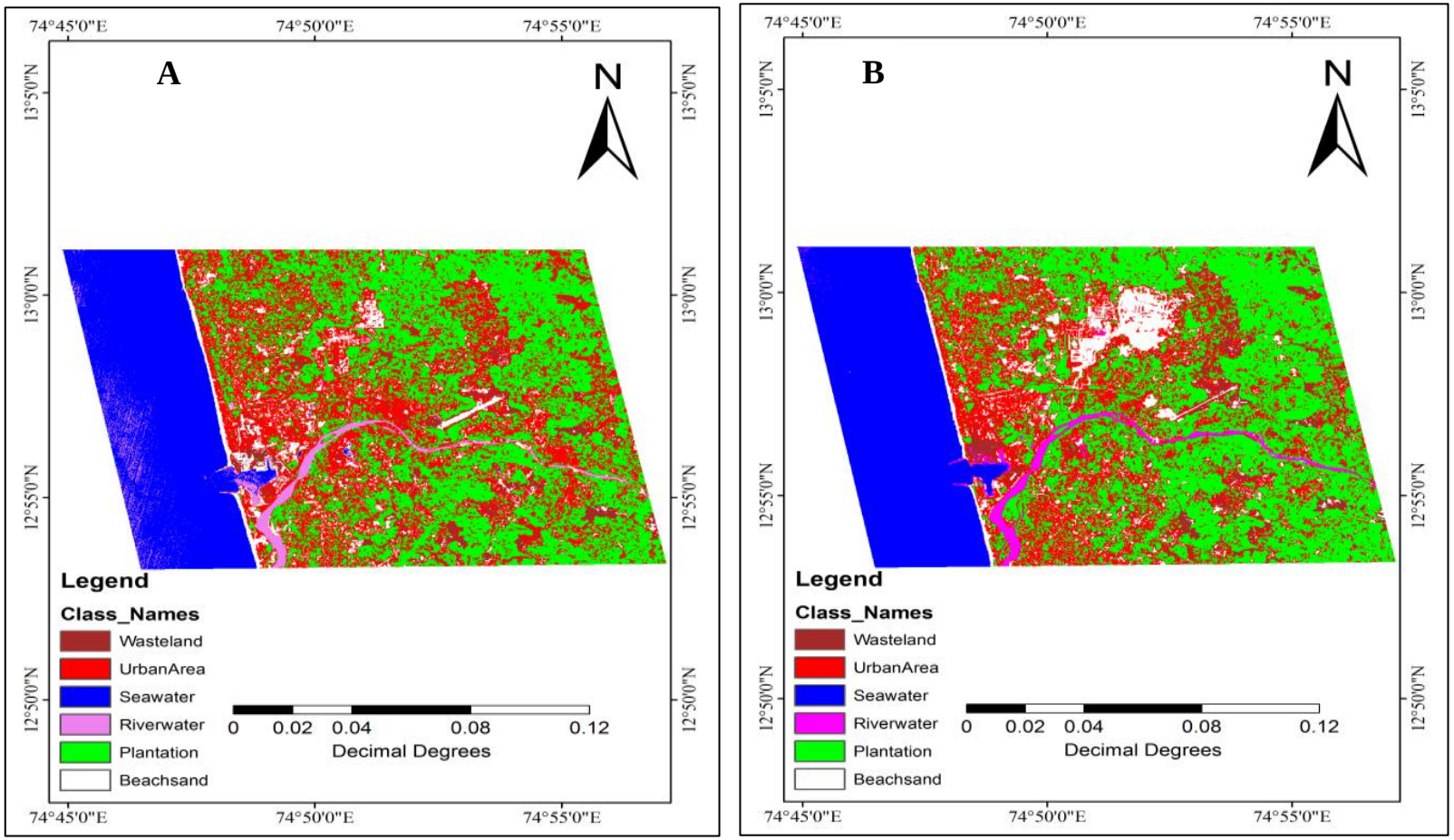

Figure 5.15 Supervised classification images of NMPT area (A). General (B). Developed Methods

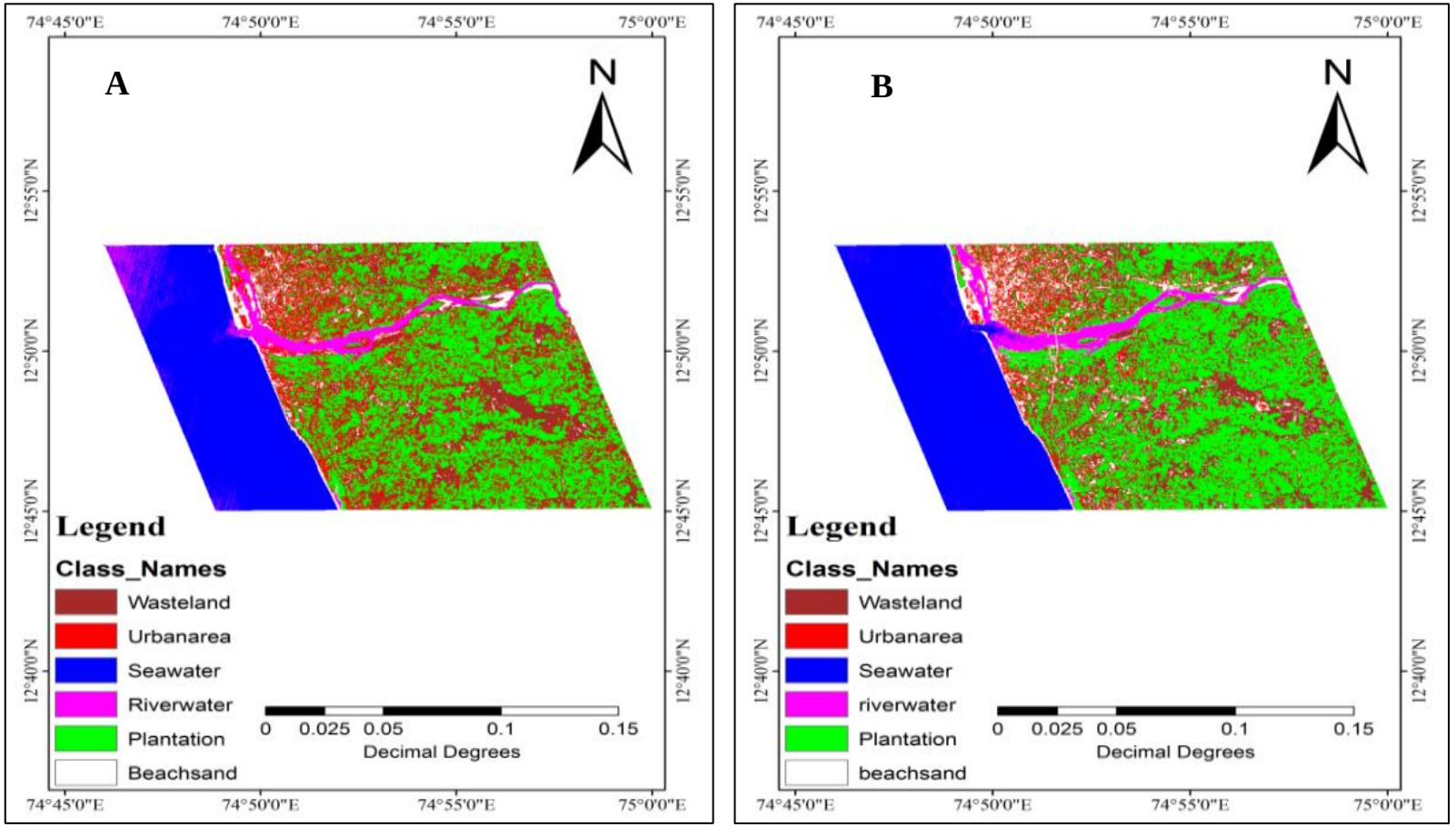

Figure 5.16 Supervised classification images of N-G rivermoth area (A). General (B). Developed Methods

Table 5.4. Accuracy Assessment and Kappa Coefficient values of General and Developed methods with respect to study area

Value / Method	M-P Rivermouth Area		NMPT Area		N-G Rivermouth Area	
	Accuracy Assessment (%)	**Kappa Coefficient**	**Accuracy Assessment (%)**	**Kappa Coefficient**	**Accuracy Assessment (%)**	**Kappa Coefficient**
General Method	75.00	0.70	78.61	0.72	76.86	0.71
Developed Method	85.42	0.83	89.66	0.88	86.93	0.85

CHAPTER 6
SUMMARY AND CONCLUSIONS

6.1. Summary

Remotely sensed satellite data is now widely used in coastal applications due to the advantage of repetitive and synoptic coverage of large and inaccessible large areas. Image processing techniques used to enhance the satellite images for accurate identification, interpretation and analysis of the earth surface features. Similar amount of energy reflected by different features and lack of consistency in features creates a low contrast satellite image. Image enhancement techniques used to improve the quality of image by increasing the contrast between different features and enhance the low contrast regions in the image. Many contrast enhancement techniques were developed to improve the quality of images and Histogram Equalization (HE) is a widely used indirect contrast enhancement technique. Because of over-enhancement due to global stretching of grey levels of histogram, HE provides loss of information in the enhanced image. To overcome the drawbacks of HE, several HE-based contrast enhancement techniques were developed and based on the modification of histogram, these methods were categorized as, Bi-Histogram Equalization (Bi-HE), Multi-Histogram Equalization (Multi-HE) and Clipped Histogram Equalization (CHE) methods.

From the comparative analysis of HE-based methods using image quality measures namely, Peak-Signal-to-Noise Ratio (PSNR) and Absolute Mean Brightness Error (AMBE), CHE methods provide excellent natural contrast enhancement and brightness preservation among HE-based methods without introducing any noise. CHE methods controlled over-enhancement of the image by clipping the high histogram regions using threshold operation and preserved the brightness of image by redistribution of clipped portions to the histogram. Based on these results, CHE-based

techniques were developed for satellite images for coastal processes including automatic shoreline detection, suspended sediment transport and land use and land cover assessment. The Mangalore Coast, from Talapdy to Mulky along West Coast of India was selected as a study area to apply the developed algorithms and to study the coastal processes.

For automatic shoreline detection, CHE-based contrast enhancement algorithm has developed to enhance coastal objects and to improve the contrast between the land and water objects. The developed CHE-based method highlighted the coastal objects without introducing any additional noise. The enhanced coastal objects were segmented using thresholding operation. The selected threshold values provided an efficient segmentation of the land and water regions by taking into consideration the mixed or wet pixels. The segmented regions were grouped and labelled by combining similar objects and removing unrelated objects. The unwanted regions were efficiently removed by using Region of Interest (ROI) technique. The shoreline was smoothed and generalized using image morphological operations and smoothed shoreline was highlighted using Robert's edge detector. The outlined shoreline was converted into vector map and used for shoreline change analysis. The extracted shoreline from developed automatic shoreline detection method has shown 96% accuracy, when compared with Global Position System (GPS) values collected from field survey. The shorelines were extracted from Indian Remote Sensing (IRS) Satellite data of IRS-P6 LISS III (2005, 2007 and 2010) and IRS-R2 LISS III (2013) and used for shoreline change analysis using Digital Shoreline Analysis System (DSAS). Shoreline change rates from 2005 to 2013 were estimated through two statistical methods namely, End Point Rate (EPR) and Linear Regression Rate (LRR). The shoreline change rates were studied separately for Mulky-Pavanje rivermouth area and Netravati-Gurpur rivermouth area of Mangalore Coast. Most significant changes were observed on Hejamadi Kodi spit, northern sector of Mulky-Pavanje rivermouth and Bengre spit, northern part of Netravati-Gurpur rivermouth.

CHE-based contrast enhancement and Principal Component Analysis (PCA) based integrated algorithm has been developed for mapping the distribution of suspended sediment along Mangalore Coast. The developed CHE-based method successfully enhanced FCC-1 (bands: 5, 6, 7) of IRS-P4 OCM 2013 image and provided good tonal variation of sediment pattern. To improve the contrast of sediment pattern further, PCA was performed and based on significance of principal components FCC-2 (PC2, PC3, and PC4) was added with contrast enhanced image. The resulted image was used for identification of sediment movement and distribution along Mangalore Coast. The identified sediment movement and distribution qualitatively analysed using previous studies done by Dwarakish et al., 2010 and Avinash et al., 2012. The identified distribution and movement of sediment along Mangalore coast using developed algorithm was matching with Dwarakish et al. (2010) and Avinash et al. (2012) studies. During the post-monsoon season, sediments moving from South to North due to the waves approaching the coast in southwest direction and currents from South to North.

CHE-based contrast enhancement and PCA based combined Land Use and Land Cover (LULC) assessment algorithm was developed for improving the accuracy of classification of satellite images. Principal components (PC1, PC2, PC3 and PC4) of IRS-R2 LISS III 2013 image were considered and each principal component of histogram was thresholded using global mean of histogram for better contrast enhancement and brightness preservation. Mixed and hidden pixels were highlighted after equalization of principal components individually. For clear understanding, study area was segmented into Mulky-Pavanje (M-P) rivermoth area, NMPT area and Netravati-Gurpur (N-G) rivermouth area. Contrast enhanced remotely sensed satellite (IRS-R2 LISS III 2013) image using developed method was classified by supervised classification with Maximum Likelihood Classifier (MLC) method and accuracy and Kappa Coefficient values were estimated. At the same time, satellite image without contrast enhancement was also classified using supervised classification with MLC

called general method and calculated accuracy and Kappa Coefficient values. By comparing the results of developed method and general method it was found that, the classification by developed contrast enhancement method has shown better accuracy and Kappa Coefficient values.

6.2. Conclusions

1. The developed CHE based contrast enhancement technique for automatic shoreline detection from satellite images has shown good contrast enhancement and brightness preservation without introducing any noise in the enhanced image compared to Bi-HE and Multi-HE based methods. It has shown *73.92 PSNR* and *7.31 AMBE* values for 2005 satellite image and *68.35 PSNR* and *5.91 AMBE* values for 2010 satellite image.
2. To overcome the drawbacks of conventional shoreline extraction, the developed clipped histogram equalization based contrast enhancement and thresholding based algorithm has shown better positional accuracy of 96%, when compared to GPS survey values. End Point Rate (EPR) and Linear Regression Rate (LRR) statistical methods inbuilt in DSAS are shown more substantial shoreline change rates in Mulky-Pavanje rivermouth area and Netravati-Gurpur rivermouth area from 2005 to 2013.

   Hejamadi Kodi Sand Spit, northern sector of Mulky-Pavanje rivermouth is under deposition and maximum shoreline accretion rate is 33.47 m/yr from EPR and 28.97 m/yr from LRR. The southern segment, Sasihitulu Sand Spit is also under accretion with the maximum accretion rate of 20.76 m/yr (EPR) and 22.8 m/yr (LRR). The shoreline accretion is observed in Sasihitulu Beach with an average shoreline change rate of 1.25 m/yr from EPR and 2 m/yr from LRR statistics due to onshore movement of sediments during post-monsoon.

Bengre Sand Spit, northern sector of Netravati-Gurpur rivermouth is under deposition and the maximum shoreline accretion rate is 8.73 m/yr from EPR and 8.89 m/yr from LRR at transect 215. The Tannirbhavi beach has shown not much change in shoreline and an average shoreline accretion rate is 1.48 m/yr (EPR) and 1.37 m/yr (LRR). The Ullal Sand Spit, southern segment of Netravati-Gurpur rivermouth, is undergoing erosion due to high concentration of wave energy with an average shoreline erosion rate of -1.93 m/yr (EPR) and -1.91 m/yr (LRR). Maximum shoreline erosion is observed in Ullal beach is -3.30 m/yr (EPR) and -2.96 m/yr (LRR). Someshwara Beach is under erosion and accretion and an average accretion rate is 3.38 m/yr (EPR) and 3.1 m/yr (LRR) and an average erosion rate is -3.87 m/yr (EPR) and -3.72 m/yr (LRR).

The developed automatic shoreline detection method is more efficient, faster and suitable for a larger area and provides high positional accuracy and applicable for global shoreline extraction.

3. The developed integrated CHE-based contrast enhancement and PCA based algorithm for suspended sediment transport mapping has shown better tonal variation of sediment concentration. The distribution and direction of sediment map matches well with the results of Dwarakish et al. (2010) and Avinash et al. (2012). The developed contrast enhancement algorithm for SSC distribution along Mangalore Coast using OCM data is satisfactory.

4. The combined CHE-based contrast enhancement and PCA based algorithm improved the accuracy of classification of land use and land cover. For Mulky-Pavanje rivermouth area the developed method has provided 85.42% of accuracy and 0.83 kappa value, for NMPT area 89.66% of accuracy and

0.88 kappa value and for Netravati-Gurpur rivermouth area 86.93% of accuracy and 0.85 kappa value.

5. Clipped histogram equalization based methods are more suitable and efficient for remotely sensed satellite images for contrast enhancement.

6.3. Scope for future study

Developed contrast enhancement algorithms can be applied for:

1. An automatic detection of wetlands along the coastal zone.
2. Identification of oil spill zones using satellite data.
3. Fine resolution satellite images for identification of sediment distribution and transport.
4. Develop an automatic classification and mapping of land use and land cover (LULC).

REFERENCES

Al Bakri, D., (1996). “Natural hazards of shoreline bluff erosion: a case study of Horizon View, Lake Huron.” *Geomorphology*, 17, 323-337.

Allee, R. J., and Johnson, J. E., (1999). "Use of satellite imagery to estimate surface chlorophyll-a and Secchi disc depth of Bull Shoals, Arkansas, USA." *Int. J. Remote Sens.*, 20, 1052-1072.

Amarsaikhan, D., Saandar, M., Ganzorig, M., Blotevogel, H., Egshiglen, E., Gantuyal, R., Nergui, B., and Enkhjargal, D., (2012). “Comparison of multisource image fusion methods and land cover classification.” *Int. J. Remote Sens.*, 33(8), 2532-2550.

Anil, A. H., Yalcin, Y., Esin, O. C., Isikhan, G., Ahmet, C. Y., and Bulet, B., (2007). “Determination and control of longshore sediment transport: A case study.” *Ocean Engg.*, 34, 219-233.

Antonio, J. S., Francisco, J. L., Antonio, A., Patricia, B., Luis, M. F. S., Victor, D. R., and Jose V. P. P., (2010). “Human driven coastline changes in the Adra River deltaic system, southeast Spain.” *Geomorphology*, 119, 9-22.

Aplin, P., and Atkinson, P. M., (2001). “Sub-pixel land cover mapping for per-field classification.” *Int. J. Remote Sens.*, 22(14), 2853-2858.

Avinash, K., Jena, B., Vinaya, M. S., Jayappa, K. S., Narayana, A. C., and Bhat, H. G., (2012). "Regionally tuned algorithm to study the seasonal variation of suspended sediment concentration using IRS-P4 Ocean Colour Monitor data." *Egyptian J. Remote Sens. Space Sci.*, 15, pp. 67-81, 2012.

Avinash, K., Narayana, A. C., and Jayappa, K. S., (2010). “Shoreline changes and morphology of spits along southern Karnataka, West Coast of India: A remote sensing and statistics-based approach.” *Geomorphology*, 120, 133-152.

Bagli, S., and Soile, P., (2003). "Morphological automatic extraction of Pan-European coastline from Landsat ETM+ images," in *Proceedings of the Fifth Int. Symp. GIS and Computer Cartogr. Coast. Zone Manag.*, Genova.

Bannur, C. R., Sherieff, A. N., Basappa Reddy, M., and Shreedhara, V., (1991). "Application of Remote Sensing Technique in Detection of Morphological Changes in the Vicinity of Estuarine Mouths - A Case Study pertaining to D.K. District." *Workshop Indian Remote Sens. Satell. Mission Appl.*

Bayram, B., Acar, U., and Ari, A., (2008). "A novel algorithm for coastline fitting through a case study over the Bosphorus." *J. Coast. Res.*, 24(4), 938–991.

Beaubien, J., (1994)."Landsat TM satellite images of forest: from enhancement to classification." *Canadian J. Remote Sens.*, 20, 17-26.

Beaubien, J., and Cihlar, J., Xiao, Q., Chen, J., Fung, K., and Hurlburt, P., (1997). "A new, nationally consistent, satellite-derived land covers of Canada: a comparison of two methodologies." *Proc. Int. Symp. Geomatics Era Radarsat*, 25-30.

Beaubien, J., and Simard, G., (1993). Methodologie de classification des donnees AVHRR pour la surveillance du couvert vegetal." Proc. 16th Canadian Remote Sens. Symp., Sherbrooke, Quebec, 597-603.

Bhat, H. G., and Subramanya, K. R., (1993). "Paleoshorelines and Coastal Processes in Dakshina Kannada, Karnataka, India: A Study Based on Remotely Sensed Data." *Int. J. Remote Sensing*, 14(17), 3311-3316.

Boak, E., and Turner, I., (2005). "Shoreline definition and detection: A review." *J. Coast. Res.*, 21, 688-703.

Bonnett, R, and Campbell, J. B., (2002). *Introduction to Remote Sensing,* New York: Taylor & Francis.

Bouchahma, M., and Yan, W., (2012). "Automatic measurement of shoreline change on Djeba Island of Tunisia." *Computer Inf. Sci.*, 5(5), 17-24, 2012.

Braud, D. H., and Feng, W., (1998). *Semi-automated construction of the Louisiana coastline digital land/water boundary using Landsat Thematic Mapper*

satellite imagery, Baton Rouge, Louisiana State University, Department of Geography and Anthropology, Louisiana Oil Spill Research and Development Program, Technical Report Series, 97-002.

Bruun, P., (1985). *Design and Construction of Mounds for Breakwaters and Coastal Protection*, New York: Elsevier Publications.

Burrough P. A., and McDonnel R. A., (1998), "Principles of Geographical Information Systems," Oxford University Press, pp. 1-135.

Byrne, G. F., Crapper, P. F., and Mayo, K. K., (1980). "Monitoring land-cover change by principal components analysis of multitemporal Landsat data." *Remote Sens. Environ.*, 10, 175-184.

Cambell, J. B., (2002). *Introduction to Remote Sensing*, 3 rd ed., The Gilford Press, New York.

Canny, J., (1986). "A computational approach to edge detection." *IEEE Trans. Pattern Anal. Mach. Intell.*, 8, 679–698.

Celik, T., and Tjahjadi,T., (2012). "Automatic image equalization and contrast enhancement using Gaussian mixture modeling.", *IEEE Trans. Image Process.*, 21, 145–156.

CERC, (1984). "Coastal Engineering Research Center US Army Corps of Engineers, Washington D C, US.", *Shore Prot. Man.*, Gov. Printing Office, 2.

Chauhan, P., (2000). "Retreival of water constituents using ocean colour data: IRS-P4 OCM data processing." *Pre-conf. train.*, 6-10.

Chauhan, P., Mohan, M., Nayak, S. R., and Navalgund, R. R., (2002). "Comparison of ocean color chlorophyll algorithms for IRSP4 OCM sensor using in-situ data." *J. Indian Soc. Remote Sens.*, 30(1), 81–94.

Chauhan, P., Nayak, S., Ramesh, R., Krishnamoorthy, R., and Ramachandran, S., (1996). "Remote Sensing of Suspended Sediments along the Tamil Nadu Coastal Waters." *J. Indian Soc. Remote Sens.*, 24, 2, 107-114.

Chen, L. C., and Rau, J. Y., (1998). "Detection of shoreline changes for tideland areas using multi-temporal images." *Int. J. Remote Sens.*, 19(17), 3383-3397.

Chen, S. D., (2012). "A new image quality measure for assessment of histogram equalization-based contrast enhancement technique." *Digital Signal Process.*, 22, 640-647.

Chen, S. D., and Ramli, A. R., (2003). "Minimum Mean Brightness Error Bi-Histogram Equalization in Contrast Enhancement." *IEEE Trans. Consumer Electron.*, 49(4), 1310-1319.

Chen, S.-D., and Ramli, A. R., (2004). "Preserving brightness in histogram equalization based contrast enhancement techniques." *Digital Signal Process.*, 14(05), 413-428.

Cihlar, J., Okouneva, G., Beaubien, J., and Latifovic, R., (2001). "A New Histogram Quantization Algorithm For Land Cover Mapping." *Int. J. Remote Sensing*, 22(11), 2151-2169.

Clark, J. R., (1995). *Coastal zone management handbook*, Boca Raton, USA: Lewis publishers.

Comber, A. J., and Law, A. N. R., (2004). "Application of knowledge for automated land cover change monitoring." *Int. J. Remote Sensing*, 25(16), 3177-3192.

Congalton, R. G., (1991). "A review of assessing the accuracy of classifications of remotely sensed data." *Remote Sensing of Envi.*, 37, 35-46.

Congalton, R. G., and Mead, R. A., (1983). "A Quantitative Methods to Test for Consistency and Correctness in Photointerpretation." *Photogramm. Engg. Remote Sensing*, 49(1), 69-74.

Constanza, R., D'Agre, R., De. Groot, R., Farber, S., Grasso, M., and Hannon, B., (1997). "The value of the world's ecosystem services and natural capital." *Nature*, 387, 253-260.

Cracknell, A. P., (1999). "Remote sensing techniques in estuaries and coastal zones-an update." *Int. J. Remote Sensing*, 20(03), 485-496.

Crowell, M. and Leatherman, S. P., (1999). "Coastal Erosion Mapping and Management." *J. Coast. Res.*, 28, 1-196.

Curran, P. J., and Wilkinson, H. D., (1985). “Mapping the concentration and dispersal pattern of dye from a long sea outfall using digitized aerial photography.” *Int. J. Remote Sens.*, 6, 17-31.

Dan, H., Yongjiu, F., and Lijun, S., (2012). "Mapping shoreline of Hangzhou Bay with remote sensing images from 1979 to 2005." *IEEE 2012 2nd Int. Conf. Remote Sens. Envir. Transp. Eng. (RSETE-2012),* 1-4.

Das, I., Mohan, M., and Krisnamoorthy, K., (2002). "Detection of Marine Aerosols with IRS-P4 cean Color Monitor." *Proc. Indian Acad. Sci. (earth & Planet Sci.).* 111.

Dattatri, J. and Kamath, M., (1997). “Littoral drifts and maintenance dredging at New Mangalore Port.” *Proc. Second Indian Nat. Conf. on Harbour and Ocean Engg. (INCHOE-97), Thiruvananthapuram, India*, 578-585.

Dattatri, J., Rao, N. B. S., Subba Rao, Dwarakish, G. S., and Nagendra, K. B., (1997). “Beach profile studies along Dakshina Kannada Coast of Karnataka State.” *Proc. Second Indian Nat. Conf. on Harbour and Ocean Engg. (INCHOE-97), Thiruvananthapuram, India*, 1135-1143.

Demirel, H., Ozcinar, C., and Anbarjafari, G., (2010). "Satellite Image Contrast Enhancement using Discrete Wavelet Transform and Singular Value Decompostion." *IEEE Geosci. Remote Sens. Lett.*, 7(2), 333-337.

Dhnawan, A., Buelloni, G., and Gordon, R., (1986). "Enhancement of mammographic features by optimal adaptive neighbourhood image processing." *IEEE-Trans. Med. Imaging*, 5, 8-15.

Di, K., Wang, J., Ma, R., and Li, R., (2003). "Automatic shoreline extraction from high-resolution IKONOS satellite imagery." *ASPRS 2003 Annu. Conf. Proc.*, Anchorage, Alaska, (2003).

Dolan, R., Fenster, M. S., Holme, S. J., (1991). “Temporal analysis of shoreline recession and accretion.” *J. Coast. Res.*, 7, 723-744.

Dolan, R., Hayden, B**.,** May, P., and May, S. K., (1980). "The reliability of shoreline change measurements from aerial photographs." *Shore and Beach,* 48(4), 22-29.

Dwarakish, G. S., Dattatri, J., and Anisha, M., (1997). "Remote Sensing application for study of rivermouth changes of Dakshina Kannada district, Karnataka." *Proc. Int. Conf. on remote sensing and GIS, Hyderabad, India*, 473-483.

Dwarakish, G. S., Dattatri, J., Rao, N. B. S., and Subba Rao, (1998). "Application of Remote Sensing to study the dynamic changes of Netravati-Gurpur rivermouth, D. K. Coast, Karnataka." *Proc. Int. Symp. Inf. Technol. Oceanogr.*, NIO, Goa, India, 72.

Dwarakish, G. S., Usha Natesan, Nayak, S. R., Chauhan, P., and Nagur, C. R. C., (2010). "Analysis of IRS-P4 OCM data for estimating the suspended sediment concentrations along the Mangalore Coast, India." *Int. J. Imaging*, 3(S10), 23-39.

Dwarakish, G.S., (2001). *Study of Sediment Dynamics off Mangalore Coast using Conventional and Satellite Data.* Anna Univ, Chennai, India

Dwarakish, G.S., and Usha Natesan, (2002). "Coastal structures Vs shoreline configuration." *NITK Res. Bulletin*, 11(3), 25-33.

Faid, A. M., and Abdulaziz, A. M., (2012). "Monitoring land-use change-associated land development using multitemporal Landsat data and geoinformatics in Kom Ombo area, South Egypt." *Int. J. Remote Sens.*, 33(22), 7024-7046.

Forget, P., Broche, P., and Naudin, J. J., (2001). "Reflectance sensitivity to solid suspended sediment stratification in coastal water and inversion: A case study." *Remote sens. Environ.,* 77, 92-103.

Forster, B. C., Xingwei, I. S., and Baide, X., (1993). "Remote Sensing of water quality parameters using Lansat TM." *Int. J. Remote Sens.,* 14, 2759-2771.

Frazier, P. S., and Page, K. J., (2000). "Water body detection and delineation with Landsat TM data.," *Photogramm. Eng. Remote Sens.,* 66(2), 1461-1467.

Frihy, O. E., Dewidar, K. H., EL Banna, M., (1998). "Natural and human impact on the northeastern Nile Delta coast of Egypt." *J. Coastal Res.*, 14, 1109-1118.

Frihy, O. E., Nasr, S. M., EL Hattab, M. M., EL Raey, M., (1994). "Remote sensing of beach erosion along the Rosetta promontory, northwestern Nile Delta, Egypt." *Int. J. Rem. Sens.*, 15, 1649-1660.

Fung, T., and Ellsworth, L., (1987). "Application of principal components analysis to change detection." *Photogramm. Eng. Remote Sens.*, 53, 1649-1658.

Garcia, C. A. E., and Robinson, I. S., (1989). "Sea surface velocities in shallow seas extracted from sequential coastal zone color scanner satellite data." *J. Geophy. Res.*, 94, 12681-12691.

Gonzalez, R. C., and Woods, R. E., (1992). *Digital Image Processing.* 2nd Edition Reading, MA. Addison-Wesley, 1992, 85-103.

Gonzalez, R. C., and Woods, R. E., (2008). *Digital Image Processing*, 3rd ed., Prentice Hall, Upper Saddle River, NJ.

Gorden, H. R., and Morel, A. Y., (1983). *Remote assessment of ocean color for interpretation of satellite visible imagery: a review*, Springer, New York.

Gowda, H. H., Ganeshraj, K., Padmavathy, A. S., and Manikiam, B., (1995). "Multidate Satellite Data for Study of Dynamic of Coastal Landforms of Uttara Kannada, South India." *Int. J. Remote Sens.*, 16(14), 2539-2553.

Hegde, A. V., and Ravindra, B., (2000). "Short-Term and Long-Term Geomorphological Dynamics of Mangalore Spits Using IRS-1A/1C Data." *J. Indian Soc. Remote Sens.*, 28(4), 233-247.

Hegde, V. S., Kanchanagouri, Hanamgond, P. T., Huchchannavar, G. K., Shalini, G., and Bhat, M. S., (2004). "Depositional Environment and silting in the Sharavati estury, Central West Coast of India."*Indian J. Mar. Sci.* 33(3), 296-302.

Hegde, V. S., Shalini, G., Nayak, S. R., Rajawat, A. S., Suryanarayana, A., Jaykumar, S., Koti, B. K., and Girish, G. K., (2009). "Low-Scale Foreshore

Morphodynamic Processes in the Vicinity of a Tropical Estury at Honnavar, Central West Coast of India." *J. Coast. Res.*, 25(2), 305-314.

Himmelstoss, E. A., (2009). "DSAS 4.0 Installation Instructions and User Guide" in: Thieler, E. R., Himmelstoss, E. A., Zichichi, J. L., and Ergul, Ayhan. 2009 Digital Shoreline Analysis System (DSAS) version 4.0 — An ArcGIS extension for calculating shoreline change: *U.S. Geological Survey Open-File Report* 2008-1278.

Hooker, S. B., Esaisa, W. E., Feldman, G., and McClain, C. R., (1992). "Overview of SeaWiFs and ocean color, SeaWiFs Technical report series." *Natl. Aeronaut. Space Adm. Technol. Memorandom 104566*, 1-24.

Horikawa, K., (1978). *Coastal Engineering - An Introduction to Ocean Engineering*, New York: Hoisted Press.

Huang, S. C., and Yeh, C. H., (2013). "Image contrast enhancement for preserving mean brightness without losing image features." *Eng. Appl. Artif. Intel.*, 26, 1487-1492.

Humied, I. A., Fatma, E. Z., Abou-Chadi, and Rashad, A. M., (2012). "A new combined technique for automatic contrast enhancement of digital images." *Egyptian Inf. J.*, 13, 27-37.

Hummel, R., (1977). "Image enhancement by histogram transformation." *Computer Graphics Image Process*, 6, 184-195.

Ibrahim, H., and Pik Kong, N. S., (2007). "Brightness Preserving Dynamic Histogram Equalization for Image Contrast Enhancement," *IEEE Trans. Consumer Electron.*, 53(04), 1752-1758.

IOCCG (2000). "Remote Sensing of ocean Color in Coastal, and other optically-Complex, waters." Sathyendranath, S. (ed.), *Reports of the International Ocean Color Coordinating Group*, No. 3, IOCCG, Dartmouth, Canada.

Jain, K., (1989). *Fundamentals of digital image processing*, Prentice-Hall.

Jayappa, K. S., Vijay Kumar, G. T., and Subrahmanya, (2003). "Influence of coastal structures on the beaches of southern Karnataka, India." *J. Coast. Res.*, 19(2), 389-408.

Jensen, J. R., (1996). *Introductory Digital Image Processing-A Remote Sensing Perspective,* 2 nd ed., Prentice hall Series in Geographic Information Science.

Jesus, A. G., Arie, C. S. and Joost, F. D., (2012). "Optimizing land cover classification accuracy for change detection, a combined pixel-based and object-based approach in a mountainous area in Mexico." *Appl. Geogr.*, 34, 29-37.

Jishuang, Q., and Chao, W., (2002). "A multi-threshold based morphological approach for extraction coastal line feature in remote sensed images." *Pecora 15/L & Satell. Inf. IV Conf. ISPRS Comm. I/FIEOS, Denver, Colorado,* 319–338.

Jorge, G., and Albert, P., (1996). "Short and medium-term grain size changes in deltaic beaches (Ebro delta, NW Mediterranean)." *Sed Geo.*, 101, 55-67.

Jyoti, S., and Rawat, P., (2007). "Image Enhancemnet method for Underwater ground and Satellite Images using Brightness Preserving Histogram Equalization with Maximum Entropy." *IEEE Computer Soc.-Int.Conf. Comput. Intel. Multimedia Appl., ICCIMA-2007,* 507-512.

Khan, M., Khan, E., and Abbasi, Z. A., (2012). "Weighted average multi segment histogram equalization for brightness preserving contrast enhancement." *IEEE Int. Conf. Signal Process., Computer Control*, ISPCC.

Kim, M., and Chung, M. G., (2008). "Recursively Separated and Weighted Histogram Equalization for Brightness Preservation and Contrast Enhancement." *IEEE Trans. Consumer Electron.*, 54(3), 1389-1397.

Kim, T., and Paik, J., (2008). "Adaptive Contrast Enhancement Using Gain-Controllable Clipped Histogram Equalization." *IEEE Trans. Consumer Electron.*, 54(4), 1803-1810.

Kim, Y. T., (1997) "Contrast Enhancement Using Brightness Preserving Bi-Histogram Equation." *IEEE Trans. Consumer Electron.*, 43(1), 1-8.

Kim,T. K., Paik, J. K., and Kang, B. S., (1998). "Contrast enhancement system using spatially adaptive histogram equalization with temporal filtering." *IEEE Trans. Consumer Electron.*, 44(01), 82-86.

Klemas, V., Bartlett, D., Pot, W., Rogers, R., and Reed, L., (1974). "Coastal and estuarine studies with ERTS-1 and skylab." *Remote Sens. Environ.*, 3, 153-174.

Komar, P. D., (1976). *Beach Processes and Sedimentation*, Englewood Cliffs: Prentice Hall.

Komar, P. D., (1976). *Beach Processes and Sedimentation*, Prentice-Hall, Inc., Englewood Cliffs, NJ.

Komar, P. D., (1998). *Beach processes and sedimentation, Upper Saddle River, New Jersey*, Prentice Hall Inc., 544.

Kong, N. S. P., Ibrahim, H., Ooi, C. H., and Chieh, D. C. J., (2009). "Enhancement of Microscopic Images Using Modified Self-Adaptive Plateau Histogram Equalization." *Int. Conf. Computer Technol. Dev.*, 308-310.

Kong, N.S.P., and Ibrahim, H., (2008). "Color image enhancement using brightness preserving dynamic histogram equalization." *IEEE Trans. Consumer Electron.*, 54(04), 1962-1968.

KREC Study Team, (1994), "Study on Coastal Erosion (Dakshina Kannada District), Input to Environmental Master Plan Study, Danida-DEE-Mangalore", KREC, Surathkal, 113-189.

Kuleli, T., (2010). "Quantitative analysis of shoreline changes at the Mediterranean Coast in Turkey." *Environ. Monit. Assess.*, 167, 387-397.

Kuleli, T., Guneroglu, A., Karsli, F., and Dihkan, M., (2011). "Automatic detection of shoreline change on coastal Ramsar Wetlands of Turkey." *Ocean Eng.*, 38, 1141-1149.

Kumar, P., Sanabada, M. K., and Parida, P. K., (1992). "Monitoring and Analysis of Shifting Shoreline Near Subarnarekha rivermouth of East Coast of India using Remote Sensing and GIS." *Proc. Remote Sens. Appl. Geogr. Inf. Syst. - Recent Trends*, Tata McGraw Hill Publ. Comp. Ltd., India, 359-362.

Kunte, P. D., (1994). "Sediment transport along the Goa-north Karnataka coast, western India." *Mar. Geol.,* 118, 207-216.

Kunte, P. D., (2008). "Sediment concentration and bed form structures of Gulf of Cambay from remote sensing." *Int. J. Remote Sens.*, 29 (8), 2169-2182.

Kunte, P. D., and Wagle B. G., (2001). "Littoral transport studies along west coast of India-A review." *Indian J. Mar. Sci.*, 30, 57-64.

Kunte, P. D., and Wagle, B. G., (1991). "Spit Evaluation and shore drift direction along south Karnataka coast, India." *Giornale di Geologia,* 53, 71-80.

Kunte, P. D., and Wagle, B. G., (1993). "Determination of net shore drift direction of Central West Coast of India using remotely sensed data." *J. Coastal Res.*, 9, 811-822.

Kunte, P. D., Osawa, T., and Sugimori, Y., (2002). "Chlorophyll and Sediment distribution study of the Gulf of Kutch using Remote Sensing." *PORSEC*, Goa.

Kunte, P. D., Wagle, B. G., and Sugimori, Y., (2003). "Sediment transport and depth variation study of the Gulf of Kutch using remote sensing." *Int. J. Remote Sens.*, 24(11), 2253-2263.

Lee, J. S., and Jurkevich, I., (1990). "Coastline detection and tracing in SAR images." *IEEE Trans. Geosci. Remote Sen.*, 28 (4), 662-668.

Li, R., Di, K., and Ma, R., (2001). *A comparative study of shoreline mapping techniques*, Halifax, Nova Scotia, Canada.

Liang, K., Ma, Y., Xie, Y., Zhou, B., and Wang, R., (2012). "A new adaptive contrast enhancement algorithm for infrared images based on double plateaus histogram equalization." *Infrared Phy. Technol.*, 55, 309-315.

Lillesand, M. T., Kiefer, R. W., and Chipman, J. W., (2004). *Remote Sensing and Image Interpretation,* John Wiley and Sons, Newyork, 1-48.

Lillesand, M.T. and Kiefer, R. W. (1994). *Remote Sensing and Image Interpretation,* John Wiley and Sons, Newyork, 1-48.

Liu, H., and Jezek, K. C., (2004). "Automated extraction of coastline from satellite imagery by integrating Canny edge detection and locally adaptive thresholding methods." *Int. J. Remote Sens.,* 25(5), 937-958.

Maiti, S., and Battacharya, A. K., (2009). "Shoreline change analysis and its application to prediction: A remote sensing and statistics based approach." *Mar. Geol.,* 257, 11-23.

Manavalan P., Adiga, S., Gangadhar Bhat, H., Subramanya, K.R., (1996). "Assessment of Coastal Environment using High Resolution IRS-IC Data." *Int. J. Remote Sens.,*

Mas, J. F., (1999). "Monitoring land-cover changes: a comparison of change detection techniques." *Int. J. Remote Sens.,* 20, 139-152.

Mason, D. C., and Davenport, I. J., (1996). "Accurate and efficient determination of the shoreline in ERS-1 SAR images." *IEEE Trans. Geosci. Remote Sens.,* 34(5), 1243-1253.

Mckim, H. L., Merry, C. J., and Layman, R. W., (1984). "Water quality monitoring using an airborne spectroradiometer." *Photogramm. Eng. Remote Sens.,* 50, 353-360.

Menon, H. B., (2004). "Calibration of an optical equation to analyse the atmospheric turbidity and water quality of an estuarine environment," *J. Indian Soc. Remote Sens.,* 32(3), 287-300.

Menotti, D., Najman, L., Facon, J., and Araujo, A. D. A., (2007). "Multi-Histogram Equalization Methods for Contrast Enhancement and Brightness Preserving." *IEEE Trans. Consumer Electron.,* 53(3), 1186-1194.

Mills, J. P., Buckley, S. J., Mitchell, H. L., Clarke, P. J., and Edwards, J., (2005). "A geomatics data integration technique for coastal change monitoring," *Earth Surface Processes and Landforms*, 30(6), 651-664.

Mishra, A. K., Dadhwal, V. K., and Dutt, C. S., (2008) "Analysis of marine aerosol optical depth retrieved from IRS-P4 OCM sensor and comparison with the aerosol derived from SeaWiFs and MODIS sensor." *J. Earth System Sci.,*117, 361-373.

Moore, G. F., Aiken, J., and Lavender, S. J., (1999). "The Atmospheric correction of water color and the quantitative retreival of suspended particulate matter in case 2 waters: application to MERIS." *Int. J. Remote Sens.*, 20, 1713-1733.

Moore, L.J., (2000). "Shoreline mapping techniques." *J. Coast Res.*, 16, 111-124.

Morel, A., (1980). "In-water and remote measurement of ocean color." *Boundary-Layer Meteorol.* 18(2), 177-201.

Morel, A., and Prieur, L., (1977). "Analysis of variations in ocean color." *Limnol. Oceanogr.*, 22(4), 709-722.

Morrow W, Paranjape R, Rangayyan R and Desautels J. (1992). "Region-based contrast enhancement of mamograms." *IEEE-Trans. Med. Imaging*, 11(3), 392-405.

Nagaraj, G., and Dwarakish, G. S., (2011). "Shoreline changes along the Mangalore Coast, West Coast of India." *Int. J. Earth Sci. Eng.*, 4(3), 63-70.

Nayak, S. R., and Sahai, B., (1985). "Coastal morphology: A case study of the Gulf of Khambhat (Cambay)." *Int. J. Remote Sens.*, 6, 559-567.

Nayak, S. R., Sarangi, R. K., and Rajawat, A. S., (2002). "Application of IRS P4 OCM data to study the impact of cyclone on coastal environment of Orissa." *Current Sci.*, 80, 1208-1213.

Neycenssac, F., (1993). "Contrast enhancement using the Laplacian-of-a-Gaussian filter, CVGIP." *Graphical Models Image Process,* 55, 447-463.

Niedermeier, A., Romaneeben, E., and Lehner, S., (2000). "Detection of coastline in SAR images using wavelet methods." *IEEE Trans. Geosci. Remote Sens.*, 38(5), 2270-2281.

Ooi, C. H., Isa, N. A. M., (2010). "Quadrants Dynamic Histogram Equalization for Contrast Enhancement." *IEEE Trans. Consumer Electron.*, 56(4), 2552-2559.

Ooi, C. H., Pik, N. S., Kong and Ibrahim, H., (2009). "Bi-Histogram Equalization with a Plateau Limit for Digital Image Enhancement." *IEEE Trans. Consumer Electron.*, 55(4), 2072-2080.

Otsu, N., (1979). "A threshold selection method from gray level histograms." *IEEE Trans. Syst. Man Cybern.*, 9(1), 62-66.

Pardo-Pascual, J. E., Almonacid-Caballer, J., Ruiz, L. A., and Palomar-Vazquez, J., (2012). "Automatic extraction of shorelines from Landsat TM and ETM+ multi-temporal images with subpixel precision" *Remote Sens. Environ.*, 123, 1-11.

Parker, J. R., (1997). *Algorithms for Image Processing and Computer Vision*. New York, John Wiley & Sons.

Patel, N., and Kaushal, B. K., (2010). "Improvement of User's Accuracy Through Classification of Principal Component Images and Stacked Temporal Images." *Geo-spatial Inf. Sci.*, 13(4), 243-248.

Pei, S. C., Zeng, Y. C., and Chang, C. H., (2004). "Virtual restoration of ancient Chinese paintings using color contrast enhancement and lacuna texture synthesis." *IEEE Trans. Image Process.*, 13, 416-429.

Pizer, S. M., (2003). "The medical image display and analysis group at the University of North Carolina: Reminiscences and philosophy." *IEEE Trans. Med. Image*, 22, 2-10.

Pizer, S. M., Johnston, R. E., Ericksen, J. P., Yankaskas, B. C., and Muller, K. E., (1990). "Contrast-limited adaptive histogram equalization: speed and

effectiveness," *In proc. the First Conf. Visualization in Biomed. Comp.*, 337-345.

Pratt, W. K., (1978). *Digial Image Processing.* New York, Wiley.

Press, W.H., Teukolsky, S.A., Vetterling, W.T., and Flannery, B.P., (1992). *Numerical Recipes in FORTRAN: The Art of Scientific Computing*, 2nd ed. London: Cambridge, 963.

Prithiviraj, M., Sengupta, S., Gosh, S. K., Ramana, I. V., and Chakraborty, D., (1995). "Documentation of the Long-term Coastal Geomorphic Changes within the Hugli River Estuary, India." *Asian-Pacific Remote Sens. J.*, 7(2), 1-9.

Rabben, E. L., (1960). "Fundamentals of photo interpretation." *Man. Photogr. Interpret., The American Soc. Photogramm.*, 99-168.

Raghavan, B. R., Vinod, B. T., Dimple, K. A., Venkatesh, P. H., Udayashankar, H. N., and Sreedhara, M. T., (2001). "Evaluation of the Netravathi spit complex, west coast of India: Integrated change detection study using topographic and remotely sensed data." *Indian J. Mar. Sci.*, 30(4), 268-270.

Raju, A., Dwarakish, G. S., Venkat Reddy, D., (2014). "Modified Self-Adaptive Plateau Histogram Equalization with Mean Threshold for Brightness Preserving and Contrast Enhancement." *Proc. 2014 IEEE Region 10 Symp., IEEE Xplore*, 202-207.

Rangayyan, R. M., and Nguyen, H. N., (1986). "Pixel-independent image processing techniques for enhancement of features in mammograms," *Proceedings of the eigth IEEE Eng. Med. Biol. Conf.*, 1113-1117.

Rao, R. V., Ramana Murthy, M. V., Manujunath Bhat and Reddy, N. T., (2009). "Littoral sediment transport and shoreline changes along Ennore on southeast coast of India: Field observations and numerical modelling." *Geomorphology*, 112, 158-166.

Rasuly, A., Naghdifar, R., and Rasoli, M., (2010). "Monitoring of Caspian sea coastline changes using object-oriented techniques." *Procedia Environ.Sci.*, 2, 416-426.

Reddy, M. A., (1993). "Remote sensing for mapping of suspended sediments in Krishna Bay Estuary, Andhra Pradesh, India." *Int. J. Remote Sens.*, 14, 2215-2221.

Ritchie, C. J., Cooper, C. M., and Schiebe, F. R., (1990). "Th erelationship of MSS and TM digital data with suspended sediment, chlorophyll and temperature in Moon Lake, Mississippi." *Remote Sens. Environ.,* 33, 137-148.

Robinson, M. C., Morris, K. P., and Dyer, K. R., (1998)."Deriving fluxes of suspended particulate matter in the Humber estuary, UK, using airborne remote sensing." *Mar. Pollut. Bulle.*, 37, 155-163.

Ryan, T. W., Sementilli, P. J., Yuen, P., and Hunt, B. R., (1991). "Extraction of shoreline features by neural nets and image processing." *Photogramm. Eng. Remote Sens.*, 57, 947-955.

Ryu, J. H., Won, J. S., and Min, K. D., (2002). "Waterline extraction from Landsat TM data in a tidal flat: a case study in Gomso bay, Korea." *Remote Sens. Environ.*, 83, 442–456.

Sanil, K. V., Pathak, K. C., Pednekar, P., Raju, N. S. N., and Gowthaman, R., (2006). "Coastal processes along the Indian coastline." *Current Sci.*, 91(4), 530-536.

Santosh, K. M., and Reddy, H. R. V., (2002). "Study of sediment movement and coastal process along Mangalore coast (Southwest coast of India) using satellite imageries." *Indian J. Mar. Sci.*, 31(4), 290-294.

Santosh, K. M., Reddy, H. R. V., Chauhan, P., and Sarangi, R. K., (2002). "Study of sediment movement and coastal processes along Mangalore coast (southwest coast of India) using satellite imageries." *Indian J. Mar. Sci.*, 31, 290-294.

Sarangi, R. K., Nayak, S., and Panigrahy, R. C., (2008). "Monthly variability of chlorophyll and associated physical parameters in the southwest Bay of Bengal water using remote sensing data." *Indian J. Marine Sci.*, 37(3), 256–266.

Schriever, J. R., and Congalton, R. G., (1995). “Evaluating seasonal variability as an aid to cover-type mapping from Landsat Thematic Mapperdat ain the Northeast .” *Photogramm. Engg. Remote Sensing*, 61(3), 321-327.

Scott, D. B., (2005). “Coastal changes, rapid, In: Schwartz M.L”., in *Encyclopedia of coastal sciences*, The Netherlands, Springer, 253-255.

Selvavinayagam, K., Surendra, A., and Ramachandran, S., (2003). "Quantitative study on chlorophyll using IRS-P4 OCM data of Tituicorin coastal waters." *J. Indian Soc. Remote Sens.*, 3, 227-235.

Sengee, N., and Choi, H. K., (2008). "Brightness preserving weight clustering histogram equalization," *IEEE Trans. Consumer Electron.*, 54 (03), 1329-1337.

Sengee, N., Sengee, A., and Choi, H. K., (2010). "Image Contrast Enhancement using Bi-Histogram Equalization with Neighborhood Metrics." *IEEE Trans. Consumer Electron.*, 56(4), 2727-2734,.

Serra, J., (1982). “Image Analysis and Mathematical Morphology.” Academic Press, London.

Shankar, R., and Karbassi, A. R. (1992). “Sedimentological evidance for a palaeobeach off Mangalire, West-Coast of India.” *J. Geological Soci. India*, 40(3), 241-252.

Sheet, D., Garud, H., Suveer, A., Mahadevappa, M., and Chatterjee, V., (2010). "Brightness Preserving Dynamic Fuzzy Histogram Equalization," *IEEE Trans. Consumer Electron.*, 56(4), 2475-2480.

Sherman, D. J., Bauer, B. O., (1993). “Coastal geomorphology through the looking glass.” *Geomorphology*, 7, 225-249.

Sim, K. S., Tso, C. P., and Tan, Y. Y., (2007). "Recursive sub-image histogram equalization applied to gray scale images." *Pattern Recognit. Lett.*, 28, 1209-1221, 2007.

Singh, A., (1989). "Digital change detection techniques using remote sensed data." *Int. J. Remote Sens.*, 10, 989-1003.

Singh, A., and Harrison, A., (1985). "Standardized Principal Components." *Int. J. Remote Sensing*, 6, 883-896.

Singh, K., and Kapoor, R., (2014). "Image enhancement using Exposed based Sub Image Histogram Equalization." *Pattern Recognit. Lett.*, 36, 10-14.

Singh, R. P., Bhoi, S., and Sahoo, A. K., (2002). "Changes observed in land and ocean after Gujarat earthquake of 26 January 2001 using IRS data." *Int. J. Remote Sens.*, 23, 3123-3128.

Sinha, P., and Kumar, L., (2013). "Independent two-step thresholding of binary images in inter-annual land cover change/no-change identification." *ISPRS J. Photogramm. Remote Sens.*, 81, 31-43.

Smith, A.W.S., Jackson, L. A., (1992). "The variability in width of the visible beach." *Shore and Beach*, 60, 7-14.

Sohn, H. G., and Jezek, K. C., (1999). "Mapping ice sheet margins from ERS-1 SAR and SPOT imagery." *Int. J. Remote Sens.*, 20, 3201-3216.

Sravanthi, N., Ramana, I. V., Yunus, A. P., Ashraf, M., Ali, M. M., and Narayana, A. C., (2013). "An algorithm for estimating suspended sediemnt concentrations in the coastal waters of India using remotrely sensed reflectance and its application to coastal environments." *Int. J. Environ. Res.*, 7(4), 841-850.

Sri Ram, P., (2014), "Development of Algorithm for the Study of Sediment Dynamics through Sediment Trend Analysis: A Case Study of Mangalore Coast, West Coast of India." M.Tech thesis, Department of Applied Mechanics and Hydraulics, NITK, Surathkal, India

Story, M., and Congalton, R., (1986). "Accuracy Assessment: A user's Perspective." *Photogramm. Engg. Remote Sensing*, 10(1), 133-146.

Surendran, A., Selvavinayagam, K., Ramachandran, S., and Manoharan, N., (2006). "Validations of suspended sediment concentration (SSC) derived using ocean colour monitor (OCM) data off Chennai coast, India." *J. Indian Soc. Remote Sens.*, 34(4), 405–413.

Tang, D., Kawamura, H., and Luis, A. J., (2002). "Short term variability of phytoplankton blooms associated with a cold eddy in the north-eastern Arabian Sea." *Remote Sens. Environ.*, 81, 82-89.

Tassan, S., (1994). "Local algorithm using SeaWiFs data for retrival of phtoplanktonpigment, suspended sediemnts and yellow substance in coastal waters." *Appl. Opt.*, 12, 2369-2378.

Tassan, S., and Strum, B., (1986). "An algorithm for the retrieval of sediment in turbid coastal waters from CZCS data." *Int. J. Remote Sens.*, 7, 643-655.

Thieler, E. R., Himmelstoss, E. A., Zichichi, J. L., Miller, T. L., (2005). "Digital Shoreline Analysis System (DSAS) version 3.0: an ArcGIS extension for calculating shoreline change." *US Geol Surv.*, 1304.

Thiemann, S., and Kaufmann, H., (2000). "Determination of chlorophyll content and tropic state of lakes field spectrometer and IRS-1C satellite data in the Mecklenburg Lake District, Germany." *Remote Sens. Environ.*, 73, 227-235.

Torre, A., Peinado, A. M., Segura, J. C., Perez-Cordoba, J. L., Benitez, M. C., and Rubio, A. J., (2005). "Histogram equalization of speech representation for robust speech recognition." *IEEE Trans. Speech Audio Process.* 13, 355-366.

Touzi, R., Lopes, A., and Bousquet, P., (1988). "A statistical and geometrical edge detector for SAR images." *IEEE Trans. Geosci. Remote Sens.*, 26, 764-773.

Viollier, M., and Sturm, B., (1984). "CZCS data analysis in turbid coastal waters." *J. Geophy. Res.*, 89(D4), 4977-4985.

Vishwanath, D. N., (1993). "Study of coastal erosion and protection works along Dakshina Kannada coast." *M.Tech Thesis*, KREC, Mangalore, India.

Wadud, M. A. A., Kabir, M. H., and Chae, O., (2008). "A Spatially Controlled Histogram Equalization for Image Enhancement." *23rd Int. Symp. Computer Inf. Sci., ISCIS '08*, .

Wadud, M. A. A., Kabir, M. H., Dewan, M. A. A., and Chae, O., (2007). "A Dynamic Histogram Equalization for Image Contrast Enhancement." *IEEE Trans. Consumer Electron.*, 53(2), 593-600.

Wahad, A., Chin, S. H., and Tan, E. C., (1998). "Novel approach to automated fingerprint recognition." *IEEE Proc. Vision, Image, Signal Process.* 145, 160-166.

Wang, B. J., Liu, S. Q., Li, Q., and Zhou, H. X., (2006). "A real-time Contrast Enhancemnet Algorithm for Infreared Images based on Plateau Histogram." *Infrared Phy. Technol.*, 48, 77-82.

Wang, C., and Ye, Z., (2005). "Brightness Preserving Histogram Equalization with Maximum Entropy: A Variational Perspective." *IEEE Trans. Consumer Electron.,* 51(4), 1326-1334.

Wang, F., (1993). "A Knowledge-based Vision System for Detecting Land Changes at Urban Fringes." *IEEE Trans. Geosci. Remote Sensing*, 31(1), 136-145.

Wang, Y., Chen, Q., and Zhang, B., (1999). "Image Enhancement Based on Equal Area Dualistic Sub-Image Histogram Equalization Method." *IEEE Trans. Consumer Electron.*, 45(1), 68-75, 1999.

White, K., and El Asmar, H., (1999). "Monitoring changing position of coastlines using Thematic Mapper imagery, and example from the Nile Delta." *Geomorphol.*, 29, 93–105.

Whitelock, C. H., Witte, W. G., Usry, J. W., and Gurganus, E. A., (1978). "Penetration depths of green wavelength in turbid water." *Photogramm. Engg. Remote Sensing*, 44(11), 1405-1410.

Wongsritong, K., Kittayaruasiriwat, K., Cheevasuvit, F., Deihan, K., and Somboonkaew, A., (1998). "Contrast Enhancemnt using Multipeak Histogram Equalization with Brightness Preserving." *IEEE Asia-Pacific Conf. Circuits and Syst.*, 455-458.

Yamayo, H., Shimazaki, H., Matsunaga, T., Ishoda, A., McClennen, C., Yokoki, H., Fujita, K., Osawa, Y., Kayanne, H., (2006). "Evaluation of various satellite sensors for waterline extraction in a coral reef environment: Majuro Atoll, Marshall Islands." *Geomorphol.*, 82, 398–411.

Yang, S., Oh. J. H., and Park, Y., (2003). "Contrast Enahncemnet using Histogram Equalization with Bin Underflow and Bin Overflow," *Int. Conf. Image Process., ICIP-2003,* 1, 881-884.

Yu, Y., and Action, S. T., (2004). "Automated delination of coastline from polarimetric SAR imagery." *Int. J. Remote Sens.,* 25(17), 3423-3438.

Zheng, G., Peng, L., Tao, G., and Wang, C., (2011). "Remote sensing analysis of Bohai Bay West Coast shoreline changes." *IEEE Int. Conf. Spat. Data Min. Geogr. Knowl. Serv. (ICSDM),* 549-552.

Zimmerman, J., Pizer, S., Staab, E., Perry, E., McCartney, W., and Brenton, B., (1988). "Evaluation of the effectiveness of adaptive histogram equalization for contrast enhancement." *IEEE Trans. Med. Imaging,* 304-312.

Zuo, C., Chen, Q., and Sui, X., (2012). "Range Limited Bi-Histogram Equalization for Image Contrast Enhancement." *Optik,* 124, 425-431.

Zuzek, P. J., Nairn, R. B., Thieme, S. J., (2003). "Spatial and temporal consideration for calculating shoreline change rates in the Great Lakes Basin." *J. Coast. Res.,* 38, 125-146.

PUBLICATIONS

International Journal Papers (Published/Communicated)

1. Raju. A, G S Dwarakish and D. Venkat Reddy, (2013) "A State-of-the-Art and Comparative Analysis of Mean Brightness Preserving Histogram Equalization based Contrast Enhancement Techniques" *International Journal of Remote Sensing and GIS,* Vol. 2 (01), pp. 41-51, 2013. http://rpublishing.org/Journal/IJRSG/Vol2Issue1/rsg2105.pdf

2. Raju. A, G S Dwarakish and D. Venkat Reddy, (2013) "A Comparative Analysis of Histogram based Contrast Enhancement Techniques for Brightness Preserving" *International Journal of Signal Processing, Image Processing and Pattern Recognition*, Vol.6, No.5, pp.353-366, 2013. http://dx.doi.org/10.14257/ijsip.2013.6.5.31

3. Ganasri. B.P, Raju. A and G. S. Dwarakish, (2013) "Different Approaches for Land Use Land Cover Change Detection: A Review" *Research and Reviews: Journal of Engineering and Technology*, Vol. 2, No. 3, pp.44-48, 2013.

4. Raju. A, G S Dwarakish and D. Venkat Reddy, *"A Comparative Analysis of Histogram Equalization based Contrast Enhancement Techniques for Detection of Shoreline using Satellite Images", International Journal of Earth Sciences and Engineering,* Vol. 07, No. 2, pp. 522-529.

5. Raju A, Dwarakish G S and D Venkat Reddy, "Automated Extraction of Shoreline from Satellite Imagery using Histogram Equalization and Locally Adaptive Thresholding based Methods", *Egyptian Journal of Informatics.* [UNDER REVIEW]

6. Raju. A, G S Dwarakish and D. Venkat Reddy, "Automatic Detection and Analysis of Shoreline Change of Mulky-Pavanje Rivermouth Area, Mangalore

Cost, West Coast of India**",** *Journal of Applied Remote Sensing.* [UNDER REVIEW]

7. Raju A, Dwarakish G S and D Venkat Reddy, "Automatic Shoreline Detection and Change Analysis of Netravati-Gurpur Rivermouth Area, Mangalore Coast, West Coast of India", *Journal of Coastal Conservation*. [UNDER REVIEW]

8. Dwarakish G S, Raju A, Sri Ram and Mrinal S Murali, "Sediment Movement in and around Mulki - Pavanje River Mouth Inferred from Sediment Trend Analysis", *Journal of Applied and Engineering Sciences*. [UNDER REVIEW]

9. Raju A, Dwarakish G S and D Venkat Reddy, "A Comparative Analysis of Histogram Equalization based Contrast Enhancement Techniques for Detection of Shoreline using Satellite Images", *Journal of Coastal Development*. [UNDER REVIEW]

International/National Conference Papers (Presented/Communicated)

1. Raju. A, G S Dwarakish and D. Venkat Reddy, (2013) "Histogram Equalization based Mean Brightness Preserving and Contrast Enhancement Techniques – A Review", *3rd International Engineering Symposium–2013*, Kumamoto University, Japan, March 4-6, 2013.

2. Raju. A, G S Dwarakish and D. Venkat Reddy, (2013) "Modified Self – Adaptive Plateau Histogram Equalization with Mean Threshold for Brightness Preserving and Contrast Enhancement", *Proceedings of the 2013 IEEE Second International Conference on Image Information Processing (ICIIP -2013), IEEE Xplore*, 208-213, 2013.

3. Raju. A, G S Dwarakish and D. Venkat Reddy, (2014) "A Comparative Analysis of Histogram Equalization based Contrast Enhancement Techniques for

Detection of Shoreline using Satellite Images", *Indian National Conference on Harbour and Ocean Engineering (INCHOE-2014),* NIO, Goa, India.

4. Raju. A, G S Dwarakish and D. Venkat Reddy, (2014) "Satellite Image Contrast Enhancement Algorithm based on Plateau Histogram Equalization" *2014 IEEE Region 10 Symposium, IEEE Xplore*, 207-212, 2014.

5. Raju A., Dwarakish G. S., D. Venkat Reddy "*Histogram Equalization Based Mean Self – Adaptive Plateau Histogram Equalization for Brightness Preserving and Contrast Enhancement*" *Proceedings of the 3rd World Conference on Applied Sciences, Engineering and Technology*, 27-29 September 2014, Kathmandu, Nepal, ISBN 13: 978-81-930222-0-7, pp 232-239.

6. Raju. A, Ganasri B P, Dwarakish G. S and D. Venkat Reddy, (2014) "Automatic Shoreline Detection and Change Detection Analysis of Netravati-Gurpur Rivermouth using Histogram Equalization and Adaptive Thresholding Techniques," *International Conference on Water Resources, Coastal and Ocean Engineering (ICWRCOE-2015),* March, 2014 (UNDER REVIEW).

BIODATA

RAJU. A was born on 10th June, 1986 in Karimnagar District, Andhra Pradesh, India. He completed his schooling in Trinity Model High School, Peddapalli, Karimnagar in 2001. He graduated from Jawaharlal Nehru Technological University (JNTU), Hyderabad, India in 2007. He has completed his post-graduation from the same university in 2009 and worked as Assistant Professor for one and half year. He has joined as a full-time research scholar in National Institute of Technology (NITK), Surathkal, India in July, 2011. He has a total of 5 technical publications in International Journals and 7 papers in International conferences to his credit. His current research interests are Digital Image Processing, Remote Sensing and GIS.